The Role of Forces During Contact Inhibition of Locomotion

Liviu Andrei Troaca Luchici

A dissertation submitted in partial fulfilment

of the requirements for the degree of

Doctor of Philosophy

of

University College London

Department of Mechanical Engineering

University College London

November 2016

I, Liviu Andrei Troaca Luchici, confirm that the work presented in this thesis is my own. Where information has been derived from other sources, I confirm that this has been indicated in the work.

To all that have stood next to
me during this process...

Abstract

Contact Inhibition of Locomotion (CIL), a process where migrating cells repel upon collision, was first observed in cultured cells more than 60 years ago. Previous work investigating *Drosophila* hemocyte collisions *in vivo* revealed that precise CIL interactions are required for hemocytes to acquire their developmental patterning. Kinematics analysis of the exact velocity and acceleration changes surrounding the contact inhibition process revealed that rapid and synchronous kinematic changes take place during collisions.

To understand the cause of such intriguing CIL kinematics I examined the actin network dynamics surrounding collisions. Pseudo-speckle microscopy tracking the actin retrograde flow dynamics during collisions revealed that the actin flow undergoes synchronous temporal and spatial reorganization across the entire lamella of both colliding partners. Also, a region of low retrograde flow develops perpendicular to the leading edge spanning colliding cells. Upon repulsion, retrograde flow simultaneously spikes in both lamellae. Further experimental investigations revealed that as hemocytes collide, an inter-cellular adhesion develops at the site of cell-cell contact which leads to the formation of an actin stress-fibre like structure transiently coupling the cells through an actin clutch-like mechanism analogous to the integrin clutch encountered in migrating cells.

I subsequently modelled the cytoskeletal stresses in freely moving and colliding cells using a linear viscoelastic model. Upon collision, lamellar stress redistributes from the cell body to the leading edge along the region of low retrograde flow. Direct laser abscission of the actin stress-fibre like structure spanning colliding cells confirmed that lamellar tension is increasing during CIL and showed that the release of this excess tension is sufficient to cause cells to migrate away from the collision. It is this haptic feedback mechanism, and the subsequent release of lamellar tension, that allows CIL to act as a productive migratory cue for the hemocyte developmental patterning.

Acknowledgements

I would like to express my deepest appreciation to BBSRC for providing the necessary funding for my studies at University College London. My special thanks go to my greatest supervisors Prof. Mark A Miodownik at University College London and Dr. Brian Stramer at King's College London for their continuous support and encouragement during the last four years. I would also like to thank to Dr John Robert Davis without who this project would not have been possible and all our collaborators, in particular Prof Graham Dunn, who greatly contributed to this work and to my training as a researcher. My final thanks go to my friends and family who stayed along side me during this whole time, and endured endless conversations about contact inhibition of locomotion and grand unified theories of cell migration.

Contents

List of Figures

List of Tables

Chapter 1

Introduction

Contact inhibition of locomotion (CIL) was discovered more than 60 years ago in cultured chick heart fibroblasts by the pioneering cell biologist, Michael Abercrombie. Initially, CIL was defined as the cessation of a cell's forward movement upon contact with another cell [8, 9]. After the initial characterisation in chick heart fibroblasts, several other cell types were observed to undergo contact inhibition, including fibrosarcoma cells *in vitro* [10], and cultured prostate cancer cells PC-3 [11]. There was a lot of speculation about contact inhibition being a phenomenon specific to a few cell types with no clear functional role. However, in recent years *in vivo* roles for this process have been discovered during embryogenesis in Zebrafish and Xenopus neural crest cells [4], *Drosophila* macrophages (hemocytes) [12], and Cajal-Retzius cells [13]. This seemingly simple intercellular interaction that takes place during CIL acts as an instructive migratory cue [4], and could even control the acquisition of embryonic patterns [5, 13].

Contact Inhibition of Locomotion plays an important role in modulating the social behaviour of cells [14, 15]. The molecular mechanisms controlling this process are still unclear. Over the years, it was proposed that a range of intercellular adhesions (e.g. cadherins [16, 17, 18, 19, 20, 21]) and intracellular signalling pathways (e.g. planar cell polarity [4], Ephrin signalling [22, 23]) are driving the observed behaviours during CIL. Contact inhibition has strong links to cell migration as it involves cells rapidly stopping and reversing their direction of movement upon contact. However, the role of the actin cytoskeleton, which is crucial for other aspects

cell migration [24], is entirely unknown during CIL. Therefore, it is impossible to achieve a complete understanding of the regulatory mechanism of CIL without knowing how actin dynamics contributes to the response.

In the present work, embryonic migration of hemocytes is exploited to understand the regulatory mechanism of CIL *in vivo*. Hemocytes are known to constantly collide with each other until they evenly disperse throughout the embryo [25, 12, 5]. Computer simulations of hemocyte movement during embryogenesis revealed that the observed even cell spacing was driven by contact inhibition dynamics [5]. Villar-Cervino and colleagues employed similar mathematical techniques to study the migration of Cajal-Retzius cells in the cerebral cortex. Their results showed that CIL is requiered during the dispersion of these cells [13], suggesting that CIL alone is a conserved mechanism capable of generating tiled cellular arrays.

During migration, the viscoelastic actin network provides the propulsion that allows a cell to generate movement. The actin cytoskeleton within the lamella of a migrating cell is in a constant state of flux. Actin polymerises at the leading edge, which pushes the cell membrane forward; subsequently, the force of polymerisation against the membrane together with Myosin II-driven contraction of the actin network drives a retrograde movement of the actin cytoskeleton. It is this actin treadmill that generates the force for cell motility [26]. When a cell generates forward movement, cell-matrix adhesion proteins, such as integrins, become engaged and bind to the extracellular matrix. Integrin activation leads to a slowing of the retrograde actin flow above this integrin-based point of friction, and the force of the moving actin network is transformed into extracellular traction stresses [27]. This integrin-actin clutch and the resultant inverse correlation between actin retrograde flow and traction force is hypothesised to be involved in the movement of nearly all cell types.

Ever since its discovery, there have been several speculations that mechanics plays a central role in directing the CIL response [9]. At that time they lacked the necessary tools to investigate this hypothesis; however, with the recent develop-

ment of fluorescent imaging techniques, advanced genetic tools, and computational resources it is now possible to dissect this process in detail. This work combines theoretical and computational materials science techniques and experimental image analysis, to understand the role of forces during CIL of *Drosophila* hemocytes.

1.1 Thesis description

This thesis contains 7 chapters. It begins with a very short introduction to contact inhibition and actin cell motility. Chapter 2 is a literature survey of the concepts needed to understand the rest of this work. It begins with a detailed exposition of actin-based cell motility focusing on the organisation and mechanics of the actin cytoskeleton. The main aspects of contact inhibition are reviewed next, including existent assays for CIL and current theories about how the process is regulated.

Chapter 3 introduces all the tools and techniques that were used to conduct this work. The chapter begins with an overview of the fly genetics that was required for characterising hemocyte CIL. Next, the theory and tools for quantifying cell kinematics are described, with emphasis on the generic kinematics platform (CSPACC) that was developed to characterise cell velocity and acceleration. Next, all the image analysis algorithms used for this work are introduced, including the pseudo-speckle microscopy technique (FLUPS) that was used for quantifying the actin retrograde flow in both freely moving and colliding hemocytes. Subsequently, an in-depth mathematical analysis of the elasticity of actin networks is conducted and the stress model used for quantifying intracellular stresses is introduced. This chapter ends with a description of the laser ablation experiments and the quantification used to convert experimental lamellar retraction rates into lamellar tension.

Chapter 4 contains an in-depth quantification of cell kinematics during CIL revealing that, at least for hemocytes, contact inhibition is a very precise process involving three distinctive kinematic phases. Furthermore, actin and microtubule cytoskeletons are identified as the main cytoskeletal players involved in the CIL response. The chapter ends with a short discussion of these findings and of the limitations of the current version of CSPACC.

Chapter 5 further investigates the role of the actin cytoskeleton during contact inhibition. As actin retrograde flow was not quantified in hemocytes before, the first part of the chapter is dedicated to quantifying the actin dynamics in freely moving hemocytes and to understanding what drives the retrograde flow movement of the networks. Subsequently, the same analysis is carried out for colliding hemocytes which revealed that during collisions there is a global and synchronous reorganisation of the actin cytoskeleton. Next this chapter highlights other cytoskeletal associated proteins that play a role during CIL. This analysis revealed that an inter-cellular adhesion between colliding hemocytes couples their actin networks which leads to the formation of an actin stress fibre-like structure synchronously in both cells suggesting that lamellar tension increased during the response. This chapter ends with a discussion of the main findings and the limitations of all the computational tools used to perform the analysis.

Chapter 6 expands the findings of the previous chapters by investigating the lamellar tension developed during hemocyte collisions using both computational modelling and direct experimental tests. Direct laser abscission experiments of the actin stress fibre-like structure spanning the colliding cells during CIL confirmed that there is indeed an increase in lamellar tension during the response. Furthermore, the release of this excess lamellar tension was sufficient to cause cells to reverse the direction in which they migrated. Next computational modelling of the stresses developed within the actin network during collisions was conducted confirming that tension plays a central role during CIL. Finally, this chapter investigates the role for CIL during *Drosophila* embryogenesis. This chapter ends with a short discussion of the main findings and an in-depth analysis of the limitations of the mathematical models and computational tools used to conduct the quantification.

Chapter 7 presents a summary and a detailed discussion of all the findings. This chapter ends with a detailed discussion the further work that has to be conducted in order to fully understand how mechanical signals are transduced at a cell level during the contact inhibition response.

Appendix A contains the legends for all the movies referenced throughout this

work.

1.2 Refereed conference and journal papers

This work has been published in:

1. Davis, J.*, Luchici, A.*, Mosis, F., Thackery, J., Salazar, J., Mao, Y., Dunn, G., Betz, T., Miodownik, M., and Stramer, B. (2015). Inter-Cellular Forces Orchestrate Contact Inhibition of Locomotion. Cell *161*, 361-373. * these authors contributed equally to the work.

Chapter 2

Literature Review

2.1 Actin based cell migration

Cell migration begins with cell polarisation, i.e. establishing a front and a back [28]. Once a cell is polarised, it begins to migrate through a cyclical process where it first extends its leading edge, then adheres to the extracellular matrix, and finally the whole cell contracts to translocate the cell body forward [29, 30]. This type of migration can be conceptualised as a whole cell treadmilling process, where the front extends and the rear of the cell then follows [31].

Actin is the common denominator for all these processes, providing the cell with both the structural and dynamic support required for it's motion [30, 31, 28, 32, 1].

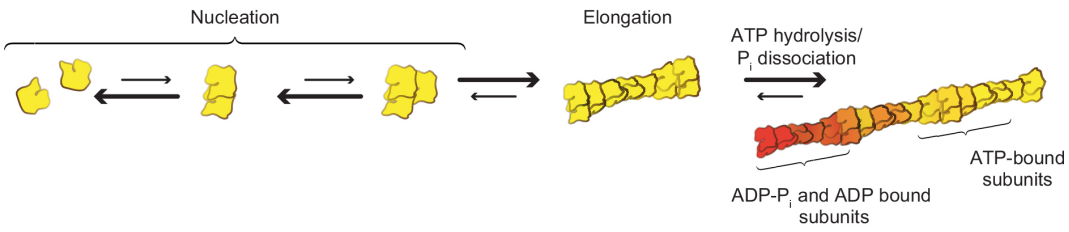

Figure 2.1: Schematics highlighting the assembly of F-actin. Assembly kinetics starts with the nucleation of actin oligomers from free ATP-bound monomers. This step is followed by rapid elongation at the barbed end while the pointed end undergoes ATP hydrolysis and phosphate dissociation. Figure recreated from [1].

Actin is a globular protein 42-kDa in diameter that can self-assemble into right-handed helical filaments (also termed F-actin). Once nucleated, actin filaments continue to grow until thermal fluctuations or other external factors break them apart [33, 1]. The geometry of the actin monomers gives rise to an asymmetric filament with two kinetically different ends: a barbed end that grows very fast [33] and a pointed end where polymerisation is a lot slower (Figure 2.1). Several studies of F-actin in solution show that addition of new monomers is highly dependent on the local monomer concentration at the filament tip [33]. As a consequence, in order for a barbed end to elongate the concentration of actin monomers has to be maintained at a critical concentration (the of free monomers at which there is no net change in the length of the filament; usually about $0.1\mu M$ in physiological conditions) [33]. Another critical aspect of actin monomers is their ability to hydrolyse ATP, and hence change their conformation, once they are incorporated into a filament in relatively short time (half-life of about 2 seconds) [34]. Once hydrolysis takes place, the γ-phosphate is released which leads to the ADP bound monomers detaching from the filament. The phosphate release is a lot slower having a half-life of approximately 350 seconds [35] (Figure 2.1). Together these two processes can be used as an internal timer to indicate the age of the filament and also to trigger the disassembly process of F-actin in physiological conditions [33].

The process of continuous recycling of actin monomers from the barbed end to the pointed end has been termed filament treadmilling [31]. Left by itself, the actin nucleation and treadmilling process is very slow (reported at about $2\mu m/h$ for *in vitro* filaments [36]), too slow to account for cell migration where cells need to constantly adapt to physical changes in their environment or to the presence of different signalling molecules. Therefore, cells exploit a diverse range of associated proteins to enhance filament assembly and disassembly [37, 33, 1].

In vitro measurements showed that single actin filaments behave like a semi-flexible material at the cell scale [38]. These results imply that filaments shorter than approximately $10\mu m$ can be modelled as stiff rods. However, long filaments tend to be more flexible and bend due to thermal energy [1]. This critical length of

$10\mu m$ is referred to as the persistence length of the filament, l_p. In other words, a persistence

The persistence length of an actin filament is directly proportional to the rigidity of a filament and inversely proportional to temperature [38, 39]. However, the cytoplasm is a very crowded space filled with numerous polymer meshworks and their accessory proteins [31]. This results in F-actin being more constrained than in a pure solution which means that even short filaments will still bend under relatively low levels of force [1]. From *in vitro* buckling experiments, we now know that a $1\mu m$ long actin filament that is capped at one end by nucleating factors such as formin and on the other by inactivated myosin buckles at a force of $0.4pN$ [40, 41]. Based on these experimental results, mathematical modelling suggested that at a constant monomer pool of $\approx 50\mu M$ (similar to the levels measured within cells), filaments as short as $0.5\mu m$ can resist a buckling force of up to $10pN$ [41, 42]. This buckling force can be even higher for filaments within the cytoplasm because nucleotides and divalent cations that bind to the filament make them up to 4 times stiffer [42, 43]. However, it will become clear later that cells also possess several proteins that soften the actin filaments, changing how much force they can withstand before buckling.

A collection of single filaments growing against a load are capable of generating force to push the entire plasma membrane forward [1]. Until now, the accepted model of how this is possible comes from the work of Mogilner and colleagues who proposed the ”elastic Brownian ratchet” mechanism. In this model, filaments are short spring-like wires that are constantly fluctuating under thermal energy. When they are in their bent configuration, there is enough space between the filament tip and the plasma membrane for a monomer to squeeze in which results in lengthening the filament. As the filament is straightening against the surface, it generates a restoring force that pushes the membrane forward [44]. Indeed, single actin filaments *in vitro* have been observed to be oscillating [45] which suggest that short filaments can be considered elastic springs, with an elastic modulus similar to rigid plastic [46]. Therefore, actin filaments in physiological conditions can be consid-

ered force generating structures capable of pushing loads up to several *pN* in magnitude.

2.1.1 Cellular organisation of the actin network

Once the polarity is established, the first step of any motility cycle is to extend new cellular protrusions in different directions. To achieve this, cells harness the self-assembly property of F-actin and form structures capable of pushing the membrane forward. Based on the organisation of actin, cells can form different types of protrusions [24]. In this work, I will only focus on a specialised force generating protrusion termed lamellipodia as this is the principal force generation mechanism for hemocytes motility.

Lamellipodia is a quasi-two-dimensional actin meshwork formed right behind the leading edge, i.e. the region of the plasma membrane extending in the direction of movement, of migrating cells. This structure forms primarily by *de novo* nucleation of actin filaments [47]. Actin polymerisation is a highly dynamic self-assembly process that is limited by the concentration of available actin monomers. As a consequence, within the cell cytoplasm there must always a pool of non-polymerised actin monomers [33]. Nucleation, growth, and disassembly of actin filaments has to be tightly controlled in order to avoid the depletion of free monomers and the stalling of the whole protrusive machinery [24, 32, 1]. To control the initial nucleation steps, cells use nucleotide exchange factors such as profilin, which binds to actin monomers and inhibits the instantaneous formation of new oligomers [48]. Profilin also catalyses the exchange of ADP-actin monomers for ATP-actin monomers, returning the resulting subunits to the ATP-actin-profilin monomer pool in the cytoplasm which remains largely at the same concentration throughout the lifetime of a cell [33]. The advantage of this mechanism is that actin monomers decorated with profilin can be assembled into filaments only in the presence of additional cellular nucleation promoting factors (NPFs) such as Arp2/3 which prevents the random nucleation of filaments within the cytoplasm. Activation of NPFs involves additional proteins such as the WASP/WAVE family proteins and formins which are controlled using small Rho GTPases and p21-activated kinases (PAK).

These proteins localise at the leading edge and signal the formation of new filaments in response to mechanical or chemical cues [37, 47] thus harnessing the actin nucleation machinery only when it is needed. Nevertheless, once NPFs are present, actin polymerisation is exclusively driven at the barbed end of the filament [49]. Under special conditions, additional proteins can be employed to increase the rate of monomer addition [1], therefore allowing cells to rapidly build the required actin architecture when it is needed.

The architecture of the lamellipodia is generated by three distinct processes. First, new filaments (called daughter filaments) are nucleated off the side of pre-existing filaments (called mother filaments or primers) at $\pm 70^{\circ}$ with respect to the primer in an Arp2/3 dependent process (the detailed biochemical control of lamellipodia formation is not essential for this work, as I will be focusing on the mechanical behaviour of this actin network. The interested reader can find a comprehensive review of how cellular protrusions are controlled in [28, 24, 32]). Furthermore, as the network branches, it has to generate enough force to push the plasma membrane forward. Single filaments would buckle under the load of the membrane, therefore the network density has to increase to ensure that enough force is being produced to generate cell movement. To achieve this, the cell uses capping proteins that block the growth at filament barbed ends [1], thus limiting the number of filaments that are in direct contact with the leading edge. In addition, capping creates new mother filaments which are subsequently harnessed by the Arp2/3 nucleation machinery to generate more filaments leading to an increase in network density (later it will become clearer why a dense network is needed to generate the force to push the plasma membrane forward). Capping also limits the number of actin filaments that are actively ”pushing” against the membrane [1] and as such ensure the required amount of force is generated. Finally, capped filaments are also sterically displaced by new branches resulting in a discrete network when viewed at filament scale, creating an inhomogeneous actin network composed of numerous branched sub-networks each nucleated from its own primer. When filaments from different such sub-networks meet, they exploit the electrostatic properties of the filaments which cause them to

entangle and merge together into a larger structure [1].

Another mechanism by which the cell ensures that lamellipodia can efficiently provide the force required for generating protrusions is to use crosslinking proteins to merge together already existent filaments or sub-networks. Based on their size and geometry, crosslinks can generate various F-actin structures [1]. For example, fascin, which has a very short bridging distance, packs together filaments into long parallel bundles [50]. On the other hand, α-actinin which has a very large bridging distance is responsible for crosslinking entire parts of the network [1].

In addition to the constant building of new lamellipodia at the leading edge, cells also constantly remodel the actin network within the lamella. Proteins from the ADF/cofilin family have emerged in the past 30 years as the principal factor for network disassembly. These proteins use fragmentation or severing to break apart the actin network [51, 52]. The exact mechanisms by which ADF/cofilin works are still under debate. However, recent experiments have shown that ADF/cofilin decreases the persistence length of the filaments to about $2\mu m$, making them very flexible [53]. These observations led to the development of a stress-based model for the action of ADF/cofilin on filaments. This framework proposed that molecules of ADF/cofilin bind preferentially to the ADP-actin part of the filament [54, 55], decreasing its stiffness which leads to a local stress accumulation at mechanical discontinuities, such as the boundaries of ADF/cofilin-decorated filament segments [56, 57]. Imaging of the interaction of ADF/cofilin with actin filaments confirmed that this is indeed the case by directly observing the fragmentation occurring at the boundary [58, 59]. These data suggest that actin filament disassembly is a stochastic fragmentation process mediated by ADF/cofilin, rather than a vectorial disassembly process, where monomers are disassembled one at a time from the filament end [1].

In recent years, myosin-driven contraction has emerged as another mechanism for filament disassembly. Myosin encompasses a large family of molecular motors that are known to associate with actin filaments to generate contractile forces. The most common protein is the myosin-II subfamily which consists of two ATPase heads and a long, rod-like tail. A myosin-II molecule is usually a dimer with the

two myosin molecules linked by their tails which enables them to cluster and form polar filaments [60]. The resulting myosin II filament has two ATPase heads on either side which attach to F-actin pointing in different directions. When myosin II is activated, it causes the filaments to slide past each other resulting in a contraction of the network [60] (molecular motors are not the focus of this report, but the interested reader can find out more about them from [61]). Studies conducted in solution have showed that myosin induces fragmentation of actin bundles in two steps. First, the actin bundles are split into individual filaments and then the resulting actin filaments are disassembled [62]. Because myosin is capable of reorganising branched networks into antiparallel filaments [1], it has been proposed that myosin-driven disassembly is a selective process, dependent on the orientation of the filaments within that particular actin structure [63, 1]. The current view on how filaments are disassembled involves a feedback loop between mechanics and biochemistry. Using this framework, ADF/cofilin binds to actin filaments modifying their elastic properties (i.e. increases their flexibility) and then myosin-driven contraction provides the mechanical stress required for fragmenting the filaments [1].

By exploiting the properties of F-actin assembly, cells are able to assemble a two-dimensional structure to push the plasma membrane forward. Furthermore, as it will become clear later, this structure is not only generating the propulsive forces required to advance the leading edge, it also offers structural support and maintains the cell shape plus generates the traction forces that propel the whole cell forward.

2.1.2 Mechanical properties of the lamellipodia

The cross-linked structure of the lamellipodia makes it a semi-flexible polymer with high elasticity at relatively small volume fractions. In other words, the actin meshwork is capable of resisting relatively high forces before becoming plastically deformed even if the network occupies a small volume from the total volume of the cell [1]. The elastic behaviour of the network is highly nonlinear and depends on both the density of F-actin and the concentration of available cross-linkers [64, 65]. *In vitro* studies of the actin network have established that the lamellipodia can be treated as a soft viscoelastic material with a shear modulus of approximately

$10^3 - 10^4 Pa$, and a relaxation time that varies from 100 to 1000 seconds [64, 66, 65]. These experimental studies of rigidly cross-linked actin networks in solution revealed that the lamellipodia can behave as both a perfectly elastic material at short time scales (of less than 1 minute), and as a viscoelastic material at longer time scales [65, 67, 68, 69, 64]. What is perhaps even more interesting is that as the applied strain increases, the elastic modulus of the network also increases nonlinearly leading to a stress-stiffening behaviour of the cytoskeleton [65, 66]. Further AFM-based microrheology of dendritic actin networks revealed that the network can also undergo "stress-softening" where individual filaments start to buckle (i.e. a sudden sideways failure which eventually leads to the breaking of the filament) if the compressive stress applied to the network is increased above a certain threshold [68]. Both stress-stiffening and stress-softening are completely reversible processes as suggested by experiments where the meshwork properties recovered to their normal values in the absence of the force [66, 70], conferring cells a very adaptive machinery to a multitude of stimuli.

The origin of the elastic behaviour of the cytoskeleton is still uncertain. Experimental and theoretical studies of the elastic properties of actin networks revealed that the elastic constants of the network depend on both the density and length of F-actin and the concentration and efficiency of cross-linkers [71, 72, 73]. In the limiting case of an actin meshwork made of long filaments in the presence of a high crosslinker density most of the shear strain caused by externally applied shearing stems from large shearing of individual filaments rather than from a network wide deformation [71, 72]. These deformations were mostly affine (self-similar at all length scales) throughout the network. In contrast, at the other extreme of a low number of short filaments in the presence of a low concentration of cross-linkers, the applied external shear stress causes filaments to bend. Surprisingly, for this case, the deformations were non-affine throughout the network [71, 72] suggesting that elastic properties of the actin cytoskeleton depend both on the number of filaments that make up the network and the available concentration of crosslinkers. Direct visualisation of the deformations of F-actin networks during application of shear

stress suggested that strongly cross-linked networks exhibited affine deformations, whereas the deformations for weakly cross-linked were nonaffine [73]. The elastic properties of cross-linked actin networks highly depend on the density and length of actin filaments and the amount of cross-linking of the network. F-actin networks are both entropic which results in affine stretching of filaments, and enthalpic which causes single actin filaments to bend in response to externally applied shear stress [74, 75, 65]. Therefore, the elastic properties of the network are highly non-linear and depend on both the network composition and architecture and on the dynamics of the cross-links and other motor proteins embedded inside the cytoskeleton [66]. This ability of the actin cytoskeleton to regulate it's mechanical properties depending on the external conditions is crucial for cells' ability to adapt in a multitude of environments when subjected to a large variety of stimuli. However, it also makes it very difficult to experimentally study, or otherwise model, the elasticity of the cytoskeleton.

2.1.3 Actin stress fibre

Stress fibers (SFs) are one of the most prominent structures of the actin cytoskeleton observed in many cultured cell types [76]. They are load-bearing, tension-generating structures, used by cells to sense changes in the physical properties of the external environment (e.g. rigidity or compliance) and to generate and transmit cytoskeletal forces during cell migration. In general, they are required for any processes where cells experience high mechanical forces, such as in wound healing or for endothelial cells under constant shear in arteries walls [76].

Stress fibers are thought to be formed from antiparallel actin filaments joined together by periodic myosin II and α-actinin clusters, which confers them a sarcomeric appearance [76]. Analysis of Swiss 3T3 fibroblasts revealed that although the myosin II and α-actinin bands maintained a complementary periodicity, they varied significantly in dimension [77]. This variation was observed not only across cell-types but also across single SF within the same cell [77]. *In vitro* studies show that the width of myosin II and α-actinin bands is shorter towards the periphery of the cell, with longer bands observed towards the middle of the lamella, suggesting

that the SFs can simultaneously contract and stretch based on their location within the cell [77]. The presence of myosin II along the stress fibre serves as an indicator that stress fibres are contractile units. Nevertheless, stress fibres are rarely observed to shorten in length which suggested that they were mostly under isometric tension [76]. Traction force measurements at focal adhesions [78, 79], together with the rapid shortening of SFs as they detach from the substratum at focal adhesions [i.e. transmembrane proteins linking the extracellular matrix to the actin cytoskeleton [80]] further support the hypothesis that SFs are mostly under isometric tension.

Recent advances in fluorescent imaging techniques allowed for the even better characterisation of stress fibres, which lead to the identification of three distinctive stress fibre types. The most common type of SFs is ventral stress fibres. These structures are anchored at both ends by focal adhesions. Ventral SFs are generally several micrometers long, extending for the length of the cell. SFs are anchored to the substratum at these focal adhesions, however it is still generally unknown how they bind to the adhesions. Recent studies suggested that talin and vinculin might be involved in connecting the end of SFs with FAs [76]. The second type of SFs are termed dorsal or radial stress fibres; they are shorter and anchored only at one end by focal adhesions. These structures usually form behind the leading edge and extend towards the cell body. They were discovered, together with the third type of stress fibres, called transverse arcs, to be the precursors for ventral SFs. Transverse arcs are usually convex shaped filaments that develop within the cell lamella, at the end of the lamellipodium. These arcs are not directly anchored by focal adhesions, therefore they are free to move with the actin network towards the nucleus [77, 81, 82, 76]. The transverse arcs are decorated by myosin and α-actinin, which results in a sarcomeric-like alternating pattern of myosin and α-actinin as arcs develop [81]. Transverse arcs are not anchored to focal adhesions, as such they are free to move with the actin network. It was observed in Human osteosarcoma (U2OS) cells that as the transverse arcs are transported towards the cell body, they fuse with dorsal SFs on opposite sides of the cells resulting in ventral SFs anchored at both ends by focal adhesions [81]. Furthermore, under certain conditions dorsal

SFs were also observed to fuse and give rise to a ventral SF [81].

There is still a lot of controversy around the exact mechanisms and processes through which stress fibres are assembled, and maintained. Analysis of human osteosarcoma (U2OS) cells *in vitro* revealed that *de novo* assembly of SFs is highly dependent on actin polymerisation. Once new dorsal SFs and transverse arcs are formed, they are then converted into ventral SFs [81]. Stress fibres are the main structures used by cells to adapt to mechanical perturbations. As they are both mechanosensing and force generating structures, it is expected that cells have some mechanisms through which they can strengthen as they undergo more and more stress. Finally, stress fibre disassembly, a less studied phenomenon, but equally important for mechanotransduction, is thought to be mainly driven by a loss of tension and decreased myosin contractility [83]. However, it is still unclear how the loss of mechanical tension contributes to the disassembly of stress fibres [76].

2.1.4 Actin retrograde flow

The cytoskeleton of migrating cells constitutes of a very dynamic structure that is continuously reorganising to generate propulsive forces. Experimental studies show that the actin network of a moving cell continuously undergoes a centripetal motion from the leading edge towards the cell body. This active transport of the actin cytoskeleton is generically termed retrograde flow [2]. The retrograde flow is thought to be driven by a combination of actin polymerisation at the leading edge which pushes the plasma membrane forward and myosin II contraction inside the lamella which pulls the whole actin network towards the cell body (Figure 2.2 and [60, 84, 85, 86]).

There is strong evidence suggesting that myosin II plays a critical role for driving the retrograde flow in migrating cells. Several studies conducted on cultured cells revealed that myosin II is primarily localised close to the cell body and at the rear of the cell [86], colocalising to the places where the retrograde flow converges, i.e. regions within the lamella where there are very little flow changes, as most of the retorgrade flow is going into these regions [85]. Furthermore, inhibition of polymerisation in *Aplysia* bag cell growth cones resulted in little change in the retro-

grade flow, further supporting the idea that Myosin II contraction is the main driver of the actin retrograde flow [87]. In contrast, when Myosin II was inhibited in cultured sea urchin coelmocytes it did not affect the retrograde flow at the periphery of the cell but did indeed slow down the flow closer to the cell body [88]. These results reveal that there is still much to discover about how actin polymerisation combines with myosin contraction to give rise to the observed retrograde flow dynamics.

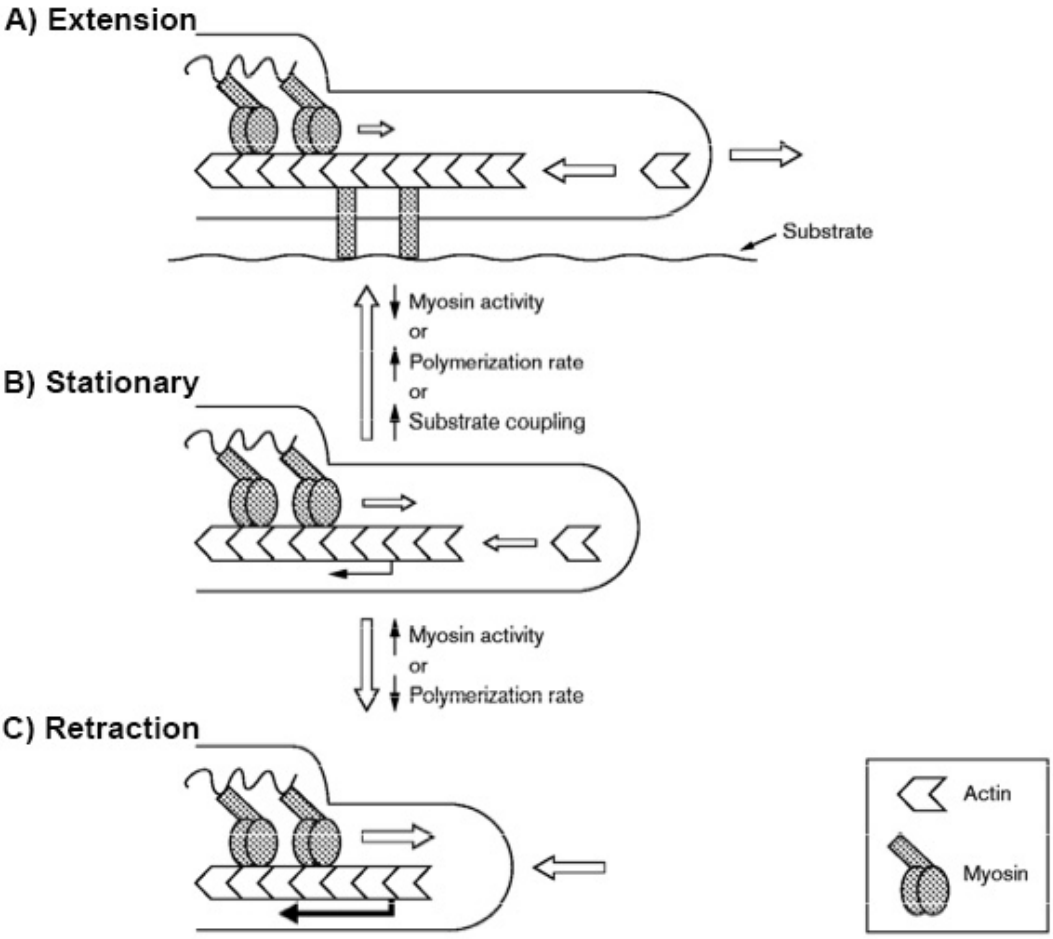

Figure 2.2: Retrograde flow overview describing extending, stationary, and retracting leading edges. A) Schematics representing the relation between myosin contraction, polymerisation rates, and cell protrusion. Note that if myosin activity is reduced or the polymerisation rate increases, a net forward protrusion will form. B) Actin polymerisation is completely balanced by the retrograde flow (black horizontal arrow). C) The increase in myosin activity or reduced polymerisation rate results in a net retraction of the leading edge. Note the enhanced retrograde flow (horizontal black line). Also, note that as the cell becomes more and more attached to the substrate, the retrograde flow will reduce. Figure recreated from [2]

Quantification of actin retrograde flow was initially performed by tracking beads attached to the lamellipodium of growth cones *in vitro* [87] or by tracking a bleached line of fluorescently labeled actin over time [89]. Both these methods had severe limitations in terms of accuracy and experimental throughput. With the advance of computer vision algorithms and image processing capabilities came several improvements in the tracking methods. These efforts culminated with the development of speckle microscopy for *in vitro* systems. Quantitative speckle fluorescent microscopy (QSF) is a single molecule technique which can capture both the movement of the actin cytoskeleton and actin polymerisation and depolymerisation rates within the cytoplasm. QSF is very powerful and has been successfully used to quantify the actin dynamics in a variety of cell types [90]. Nevertheless, for QSF to be successful, the samples have to prepared in a specific way which makes it difficult to use in most situations [91]. Fortunately, Vallotton and colleagues observed that phase contrast images of cultured keratocytes displayed bright, dynamic fluorescent actin features when the actin cytoskeleton was treated with either a rhodamine or a phalloidin probe [85]. The signal was strong enough to allow for these features to be subsequently tracked over time. Because of the striking resemblance between the results obtained using the latter approach and single molecule speckles, tracking larger actin features (e.g. parts of actin filaments rather than individual monomers) became known as pseudospeckle fluorescent microscopy [85]. Its main advantage over true speckle is that it does not require individual actin monomers to be fluorescently labeled which reduces the complexity and time needed to correctly prepare the samples allowing for its application to a far greater number of systems. However, one major limitation of pseudospeckle microscopy is that it cannot quantify actin polymerisation and depolymerisation rates, just the bulk movement of the actin network over time [85].

Maps of retrograde flow speed computed in different cell types show that the network is highly noncoherent, with regions of high flow rates separated by zones of slow flow speed. Convergence zones are not accompanied by an increase in F-actin density suggesting that these zones are actually regions where meshwork

contraction causes network depolymerisation. These studies also revealed a clear separation of the actin network into distinct regions with different actin retrograde flow speed, polymerisation kinetics and myosin activity. The variation in actin flow dynamics, actin polymerisation kinetics and myosin activity have later been attributed to the existence of two distinct structures: a lamella and lamellipodia [84, 92, 85, 86]. The latter is thought to exist right behind the leading edge, where the retrograde flow is very fast and speckles are short lived. Furthermore, in this region two distinct zones of actin activity have been observed. Immediately behind the leading edge there is a clear band where most of the actin polimerisation takes place. Right behind this polymerisation region, there is a second band populated by short-lived actin speckles where most of the depolymerisation takes place [93]. In contrast the retrograde flow in the lamella is slower, speckles are long-lived, and there is a punctate pattern of filament turnover together with high concentrations of myosin II [93].

These observations led to the belief that lamella and lamellipodia are two materially distinct and nearly decoupled networks. There is some limited evidence that lamella serves primarily as a structural element, offering the support required to maintain cell shape and generate traction forces while the lamellipodium is helping extend the leading edge forward. Nevertheless, there is a lot of controversy about how these two networks are connected. For example, in Newt lung and PtK1 epithelial cells it is observed that the lamellipodium is ”riding” on top of the lamella. There was a lot of critique surrounding this result as there is no definite proof that the two networks are sliding on top of each other [84, 93]. Furthermore, it could be that the observed decoupling between lamella and lamellipodium is just an artifact of the tracking methods employed. Another study using cultured fish keratocytes showed that in fast moving cells the retrograde flow displayed a clear boundary between lamellipodia and lamella. This boundary colocalised with the location where focal adhesions remained anchored and matured (see section 2.1.5 for further details on adhesions) [94, 95].

The actin retrograde flow is closely linked to cellular movement, possibly being

the main force generator during cell migration. The details of how the retrograde flow contributes to cell movement are still unknown. The theory for random cell migration postulates that cells extend protrusions in random directions and subsequently translocate in the direction of the largest of these protrusions. Current findings suggest that the retrograde flow is somehow limiting cellular protrusions [93, 96] and directly regulates cell speed. Therefore, it is possible that for a randomly moving cell the actin retrograde flow dictates the direction of movement, irrespective of the leading edge ruffling.

2.1.5 Actin clutch and force transduction

Most of the mechanotransduction in migrating cells is done via specialised subcellular adhesion complexes which are highly specialised structures in charge of making sense of both mechanical and chemical information coming in from the extracellular environment [97]. In general, every adhesion requires two principal components: an integrin and an extracellular counterpart for the integrin to bind to. Once such a pair is formed, cytoplasmic proteins that link with the actin cytoskeleton are recruited to help lock the cell in place. Adhesions to the extracellular matrix involve a more complicated integrin-extracellular matrix proteins complexes, which is usually formed from heterodimers composed of α and β subunits that bind to specific ECM proteins (e.g. fibronectin, vitronectin, collagen) [60, 97]. The exact biochemistry of cell-ECM adhesions is beyond the scope of this work but can be found in several review articles ([98] for cell-ECM adhesions). In the remaining of this section, an overview of how focal adhesions form, grow and mature will be given in the context of mechanotransduction.

Focal adhesions (FAs) are initiated at the leading edge of the cell as dot-like adhesion sites, termed focal complexes. Initially, the adhesions are very small, with an area less than 1 μm^2 [97]. As focal complexes link to the actin cytoskeleton, the retrograde movement of the actin network causes the adhesions to stretch which leads to an increase in their size. A small fraction of these nascent focal adhesions undergoes further myosin-dependent maturation as they are transported towards the cell body by the retrograde flow [28, 99]. Over time, focal adhesions continue to

stabilise, grow in size, elongate and even change their composition. At the end of this process, the resulting FA plaque either disassembles or transforms into a fibrillar adhesion (cell-matrix adhesions composed mainly of thin actin cables crosslinked by actin-binding proteins that are located towards the centre of the cell), and the process is restarted [100].

Focal adhesion maturation depends on cytoskeletal tension [97]. The main mechanism to generate tension at FAs sites is thorough stress fibre anchoring to FAs which subsequently generate isometric tension via a Myosin II-induced contraction (see section 2.1.3). To test if tension alone is inducing FA maturation, Oakes and collegues perturbed the stress fibre assembly pathways without affecting the contractility of the actomyosin network in cultured U2OS human osteosarcoma cells [82]. This experiment revealed that focal adhesions still assembled even if stress fibres were not present. However, FAs did not reach compositional maturation, suggesting that myosin II generated contraction alone is not sufficient to induce adhesion maturation [82]. In contrast, maturation of FAs still occurred even when myosin II-dependent cellular tension was decreased to up to 80% of its unperturbed level [82]. These results were confirmed by a more recent study from Stricker and collegues where they showed that focal adhesion growth rate remained constant even when the myosin II-mediated cellular tension was decreased to about 75% of its normal level [101]. However, these studies cannot explain how much Myosin II-induced contraction contributes to FA maturation because cells must retain some myosin activity to drive the retrograde flow and the assembly process for stress fibres [101]. Therefore, further studies are needed to clearly distinguish between isometric stress-fibre generated tension and general myosin II contraction within the lamella during focal adhesion maturation.

Once a migrating cell is anchored to the extracellular matrix, it will immediately use that adhesion as a traction force transmission relay. Pioneering traction force microscopy studies from [78] found that migrating cells *in vitro* are capable of exerting a consistent traction stress of the order of $5nN\mu m^{-2}$. Surprisingly, the generated traction force grew linearly with the adhesion size, measured by the flu-

orescent intensity of the respective region [78]. In contrast, Beningo and collegues revealed that there is a strong inverse correlation between the size of the focal adhesions and the measured traction force. They showed that small adhesions near the leading edge are responsible for transmitting strong traction stresses, whilst mature FAs only exerted weaker forces [79]. More recent studies were able to partially reconcile these apparently contradictory findings showing that there is indeed a strong correlation between adhesion size and the magnitude of the traction stresses, but only during initial stages of the adhesion maturation process. After the focal adhesions matured, this correlation disappeared, and the size of the FA remained constant while the traction forces either increase or decrease, based on the FA's relative position to the cell edge [102]. These findings suggest that cells could use the rate of adhesion maturation as a mechanism to modulate the transmitted force, and thus adapt to different substrates on which they migrate.

The retrograde flow, coupled to myosin contraction, is generally believed to be the main generator of cytoskeletal stress that is converted via focal adhesions into productive traction forces. However, the exact mechanisms through which this is achieved are not fully understood. Mathematical modells of the interaction between the actin network and FAs revealed that retrograde flow dynamics depends significantly on the coupling between the cytoskeleton and the extracellular matrix [103]. This study suggested that the actin network is directly coupled to the extracellular matrix through a clutch mechanism that strongly depended on the substrate stiffness. The cellular clutch works similarly to the clutch on a car. When the clutch is engaged (i.e. the actin network is linked to FAs) the retrograde flow slows down suggesting that part of the forces that would normally drive the flow are transmitted to the extracellular matrix via cell-ECM adhesions. In contrast, when the clutch is not engaged (i.e. the actin networks is not linked to FAs) the retrograde flow speed is increased suggesting that all the forces developed within the lamella are directed towards driving the flow. In addition, this actin clutch model also showed that retrograde flow dynamics is greatly affected by the stiffness of the substrate on which cells migrate. When simulated cells migrated on a soft substrate, the retro-

grade flow slowed down allowing cells to move using a "load-and-fail" mechanism where integrins were constantly binding to the actin network until the forces acting on them were to high and caused them to break. As the stiffness of the substrate was increased, the flow speed started to increase which caused a lot of slippage between the cell and the substrate where integrins were constantly binding and unbinding to the actin network. In the second scenario, they showed that cells generated less traction forces than when they were migrating on a soft substrate [103]. Confirmation of these results came from traction force microscopy studies that revealed an inverse relationship between F-actin speed and traction stresses developed at focal adhesions, where low flow velocities correlated with large stress values and fast retrograde flow were observed for low traction stresses [104]. Together these two studies strongly suggest that the retrograde flow is fundamental for regulating traction forces at focal adhesions during cell migration. However, the detailed physical and molecular mechanisms of how this takes place are still under intense scrutiny in the community.

Complementary studies revealed that cultured cells use stress fibres to transmit force to the ECM via focal adhesions [105, 97, 106]. For example, cells under cyclic stretch, such as the pulsatile stretching and shear experienced by endothelial cells and vascular smooth muscle [76], display a step-wise response to the external perturbations. First stress fibres form and then remodel to become better suited for withstanding the given perturbation. Subsequently,stress fibre begin to reinforce and repair, as the external tension causes some filaments to break [107]. This response is clearly seen in cultured fibroblasts exposed to cyclic stretch as they rearrange their SFs perpendicular to the direction of the force. This process of cytoskeletal and cell reorientation was found to be highly dependent on both the amplitude and frequency of the applied stress [108], and the substrate stiffness [109]. In order to sustain this remodelling and reorganisation of stress fibres's, a concomitant reinforcement and repair of the stress fibres has to occur [76]. Surprisingly, Zyxin, a protein usually encountered in FAs, redistributes along the SF as applied forces increase causing the SF to thicken [110, 111]. This fibre reinforcement does not depend on ROCK

signalling (an important protein for controlling actin assembly and reorganisation [37]), instead it appears to be mediated by an MAPK-dependent phosphorylation of Zyxin [111]. Several other studies confirmed that SF reinforcement is Zyxin dependent by showing that Zyxin together with α-actinin and VASP were recruited to sites of strain-induced breaks [110], but were not involved in the cell reorientation process [76].

2.1.6 Actin driven cellular motility

The actin cytoskeleton is a very complex material which is constantly undergoing a tremendous reorganisation to fulfil a myriad of functions. During lamellipodia-based migration, the cell needs to i) extend it's leading edge ii) adhere to the substrate iii) contract and translocate its whole cell body forward. As we saw in the previous sections, actin is the principal driver of these processes. Interestingly, the retrograde flow appears to be the linker between all these seemingly separate processes. However, the details of how this is achieved are still missing.

The current theory postulates that actin polymerisation right behind the leading edge pushes the edge forward [24]. As newly assembled filaments push the membrane forward, the membrane generates a reaction force which is subsequently transmitted to the bulk of the actin network partially contributing to moving the whole actin meshwork [112, 113]. Simultaneously with actin polymerisation, myosin II contracts providing the remaining of the force required to generate the actin retrograde flow. As the plasma membrane is pushed forward, a clutch-like mechanism is engaged (see section 2.1.5) that links the actin cytoskeleton to the extracellular matrix via specialised proteins [114] (Figure 2.3A). Engagement of the clutch (i.e. integrins are bound to the actin network) leads to a decrease in retrograde flow rates as the network cannot flow freely anymore which causes a build up in intracellular tension [96] (Figure 2.3B). This tension build-up eventually leads to the disengagement of the clutch. When the clutch is disengaged, the accumulated tension is released providing the necessary 'push' to move the whole cell [103] (Figure 2.3C).

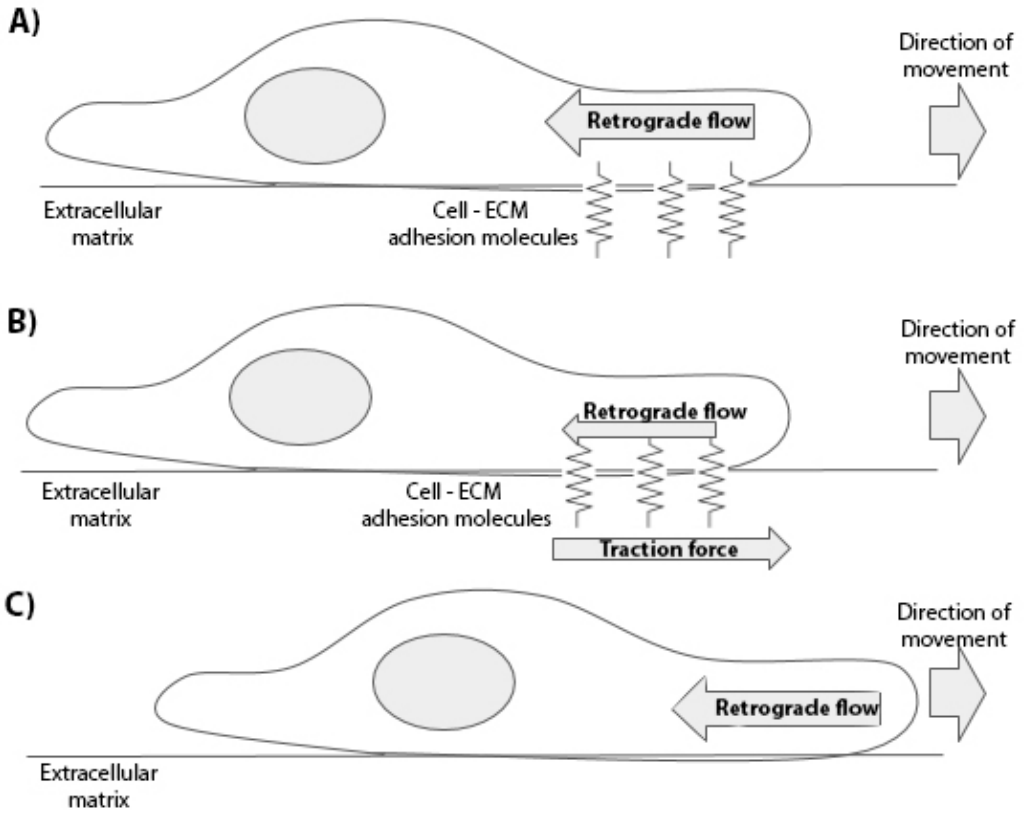

Figure 2.3: Schematic highlighting the actin-ECM clutch. A) Prior to adhering to the substrate, the whole actin network is moving towards the cell body driven by a combination of actin polymerisating against the leading edge and myosin contraction within the lamella. B) The cell adheres to the substrate and integrins link to the actin cytoskeleton, causing the retrograde flow to slow down causing part of the force previously driving the flow to get transmitted to the ECM. C) The adhesion between the cell and the substrate disassembles or breaks leading to the whole cell translocating and the retrograde flow rate returning to the values it had before the cell-ECM adhesion was engaged.

In vitro studies trying to investigate the connection between retrograde flow and cell movement showed that there is a biphasic relationship between retrograde flow speed and the amount of force that can be transmitted to the extracellular matrix [102]. Support for this hypothesis came from studies that showed a biphasic relationship with the amount of adhesiveness to the substratum and the cell speed suggesting that efficient migration requires an optimal level of adhesiveness [115, 116, 117]. Furthermore, adhesion maturation and transmission of traction forces is directly dependent on the retrograde flow rate [96]. Probably the most

striking evidence for the direct connection between whole cell movement and the retrograde flow dynamics comes from studies of keratocytes migrating in culture where the retrograde flow was observed to be inversely proportional with the cell speed [96] hinting to a possible regulation of motility via regulation of the actin cytoskeleton in general, and the retrograde flow in particular.

2.1.7 Continuous models of the actin cytoskeleton

A comprehensive multiscale model of the actin cytoskeleton that allows for direct manipulation of all the relevant parameters controlling the behaviour of the meshwork has been a long quest for many researchers in the field. Unfortunately, up to this date, there is no clear model on how all the intracellular processes (e.g. actin polymerisation, myosin II contraction, retrograde flow) are integrated at the cellular level during cell migration (see [118] for a comprehensive review on mathematical models of actin during cell migration). Out of this quest two different classes of models emerged: passive and active models.

Passive models of the actin cytoskeleton are by far the most established modelling approach because they can capture the behaviour of the actin network at different spatial and temporal scales. The main assumption made by every passive model is that the cytoskeleton can be regarded as an elastic or viscoelastic material. In short, elastic models assume that the deformation of the actin network is directly proportional to the applied force (deformations are not time dependent, they can withstand shear stress and do not dissipate energy over time) while the viscoelastic models are based on the assumption that the actin network can exhibit both viscous (deformations are time-dependent, they cannot withstand shear stresses, and energy is dissipated over time) and elastic behaviours. One notable example of passive models is the elastic model for forces developed within the cytoskeleton created by [67]. In this model, the authors assumed that the actin network behaves as an isotropic (i.e. deformations are not dependent on the direction in which they occur) elastic material in a permanent quasi-steady state that does not undergo active contraction. In addition, they completely ignored any viscous characteristics of the network. Using these simple assumptions, the model suggested that inside the lamel-

lipodium there are three distinct force zones based on the predominant force generation mechanisms. The model revealed that contraction forces are predominant at the rear of the lamellipodium, adhesion forces are primarily at the leading edge, and a combination of adhesion and contraction forces exists in the rest of the network [67]. Betz and collegues relaxed the constraint that the actin network behaves like a purely elastic material by assuming that the cytoskeleton of growth cones can be modelled as an isotropic, homogeneous, linear viscoelastic material [7]. Using only the local gradient of the stress tensor, they modelled the forces produced by the actin retrograde flow within the lamellipodium of growth cones *in vitro*. Their model revealed that the stress is rapidly dissipated at the leading edge which suggested the presence of a mechanism capable of absorbing and transmitting lamellar tension to the extracellular matrix [7], similar to the clutch-like mechanism coupling the actin cytoskeleton to the extracellular matrix during cell migration. Unfortunately, the model developed in [7] does not take into account myosin contraction or any information about the signalling cascades controlling actin polymerisation [7]. There have been several attempts to add network contractility to viscoelastic models of the actin retrograde flow within the lamella of migrating cells. For example, Rubinstein and collegues recreated most of the known behaviour of the retrograde flow in rapidly moving cell by coupling a viscoelastic Maxwell model of the actin network with a transport equation for myosin [119]. Contraction stresses were assumed directly proportional to the concentration of myosin molecules linked to the actin cytoskeleton. To incorporate actin polymerisation, the authors assumed that actin turnover is given by a reaction-drift density equation with constant disassembly rate [119]. Following a similar idea, Craig *et al* (2012) developed a different mechanical model of the actin treadmill by assuming that myosin pulling forces and membrane tensions are fully balanced by a drag force caused by filament resistance to buckling and breaking. This model predicted that if myosin activity is inhibited, membrane tension increases to drive the retrograde flow in growth cones [120].

In contrast, active models of the actin network consider that the cytoskeleton is a system far from chemical equilibrium, constantly consuming energy. Usually,

active models use one of two distinct approaches, depending on the timescale of interest: liquid crystal theory at long timescales or an active polar gel abstraction at short timescales [121]. When applied to the actin network of moving keratocytes, several active models successfully predicted the behaviour of the retrograde flow and estimated the principal physical parameters describing the contractility of the network [121]. Nevertheless, models of active matter are still in their youth, with a lot of work left to be done until they will be capable of capturing the details of the coupling between actin networks and the external environment. Finally, a drawback of both active and passive models is that in their current formulation, they are incapable of describing the actin network at a microscopic level nor can they include detailed biochemical properties of actin dynamics.

Therefore, even if modelling of the cytoskeleton has a long history in biomechanics, there are still numerous questions that need to be answered before we will be able to completely describe the behaviour of the actin network using solely a mathematical framework. Nevertheless, current models are providing an alternative to biological experiments by identifying some of the most important parameters for driving cell migration. Ideally, these predictions would be tested experimentally which would allow us to get a much more comprehensive understanding of the biological mechanisms that drive cell motility.

2.2 Contact Inhibition of Locomotion

Contact inhibition of locomotion (CIL) was first described by the pioneering cell biologist M. Abercrombie in a series of three papers published between 1950 and 1953 on the migration of chick fibroblasts *in vitro*. In his words, contact inhibition was defined as "the stopping of the continued locomotion of a cell in the direction which has produced a collision with another cell; so that one cell does not use another as a substratum" [8] (Figure 2.4).

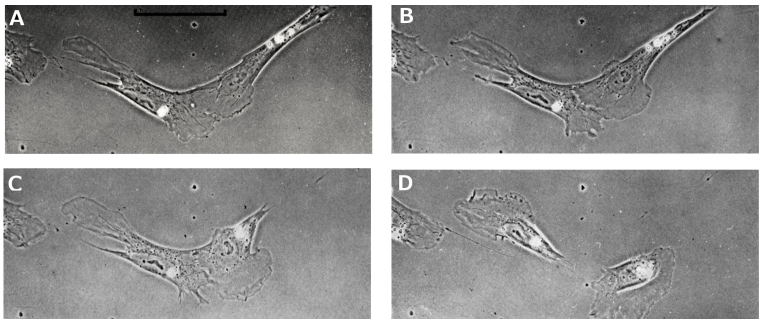

Figure 2.4: Time series of phase contrast *in vitro* chick heart fibroblasts undergoing contact inhibition. A) 5min post-collision B) 10min post-collision C) 15min post-collision D) 30min post collision Scale bar 25 μm.[3]

Besides providing the first characterisation of CIL, the initial studies of this process investigated the "monolayering" effect encountered when two *in vitro* populations of fibroblasts met to form a uniform sheet of cells. Analysing the motion of fibroblasts emanating from opposite explants showed that after the establishment of the junction between explants, the newly formed cellular sheet did not experience any further growth, and did not penetrate the junctional area. In contrast, they observed an outgrowth from the sides of the newly formed cell layer which resulted in a circular monolayer of cells. These data suggested that the distribution of fibroblasts within the monolayer was driven by CIL as it prevented the cells to migrate over each other [122]. Using a similar experimental set-up where one of the explants was derived from sarcoma cells rather than fibroblasts revealed another interesting behaviour of fibroblasts *in vitro*. When fibroblasts and sarcoma cells collided, no inhibition of the motion of sarcoma cells and just a slight inhibition of the fibroblasts movement was observed [123]. These data showed that cancer cell lines might lose their ability to contact inhibit when they collide with a different cell type which suggested that CIL could play a major role in enhancing malignant invasion [123, 8, 14, 9].

Since its initial discovery, several cell types were observed to undergo contact inhibition such as neural crest cells, *Drosophila* macrophages, and Cajal-Retzius cells [4, 12, 13]. Out of this work, it emerged that CIL is not a single response, will different cell-types showing slightly different behaviours upon collision which lead to a complex contact inhibition responses. One possible distinction that was

made was to separate the CIL response for cells colliding with the same cell-type (i.e. homotypic collisions) or with a different cell type (i.e. heterotypic collisions) [124, 125, 126, 10]. Furthermore, Parkinson & Edwards (1978) showed that heterotypic collisions between embryonic pigmented retina epithelial cells and choroid fibroblasts *in vitro* resulted in fibroblasts undergoing contact inhibition while the collision did not affect the movement of epithelial cells. These data lead to a further classification of heterotypic collisions into reciprocal where cells inhibit each other, and non-reciprocal where just one colliding partner is affected by the collision [127, 128, 123, 126].

Contact inhibition is a complex process involving the coordination of several cytoskeletal players, including the actin and microtubule networks (see the remaining of this chapter for more details) which leads to diverse CIL behaviours where contact inhibiting cells displaying significant speed differences before and after collision [9, 129], differences in the amount that cell's overlap [130], cessation of lamellar ruffling [130, 131, 132, 133, 134, 135], presence or absence of lamellar contraction after the two colliding cells collided [9, 130, 136, 133], or change in the direction of movement [130, 18]. In addition, populations of cells that undergo contact inhibition also displayed differences in how the colony expanded [124]. Given the broad range of CIL behaviours, Martz & Steinberg (1973) proposed a more comprehensive classification of contact inhibition into six different classes with a type 1 to 6 based on speed difference, overlapping area, the ruffling activity of the lamella, neighbour exchange, direction of movement and colony expansion, respectively. The split of contact inhibition into so many distinct classes was aimed at to bring together the different observation from different systems about the process. Nevertheless, some of these classes are purely based on subjective observation, without any quantitative index to back them up which I believe created a lot of confusion among researchers. In my view, a far more elegant and useful distinction for separating CIL behaviours is the one introduced by Abercrombie himself, where contact inhibition was classified solely based on the presence or absence of lamellar contraction. In Abercrombies view, there are two main types of CIL; a type 1 CIL

where colliding cells undergo a lamellar contraction after the lamellar overlap, and a type 2 CIL where contraction is not observed following the initial cell-cell contact [8]. In the present work, I will be adopting Abercrombie's classification of CIL into a type 1 and a type 2.

Another debated aspect of CIL is cell repolarisation following the cell-cell contact. Although numerous studies tried to elucidate the exact sequence of events during this last phase of CIL, it is still unclear how repolarisation starts during CIL [130, 3, 137]. For example, in chick heart fibroblasts protrusions first collapse at the site of cell-cell contact before the cells form new protrusions away from the contact site [3, 130]. In contrast, neural crest cells the opposite was shown to happen where cells first form protrusions away from the contact site and then they begin to separate [137]. Regardless of the order of events, it is clear that cell repolarisation is crucial for a normal CIL response, therefore, it is important to understand what happens with cells after the contact to understand the bigger role CIL plays in different biological processes.

2.2.1 Assays for contact inhibition

Contact inhibition is a multifaceted phenomenon, closely linked to cellular motility which makes it tremendously difficult to dissect phenotypes strictly due to CIL versus random variability in migration. In the initial characterisation of the process, Abercrombie and colleagues were the first to realise that relying on qualitative analysis would not be sufficient to understand the cellular dynamics involved in CIL. In their view, to fully understand the mechanisms behind CIL we first need to develop quantitative tools to objectively study the process [9, 130, 138, 126, 10].

The invasion index is one of the first measures for assessing if two cells are undergoing contact inhibition which was initially introduced by Abercrombie and colleagues to quantify the interaction between two explants of chick heart fibroblasts *in vitro* [125]. Observing the motion of fibroblasts emanating from two opposing explants, showed that when cells come in contact, they continued to contact inhibit leading to the formation of a junctional zone between explants where cells are constantly interacting. In contrast, cells that were not capable of undergoing

contact inhibition did not form a junctional zone, invading the opposite explant. The invasion index was subsequently defined as the width of the junctional zone forming between two population of cells migrating radially from opposing explants [122]. These results suggested that a width significantly different from zero could be immediately connected with cells that undergo contact inhibition. Nevertheless, using only the invasion index is not sufficient for assessing with 100% certitude if cells are indeed contact inhibiting because the low values of the index could also be explained by cells inability to migrate far enough from the explant in order to establish a junctional zone. To complement this measurement, it is necessary to quantify the dispersal distance of cells from their respective explant in the absence of an opposing explant with which they can interact [125]. The invasion index together with the cellular displacement represents a set of measurements for assessing if cells are capable of undergoing contact inhibition.

Another tool for quantifying cellular behaviour during collisions was introduced by Dunn and colleagues who abstracted the cell to a material particle and subsequently analysed the changes in cell velocity and acceleration during collisions (see section 3.2 for an introduction to particle kinematics) [126]. In contrast to the invasion index, analysing cell velocity and acceleration can identify if the contact with another cell influences motility. The core assumption of this idea is that any non-random movement of the cells would result in a biased acceleration. The success of this method depends on prior normalisation of cell position to eliminate any variation in the movement not directly related to their interaction. The best normalisation is to align the tracks which result from tracking either the cell nucleus or cell centroid to a common origin such as the position of the colliding partner in such a way that the two cells are horizontal at the time of the collision (see Figure 2.5A,B; Section 3.6.2). After the tracks are aligned, cell acceleration vectors are computed and plotted from a common origin which results in a vector plot like the one showed in Figure 2.5C.

Summing all the acceleration vectors provides an indicator of the average cell acceleration of all cells in the sample. This quantity was used to identify any effects

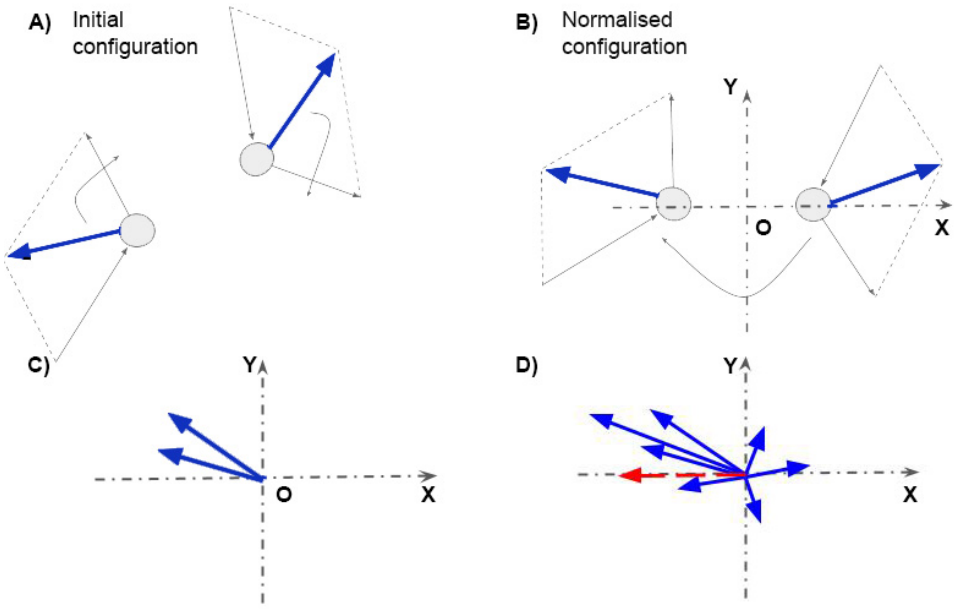

Figure 2.5: Schematic with a normalised sample acceleration plot. A) Fictitious scenario of two interacting cells. The blue arrows represent the acceleration vectors of the two cells at the time of interest. The curved arrows show the direction in which each acceleration vector has to be rotated to make both cells horizontal. B) Acceleration vectors normalised to the direction of a colliding partner. The curved arrow shows the direction in which the acceleration vector of the cell on the right needs to be rotated to complete the normalisation. C) Acceleration vectors normalised and translated to a common origin. D) Example acceleration plot for a population of cells. Each blue arrow represents the acceleration of a cell at a given time point. The red arrow represents the resultant horizontal acceleration.

of the colliding partner on cell motility because any bias in the movement will show as a significant acceleration in that direction. In other words, a significantly negative horizontal component of the acceleration vector indicates that the two colliding cells are moving away from each other and/or slowing down. The core assumption behind this is that for a system of interacting partciles, there is a significant acceleration only when there is an imbalance in the system. Applied to collisions, this imbalance would be created by the presence of the colliding partner. Unfortunately, this method is not foolproof either as it greatly depends on the reference point used to normalise the trajectories. Several studies succesfully used this method to investigate contact inhibition between chick heart fibroblasts and fibrosarcoma FS9 cell line [126, 10]. These investigations revealed different distributions of the acceler-

ation based on the reference used to normalise the vectors (i.e. either aligning the acceleration with the horizontal axis or by making the velocity vector at a previous time point horizontal)[126]. For the first case, they observed a clear bias in the acceleration away from the collision, however, in the second case they were unable to show any significant bias in cell movement [126]. Furthermore, this method cannot be used if the acceleration vectors result in a multi-modal distribution, i.e. the same number of vectors in different directions (see 3.5 for how to deal with this situations). Nevertheless, this assay has been crucial for identifying when cells are undergoing contact inhibition [126, 5] or how different genetic perturbation affect the contact inhibition response [4].

Dunn and colleagues proposed another kinematic technique for identifying if a cell is undergoing contact inhibition still relying on velocity and acceleration as fundamental measures of cell movement (see Section 3.2 for more information about particle kinematics) [10]. Because contact inhibition involves the cessation of forward movement upon contact with another cell, it is possible to use the horizontal component of the acceleration vector, termed C_x, to establish if cells stop moving forward following a collision [10]. The main advantage of this technique is that it allows for comparison between different cell types simultaneously, even if they have different speeds and persistence. To achieve this, C_x is normalised using the direction of the velocity vector and scaled by cell speed computed during the same interval. This makes the value of C_x between -1 and 1, where 0 indicates no change in velocity over that time interval. When applied to the study of collisions between different cell types or treatments, this index is usually compared for both freely moving and colliding cells. Therefore, if a cell is undergoing CIL it's C_x index is computed for both freely moving and colliding cases and if there is a significant reduction from one mode of migration to another, then it can be asserted that the collision is indeed a contact inhibition event, irrespective of cellular persistence [10]. In other words, regardless of the variation of the direction in which a cell migrates, C_x is capable of distinguishing when a cell is undergoing CIL or not.

Cellular behaviour after the initial contact with another cell is not the same for

all cell types, with some cells simply stopping their forward movement and others changing their direction of travel [139, 128, 127, 136]. To account for this subtle, but crucial difference between the two behaviours, the acceleration analysis was extended to include the vertical component of the vectors, C_y [10]. This offers information about any changes in later movement as follows: if a cell completely stops, then both C_x and C_y will be reduced, however, if the cell is just changing its direction of movement, then $C_y$increases after the contact. The introduction of these two indices has indeed been a step forward in analysing cellular collisions, as this method is still employed today to shed light on the regulatory mechanism of contact inhibition in a range of systems [22, 11, 23]. However, it is not a foolproof method. Because they rely on comparing the movement of cells during collisions with respect to their motion prior to the cells coming in contact, these indices are by definition sensitive to how variable is the cell movement in the first place; too much variation will potentially mask any effects of the collision as measured by C_x and C_y. This observation is particularly pertinent when cell position is recorded with short temporal resolution as this will produce a noisier speed because all speed computations are greatly dependant on the time interval over which they are performed. Furthermore, tracking errors at short time scales also introduces additional variations in the movement (see section 3.2) limiting the application of this method to relatively large time-scales, of the order of minutes.

Therefore, up to this date there is no universal assay capable to objectively establish with a very high degree of accuracy whether a collision between two cells is a contact inhibition event. The assays developed so far were mainly concerned with identifying if a collision constitutes a contact inhibition event, paying little attention to the development of quantitative tools that can reveal insights into what controls the response. Nevertheless, there are a few example where the assays reviewed in this section have successfully been employed to identify contact inhibition across different cell types [22, 140, 141, 5]. The same assays have sometimes laid the foundation for further experiments that aimed to provide information about the role of genetics in the process [4].

2.2.2 Characterisation and mechanisms driving contact inhibition

Abercrombie and colleagues designed two experiments to test if CIL is cell specific where they characterised the behaviour of chick heart fibroblasts emanating from two confronting explants which were derived from either same cell-type or from two different cell-types. The first experiments where cells belonging to the same cell type collided revealed that both cells undergoing contact inhibition of locomotion [124, 125, 132, 133, 8, 139]. Interestingly, the second series of experiments where chick heart fibroblasts collided with sarcoma cells revealed that although sarcoma cells were capable of inhibiting the movement of other sarcoma cells, they showed no signs of CIL when they collided with fibroblasts. These results proved that contact inhibition is indeed cell type specific rather than a common phenomenon to any cell type. Nevertheless, the results still left open one big question: what is the mechanism that allows some cell-type to contact inhibit each other while having no effect on the movement of cells from other cell types? [127, 126].

A critical part of contact inhibition is the cessation of forward motion upon contact with another cell. Therefore, cell architecture, especially the components of the cell involved in cell migration, was the first place to start the investigation for uncovering the underlying mechanism behind contact inhibition of locomotion. Out of a myriad of studies aiming to understand the mechanisms behind CIL in various cell types, it emerged that a stereotypical series of events takes place during the process. In short, Abercrombie's original experiments using fibroblasts colliding *in vitro* [9] and more recent studies of collisions between prostate cancer cells [11, 22] revealed that at least for these cell types, CIL is a four step process. An intercellular adhesion is established which causes the paralysis of membrane ruffling leading to a contraction of the lamellae and the subsequent separation of the two colliding cells. However, there is some uncertainty surrounding the second step of this timeline because most of the studies where the cessation of membrane ruffling was observed were based on phase contrast time-lapse movies of colliding cells with a temporal resolution of about $5min$ per frame [122, 130, 8, 132, 133, 127] without

any other assay to confirm them. This is not the only sequence of events proposed to take place during CIL. Studies conducted by Mayor and colleagues on the contact inhibition of neural crest cells suggested that a different series of events takes place during CIL. They suggested that as two cells collide, a cell-cell adhesion is established which leads to the local inhibition of new protrusions in the direction of movement (without any sudden lamellar contraction event taking place) and the generation of new protrusions in other directions which subsequently leads to cells repolarising and migrating away from the collision [20, 142].

Irrespective of which sequence of events is considered, the first step of contact inhibition is the establishment of an intercellular adhesion. This was originally speculated by Heaysman and colleagues using data from an electron microscopy study investigating CIL [138]. Since this initial observation, there have been numerous other studies that tried to identify the exact molecular nature of the adhesion that formed between colliding cells. Studies conducted in various cell types undergoing CIL highlighted proteins from the Cadherin family as the most likely candidate for linking the two colliding cells [16, 17, 18, 19, 20, 21]. Cadherins are usually membrane-bound proteins that have one intracellular end connecting directly to the actin cytoskeleton primarily through α and β catenin and another extracellular end connecting to the extracellular region. Furthermore, cadherins are known to form homophilic interactions between cells [143] and have multiple isoforms. These properties of the cadherin molecule led to the proposal that during contact inhibition, colliding cells distinguish between cell types by exploiting the different isoforms of the cadherin protein where cells expressing the same isoform recognise eachother and undergo a CIL event [142, 144]. Nevertheless, this explanation is not complete because a recognition mechanism based solely on cadherins cannot explain how cells of different cell types, i.e. with different isoforms of the cadherin protein, are still capable of undergoing CIL.

An alternative way for how cells are able to recognise each other was proposed by Heaysman and colleagues whereby they envisioned that a receptor-emitter pair allowed cells to behave independently during collisions [123]. More recent stud-

ies of contact inhibition suggested that Ephrin ligands and their specific receptors (Eph) could be the main receptor-ligand pair coupling colliding cells during contact inhibition between prostate cancer cell PC-3 lines and fibroblasts or between two prostate cancer cells [22, 23] or during collisions between Cajal-Retzius cells [13]. These studies suggested that there are two ways in which Ephrin mediated contacts lead to CIL. First, Ephrin A and Eph A pair promoted lamellar contraction while Ephrin B2 and Eph B3/B4 pair promoted cell migration of prostate cancer line PC-3 [22]. Second, Ephrin signalling modulated Cadherin complexes and as a consequence could play a role in modulating the adhesion between two colliding cells. These findings lead to speculations about an overarching mechanism for contact inhibition where lamellar contact triggers some chemical cascade, such as an Ephrin-Eph signalling or Cadherin activation in such a way that subtle changes in the protein concentration or localisation are responsible for the multitude of contact inhibition behaviours [21].

The paralysis of membrane ruffling and contraction of the lamella was signalled as a hallmark of CIl for certain cell types [129]. However, not all cell types appear to undergo both these steps. For example, chick heart fibroblasts were reported to cease their lamellar activity right after the contact with another cell and then undergo a rapid contraction event which led to the cells separating [9]. These observations lead to the hypothesis that the actin cytoskeleton plays a role during the CIL response. Until today our understanding of the role and regulation of actin during CIL is very limited. Studies of neural crest cells colliding *in vivo* have showed that the PCP pathway (an important signalling transduction cascade for cell polarity [145]) and small GTPases are triggering the remodelling of the actin network which leads to the repolarisation of colliding cells [4]. In another study, Kadir and collegues showed that fibroblasts collisions require Rho and ROCK activity [11]. Furthermore, studies of heterotypic collisions between NIH3T3 and chicken heart fibroblasts further showed that Rac1 and RhoA are required for a normal CIL response. These studies suggest that controlled remodelling of the actin cytoskeleton is required during CIL either for enabling cells to repolarise or for stopping them

to migrate forward upon contact with another cell. However, there is still no clear mechanism on how the actin cytoskeleton and it's associated proteins give rise to the observed repolarisation and migration away from the cell-cell contact site during CIL. Investigating cell repolarisation, Mayor and colleagues proposed that as the cells come in contact, they stop polymerising new actin around the site of cell-cell contact and instead begin generating new protrusions in other directions which eventually leads to cell repolarisation [142, 20, 140, 16, 146]. The generation of new protrusions away from the site of cell-cell contact while the cells are still in contact could act as a tension generation mechanism directly contributing to the breaking of the cadherin-mediated cell-cell junction leading to the subsequent separation of the colliding cells [137]. Furthermore, Abercrombie envisioned a mechanical explanation of how cells are capable of migrating away from each other during CIL whereby the tension developed within the actin cytoskeleton is the main driver of the response. In his words, "As a result of the adhesion between them, they push or pull against each other to some extent; some of the energy which would normally go into movement is thereby dissipated or becomes potential energy of elastic tension between the cells [...]. When an adhesion breaks, the release of potential energy stored as elastic tension produces the observed sudden acceleration" [9].

The final step of the contact inhibition response is cell repolarisation. Even if this is a very active research topic in the contact inhibition community, there is still no clear understanding of what causes colliding cells to repolarise. Recent investigations into CIL revealed that microtubules are undergoing tremendous reorganisation during CIL. Studies of rat kidney epithelial cells were one of the first to show that microtubules are remodelled away from the contact site as the cells were colliding [147]. Furthermore, studies of collision between chick heart fibroblasts where Glu MTs were stabilised such that they did not undergo any catastrophe events during the response showed that in order for colliding cells to separate, they need to maintain an unstable microtubule cytoskeleton [11]. Additionally, *in vivo* studies of *Drosophila* hemocytes revealed that microtubules are playing a role during CIL because overexpression of a microtubule severing protein (spastin) or losing the ability

to stabilise microtubules disrupted the contact inhibition process as hemocytes were not able to separate [12]. Therefore, remodelling of the microtubule cytoskeleton alongside with the remodelling of the actin cytoskeleton plays an important role in a normal CIL response. However, it is still unclear how the remodelling of microtubules upon cell-cell contact relates to the subsequent cell separation and repolarisation events. I believe that for a full understanding of the mechanisms behind CIL, an integrated study needs to be conducted where the interaction between cell-cell adhesion, actin cytoskeleton, and microtubules is addressed.

2.2.3 The role of contact inhibition *in vivo*

In 2008 Carmona-Fontaine and colleagues reported, for the first time in a living organism, that CIL is required for the normal developmental migration of Xenopus and Zebrafish neural crest cells (Figure 2.6A) [4]. These cells are capable of differentiating into a diverse range of cell types, e.g. craniofacial cartilage, smooth muscle, peripheral and enteric neurones and glia [148]. Recently, it was suggested that contact inhibition plays a crucial role in enhancing *in vivo* neural crest dispersal [4]. Furthermore, there is some evidence that when neural crest cells collide with other cell types, they fail to contact inhibit which allows them to migrate throughout the embryo and invade various tissues where they will differentiate into a host of cell type [149]. This intriguing behaviour resembles malignant invasion [150, 151]. Using a discrete computer model where changes in polarity are converted into directional changes, Woods and collegues successfully replicated the collective cell migration of neural crest cells [152]. In their simulation, cells were allowed to both repel following a collision and experience co-attraction from other cells in the population. Inhibiting co-attraction in the simulation was sufficient to recreate the neural crest behaviours observed *in vivo* where restriction of co-attraction lead to an invasive phenomenon. Interestingly, these simulations suggested that guidance of neural crest migration stems from the interplay between contact inhibition and co-attraction [152].

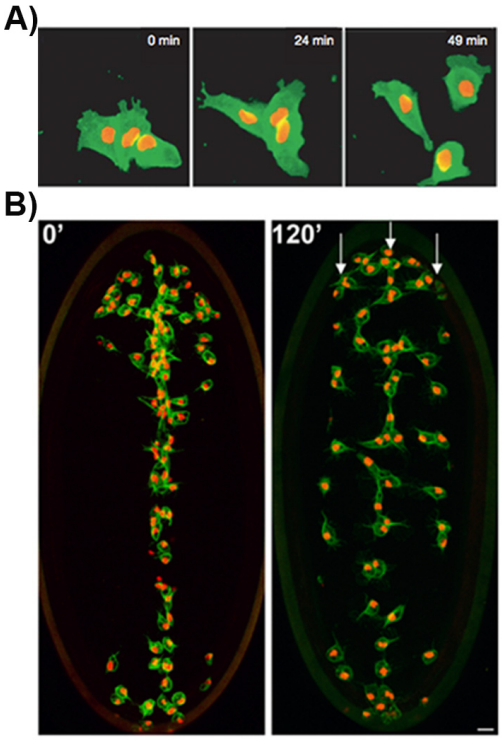

Figure 2.6: Contact inhibition of locomotion both *in vitro* and *in vivo*. A. Time-lapse movie of Zebra fish neural crest cells undergoing contact inhibition [4]. B. *Drosophila* hemocytes containing a red nuclear marker and a GFP microtubule label (green). Note how contact inhibition drives the cells into a three rows pattern. Scale bar = 10 μm [5]

Stramer and colleagues identified another model system for contact inhibition in the embryonic migration of *Drosphila* macrophages (hemocytes) (Figure 2.6B) [12]. These highly migratory cells are very similar to mammalian macrophages, playing an important role in the fly immune response [153]. Additionally, hemocytes are the main producers of extracellular matrix during development. Their primary role is to produce and secrete the majority of proteins required for the development of basement membranes [154].

Hemocyte embryonic dispersal differs significantly from the neural crest cells. They develop from the head mesoderm and disperse throughout the *Drosophila* embryo taking defined migratory routes [154]. One of these routes occurs along the ventral surface where their superficial position in the embryo allows them to be imaged live at a very high spatial and temporal resolution [12, 155, 25]. Time-lapse imaging has revealed that hemocytes spread out to form an even distribution pattern

throughout the entire ventral surface within a thin acellular cavity (the hemocoel) [12, 5].

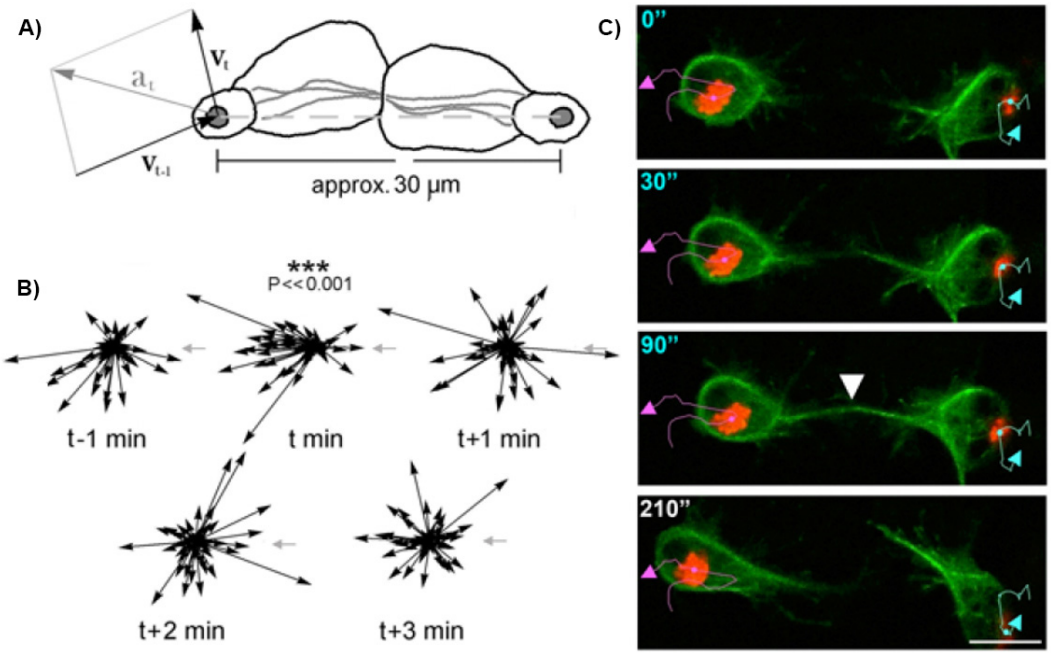

Figure 2.7: *In vivo* tracking of *Drosophila* hemocytes during contact inhibition of locomotion. A) Sketch of two colliding hemocytes at the moment of microtubule alignment (time t). The distance between nuclei upon the collision response was measured to be $30.0 \pm 5.2 \mu m$. B) Five samples of the acceleration vectors surrounding a collision (labeled as *t min* in the figure) from times t-1 to t+3 min oriented so that the target cell is directly on the right as in 2.7A. C) Stills from a time-lapse movie of a hemocyte collision pair. Note the microtubule bundles marker for contact inhibition (arrowhead). Scale bar = 10 μm [5]

.

Time-lapse movies of hemocyte developmental migration showed that almost all frontal collisions were a contact inhibition event where hemocytes stopped their forward movement and very quickly repolarised and migrated away from each other. By expression of fluorescent actin and microtubule probes to examine cytoskeletal dynamics in both freely moving and colliding *Drosophila* hemocytes revealed a large actin-rich lamella, which contains many dynamic microtubule filaments similar to culture cells (Figure 2.7A and Figure 2.7C) [12]. The dynamics of the microtubule cytoskeleton appeared to alter when two cells collide; as cells were coming in contact, a transient bundling and subsequent alignment of dynamic microtubule arms occurred. At the end of this alignment, hemocytes reversed their

direction of movement and migrated away from the collision [12, 5]. Subsequent statistical analysis of this response revealed that, although not fully understood how, the microtubule alignment can be used as an accurate fiduciary marker of a collision [5]. Analysis of cell acceleration including data from one minute prior and after the collision event revealed that upon collision, hemocyte acceleration suddenly changed from a random distribution to pointing away from the colliding partner (Figure 2.7B) suggesting that the presence of the other cell is directly contributing to cessation of movement in the direction of the colliding partner characteristic of the CIL response.

Davis and collegues simulated the migratory pattern and spacing of hemocytes along the ventral surface of the embryo using the kinematics of free running and colliding cells [5]. The model was build using the observed kinematic changes during CIL, and as such it could not be exploited to give any insights into what drives these changes *in vivo*. Nevertheless, successive computer simulations of their model with variable parameters suggested that CIL is required for an even dispersal pattern to emerge [5]. Hemocytes are highly dynamic motile cells that perform a wide variety of roles during embryogenesis. There is some evidence suggesting that hemocytes are capable of turning CIL on or off when they are recruited for wound healing [12] which raises the question what is the connection between hemocytes functions and contact inhibition?

Chapter 3

Materials and Methods

3.1 Fly genetics

All work related to fly genetics was carried out by our collaborators, Dr. John Robert Davis and Dr. Brian Stramer, at King's College London. For this work labeled wild-type, UAS-Dia-CA, zip^1, and dia^5 mutant hemocytes (Bloomington Stock Center) using the following promoters: *Srp*-Gal4 or *Sn*-Gal4 were used. Furthermore, all the crosses with the dia^5 mutant were kept at 25°C as this mutation was reported to be temperature sensitive [156]. Additionally, to visualise cell nuclei or different parts of the cytoskeleton several fluorescent probes were used as summarised in Table 3.1 below.

Labelled component	**Fluorescent probe**	**Source and/or reference**
Nuclei	UAS-RedStinger	N/A
Microtubules	UAS-Clip-GFP; UAS-Clip-Cherry	[12]
Actin	UAS-Lifeact-GFP; UAS-Moesin-Cherry	N/A
Diaphanous	UAS-GFP-Dia	[156]
Myosin II heavy chain	UAS-GFP-Zip	[157]
Zyxin	UAS-Zyxin-Cherry	Bloomington Stock Center

Table 3.1: Fluorescent labels for visualising cell nuclei and cytoskeleton components.

3.2 Particle Kinematics in 2D

When analysing a mechanical system about which we do not not have any information, we usually begin by investigating the movement of the system as a whole. A special case of this is when the system can be divised in several, even infinite, parts (*i.e.* discretised) such that the relative motion of it's components can then be studied. This analysis, does not make any assumptions about the rules or mechanisms generating the observed movement of the system. As a consequence, we can approximate the components of the system that we are interested in studying as material points, or particles (*i.e.* geometric points) that may or may not interact with each other or external factors. In other words, using this abstraction we ignore any additional information about the constitution of the system and consider that all of it's mass and information is concentrated at a set of discrete points, usually the centres of mass of each constitutive part we chosed. However, that is not the only available choice; you can choose any internal or external points to abstract the system under scrutiny, as long as they are representative for the observed motion [158, 159]. In fact, there are situations when the centre of mass might not be the best descriptor for the movement and cell biology offers numerous examples for this, especially for cells that are rapidly changing their shape as they migrate. Therefore, great care has to be taken in discretising the system before proceeding with any of the subsequent analysis of it's motion.

Once an adequate reference point has been selected within a given reference frame, we can start to describe the changes that take place in motion by analysing two quantities: velocity, $\vec{v}$, and acceleration, $\vec{a}$. Analysis of these two vector quantities is sufficient for describing the movement of any particle, without having any information about the forces causing it [158, 159]. Nevertheless, by inspecting these two quantities in both space and time, we are able to formulate and test hypotheses about the causes of any instantaneous disturbances to the otherwise uniform motion of the system [126].

The first step before commencing any kinematic study, is to select an adequate coordinate system. In the case of a particle moving on an arbitrary plane, the most

convenient choice is to use Cartesian coordinates, defined by any two mutually perpendicular unit vectors, $\{\vec{i},\vec{j}\}$, with an origin placed arbitrarily in the XY plane. In this frame of reference, the position of a particle can then be represented by it's position vector defined as $\vec{r} = x\vec{i} + y\vec{j}$ (Figure 3.1A). Using the coordinate system I just introduced, we now derive suitable mathematical expressions for velocity and acceleration vectors.

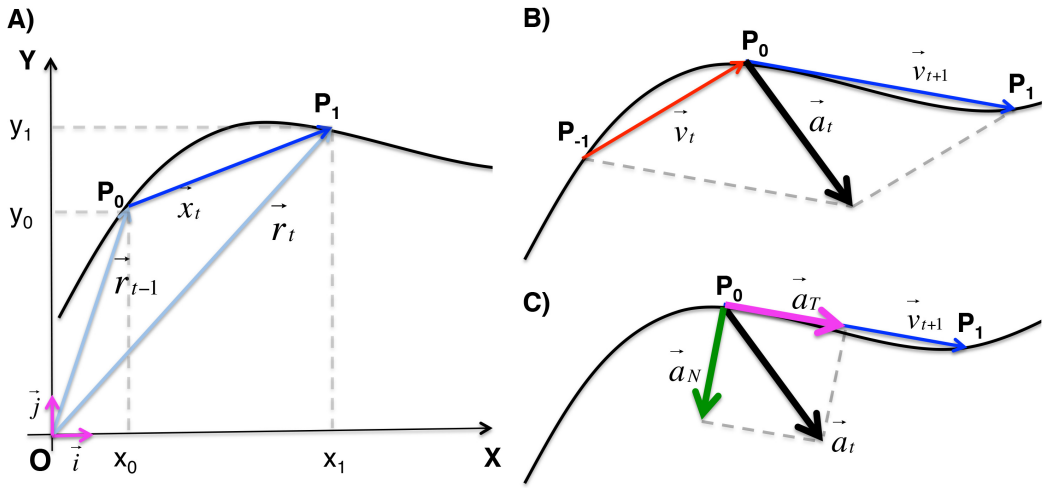

Figure 3.1: Particle kinematics in 2D. A) Schematic of a particle moving along an arbitrary trajectory. Light blue arrows represent the position vectors of the particle with respect to the chosen origin of the coordinate system, O, at two successive time points, P_0 and P_1. The two magenta arrows represent the unit vectors (*i.e.* direction) of each coordinate axis. Note that using Cartesian coordinates, the location of the particle at each time can be summarised by it's position along each coordinate axis, OX and OY. Furthermore, by subtracting the two position vectors you obtain the displacement of the particle over that time interval (blue arrow). B) Schematic of a particle moving along an arbitrary path. Blue arrow represents the average velocity vector between $t-1$ and t and red arrow represents the average velocity vector between t and $t+1$. Note that both these vectors are an approximation of the instantaneous velocity of the particle. Black arrow represents the acceleration of the particle at time t. Note that the acceleration vector represents the vector difference between $\vec{v}_t$ and $\vec{v}_{t-1}$. Furthermore, this acceleration is also a discrete approximation of the acceleration of the particle between $[t-1, t+1]$ interval. C) Decomposition of instantaneous acceleration (black arrow) into tangential (magenta arrow) and normal component (green arrow). Note that the tangential component is a good measure of the particle's behaviour in the direction of travel (blue arrow), while the normal component is measuring the rate at which the particle is changing direction.

The velocity of a particle is defined as the rate of change of displacement over a fixed interval of time using Equation 3.1 (Figure 3.1B)). For example, assuming

that a particle that at time t_{-1} is at P_{-1} moves to point be P_0 at time t_0, then the velocity of the particle as it moves between these two position is defined as:

$$\vec{v} = \lim_{\Delta t \to 0} \frac{\Delta \vec{x}}{\Delta t} = \frac{d\vec{x}}{dt}, \tag{3.1}$$

where $\vec{x} = \vec{r}_{t_0} - \vec{r}_{t_{-1}}$ and $\Delta t = t_0 - t_{-1}$ is the time between the two positions at which the particle is observed. Equation 3.1 defines velocity as the instantaneous rate of change of the particle's displacement. From this it can be concluded that the velocity vector contains information about the direction in which the particle is moving, and how fast it is moving in that direction.

In practice, however, it is impossible to measure the position of the particle with such infinitesimal precision, which leads to an approximation of the instantaneous velocity by an average velocity over the time between two subsequent observations. Therefore, for all practical purposes, Equation 3.1 can be approximated by:

$$\vec{v} = \frac{\vec{r}_t - \vec{r}_{t-1}}{t_0 - t_{-1}} = \frac{\Delta \vec{x}}{\Delta t} \tag{3.2}$$

In contrast to the continuous formulation of the velocity, when Equation 3.1 is used it is important to accurately control for Δt as value too small or too big would introduce spurious measurements [126]. Using the movement of a cell as an example, what this means is if Δt is very small, then the cell will probably be stationary for a very large number of times and when it will finally appear that it was moving it will look like it suddenly jumped from one location to the next.

Although velocity is a very good indicator of the particle's movement, it is not able to distinguish if changes in movement are caused by internal or external factors. In practice, most interesting systems involve either heterogeneous environment or fast changes in motion which means that another measure is needed to characterise the movement of particles. For these systems, acceleration vectors are a much suitable measure for quantifying motion.

The acceleration vector is defined as the instantaneous rate of change in velocity (Figure 3.1B). Mathematically, this can be written as:

$$\vec{a} = \lim_{\Delta t \to 0} \frac{\Delta \vec{v}}{\Delta t} = \frac{d\vec{v}}{dt} \tag{3.3}$$

As with velocity, Equation 3.3 relies on the continuous assumption where the time interval, dt is taken to be infinitesimally small. However, we saw before that infinitesimal time intervals are just a theoretical construct, very challenging to realise experimentally. As a consequence, in practice, instantaneous acceleration is computed as a discrete approximation by calculating the change in velocity as the particle moves from position P_{-1} to position P_1 in the time interval $[t_0, t_1]$:

$$\vec{a} = \frac{\vec{v}_t - \vec{v}_{t-1}}{t_0 - t_{-1}} = \frac{\Delta \vec{v}}{\Delta t} \tag{3.4}$$

Now that acceleration is defined, it is important to uncover what information it can convey about the system. By rewriting Equation 3.3 as Equation 3.5 it is possible to split the acceleration into a component that is tangent to the direction of movement, $\vec{a}_T$, and a component perpendicular to this direction, $\vec{a}_N$ (Figure 3.1C). Following from this decomposition, see that inspecting the acceleration of a particle reveals if the particle's speed is either increasing (positive acceleration) or decreasing (negative acceleration) (Figure 3.1C). Note that zero tangential acceleration does not necessarily imply that the particle is at rest; in most cases zero acceleration vector means that the particle is moving at constant speed in the direction of motion. Furthermore, from the diagram and Equation 3.5 we can conclude that the tangential acceleration represents the instantaneous change in speed with respect to time of the particle (Figure 3.1C). To have complete information about the changes in the motion of a particle, we also need to consider it's acceleration perpendicular to the direction of travel. As it turns out, this acceleration component is a very good measure of the rate of change of the direction of travel with respect to time, scaled by the speed at which the particle is moving (Figure 3.1C)).

$$\vec{a} = \vec{a}_T + \vec{a}_N \tag{3.5a}$$

$$= \frac{|\vec{v}|}{dt} + \frac{d\theta}{dt}|\vec{v}| \tag{3.5b}$$

where $\theta = \theta(t)$ is the direction of travel as a function of time of the particle.

In conclusion, observing the velocity of a particle over time is a good estimate for its motion. However, velocity alone is not informative for any rates of change of motion. A more appropriate measure for changes in motion is the particle's acceleration as this quantifies both internal and external factors that affect the motion of a particle.

3.3 Vector Components

In Section 3.2 we saw that once a coordinate system and an origin are chosen, we can start to pair a position vector with every point in space.

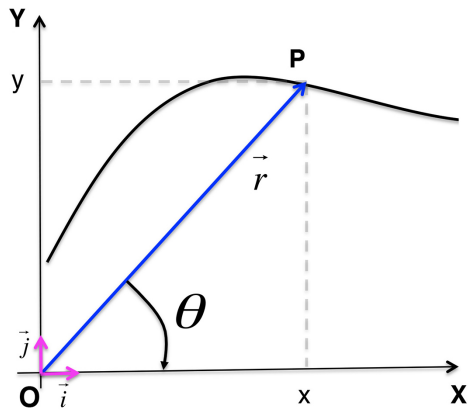

Figure 3.2: Decomposition of vectors in 2D. Example of a position vector (blue arrow) for a particle moving along a 2D path (black curve). Note magenta arrows show unit vectors for each of the coordinate axis and θ indicates the direction of the particle.

In addition to representing a vector by it's components along each dimension of space, they are often represented using their magnitude and direction. Mathematically, any $2D$ vector $\vec{v} = x\vec{i} + y\vec{j}$ can also be represented using the vector's

magnitude, $|\vec{v}|$ and one angle for direction, θ, as [158]:

$$\vec{v} = |\vec{v}|\,(\cos\theta, \sin\theta)^T \tag{3.6}$$

For the purpose of this work, θ was defined as the angle between the OX axis and the projection of the vector in the XY plane [158] (Figure 3.2).

$$|\vec{v}| = \sqrt{x^2 + y^2} \tag{3.7a}$$

$$\theta = \tan^{-1}\frac{y}{x} \tag{3.7b}$$

3.4 Homogeneous Coordinates

A very practical representation of points in space is to use homogeneous coordinates. In this new coordinates system, a point $P_0 = (x, y, z)^T$ will be identified with $P_0 = (x, y, z, W)^T$, where x, y, z, W cannot all be zero at the same time. Furthermore, coordinates $(x/W, y/W, z/W, 1)^T$ represent the same point in homogeneous coordinates [160]. In this work I made extensive use of this property of homogeneous coordinates and represented all coordinates as $(x, y, z, 1)^T$.

The main advantage of homogeneous coordinates is that they can be used to compose complex transformations from more basic ones, such as translation, rotation or scaling, into a single operation. Furthermore, a 2D system can easily be represented using the same formulation by setting the z-coordinate to 0 [160].

Using this new coordinates system, the mathematical formulation of translation from a fixed reference point is given in Equation 3.8 below.

$$T(d_x, d_y, d_z) = \begin{bmatrix} 1 & 0 & 0 & d_x \\ 0 & 1 & 0 & d_y \\ 0 & 0 & 1 & d_z \\ 0 & 0 & 0 & 1 \end{bmatrix} \tag{3.8}$$

where d_x, d_y, and d_z represent the amount by which point P is translated. Furthermore, the rotation about each of the axis of the coordinate systems by an angle

θ are given by R_x, R_y, R_z respectively:

$$R_x(\theta) = \begin{bmatrix} 1 & 0 & 0 & 0 \\ \cos\theta & \sin\theta & 0 & 0 \\ -\sin\theta & \cos\theta & 0 & 0 \\ 0 & 0 & 0 & 1 \end{bmatrix} \tag{3.9}$$

$$R_y(\theta) = \begin{bmatrix} \cos\theta & 0 & \sin\theta & 0 \\ 0 & 1 & 0 & 0 \\ -\sin\theta & 0 & \cos\theta & 0 \\ 0 & 0 & 0 & 1 \end{bmatrix} \tag{3.10}$$

$$R_z(\theta) = \begin{bmatrix} \cos\theta & \sin\theta & 0 & 0 \\ -\sin\theta & \cos\theta & 0 & 0 \\ 0 & 0 & 1 & 0 \\ 0 & 0 & 0 & 1 \end{bmatrix} \tag{3.11}$$

Using the above definitions for translation and rotation matrices, multiple geometric transformations can easily be combined into a single mapping obtained by multiplying together the basic transform required in the reverse order in which they are applied [160]. In other words, a rotation about the origin through an angle α of a point $P = (x, y, z, 1)^T$ can be achieved by the following transformation:

$$P' = [T(x, y, z) \times R(\alpha) \times T(-x, -y - z)] \times P \tag{3.12}$$

3.5 Vector Statistics

A very powerful test for randomness of a vector sample is to check if the components of the resultant vector are significantly different from zero. To this aim, I apply a two tailed T-Test to each component of the resultant vector [126, 10]. The power of this approach stems from the fact that it allows to also check for randomness of each vector component which then could be used to make inferences about changes in cell movement along specific directions.

Sections 3.2, 3.3, and 3.4 introduced three alternative ways of representing a vector. All these representations are equivalent, and which one you choose to use depends on the hypothesis that are formulated.

Regardless of which mathematical representation is chosen to represent a vector, it is useful to treat the respective vector components as random variables of time and/or space. This formulation opens up a wide range of statistical tools, that we can use to investigate various hypotheses about a population of vectors. For example, it is a well known fact that a population of random vectors will have a resultant very close to zero. Therefore, any resultant vector that is significantly different from zero is clearly an indicator that the process generating it is not a random process [126].

To compute the average direction of a sample of vectors, special consideration has to be given to the direction of a vector, as it is a periodic random variable, of period 2π. Because of this periodicity, circular statistics have to be employed for computing statistical quantities for direction. To quantify the average direction of velocity and acceleration vectors for a population of cells at each time point, is equivalent to finding the resultant vector with respect to some predefined reference [161, 162]. In this work, the reference direction was chosen as 0 radians, except otherwise specified.

$$\vec{x}_0 = \frac{1}{N}\sum_{j=1}^{N}\vec{x}_i, \tag{3.13}$$

where N is the number of vectors in the sample.

The average direction can also be represented using Equation 3.6 or by it's $\{x, y, z\}$ components, depending on the hypothesis that is being investigated. The advantage of treating vectors as circular data is that it is easier to assess the clustering of the data around the mean direction by inspecting the magnitude of $\vec{x}_0$. This is possible because a value of $\bar{R} = |\vec{x}_0|$ close to 0 means that the vectors are widely dispersed about the mean direction. In contrast, a value of $\bar{R}$ close to 1 means that heavily concentrated around the mean direction [162].

It is important to note that the method introduced above is applicable only to uni-modal distributions. If the vectors are pulled from a bi-modal distribution, i.e.

half of the vectors are forward and half of them are pointing backwards, then a different test for significance has to be used. In these situations one can divide the unit circle into equal sectors and test the significance of the vectors in each sector.

3.6 Quantification of cellular kinematics

3.6.1 Cell Speed and Acceleration Analysis (CSPACC) platform

CSPACC is an user friendly statistical platform in Matlab [163] that I developed for computing, summarising, and testing various hypotheses about cell velocity and acceleration for cells migrating in both 2D and 3D environments. This platform allows the user to identify instantaneous changes in cell kinematics (see section 3.2 for further details), and to describe and/or compare movement of different cell populations. In the current implementation acceleration and velocity vectors are treated as random variable generated by an unknown distribution. Internally, vectors are represented as either a doublet of components (v_x, v_y) or by their magnitude and direction, θ, which makes it possible to compute any statistical descriptors for the gross migration of the observed cells that are adequate for the problem at hand.

The current version of the code does not rely on very specialised Matlab packages which makes it accessible for anyone having a basic Matlab version. The only dependencies for CSPACC are CircStats2D (an open source circular statistics Matlab package for 2D data [164]).

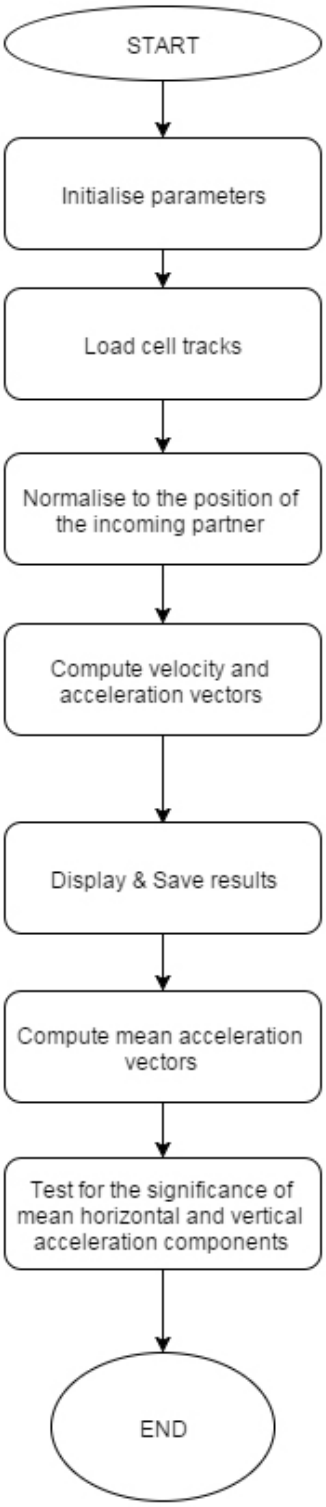

Figure 3.3: Flowchart summarising CSPACC algorithm. Example analysis used to quantify hemocyte kinematics during CIL.

3.6.2 Normalisation of cell tracks with respect to the position of the colliding partner in 2D

To test various hypotheses about the behaviour of cells, velocity and acceleration vectors, which are fundamental measures of cell kinematics (see section 3.2), can be normalised to any reference point that is relevant for the question. Normalising cellular trajectories prior to determining velocity and acceleration vectors is required due to the random nature of cell movement.

For studying CIL and other cellular collisions in general, it is important to understand how colliding partners affect each others behaviour. Furthermore, for the kinematics analysis conducted in this work, a collision is recorded as the moment when the two microtubule bundles are aligned, as this has been showed to be a good temporal registrar of collisions [5]. To investigate how colliding partners influence each other I implemented a normalisation procedure where cell position is transformed such that the two interacting cells are always facing each other. Using this normalisation it is possible to investigate if the interaction is actively contributing to cells slowing down (i.e. if the resultant x-component of the acceleration is significantly different from zero) as opposed to passively avoiding each other (i.e. if resultant of the other acceleration components is not significantly different from zero). Within this framework, the centre of the coordinates system is chosen as an arbitrary $(0, 0)$ point corresponding to the zero-point of the frames from which cells are tracked. This is usually the upper-left corner of the frame. Furthermore, each cell is tracked using the centroid of the nucleus, therefore, the coordinates of each cell are abstracted to the coordinates of the nucleus.

Mathematically, normalising cell tracks with respect to the position of the colliding partner is equivalent to connecting the two colliding cells by a vector and then making this vector parallel to the OX axis. To achieve this, first I convert cell position from Cartesian to homogeneous coordinates and subsequently create the normalisation matrix by combining a translation with a rotation about the origin of the coordinate system (see section 3.4 for more details on homogeneous coordinates and transformation matrices). Note that this transformation will be applied to pairs

of three consecutive time points, because computation of cell acceleration requires the velocity at previous and current time points (see section 3.2).

To determine the transformation matrix for the 2-tuple, I translate the points A_0 and B_0 by a translation matrix $T(-x_0, -y_0)$ (Fig. 3.4A). Following this transformation, I compute the angle, θ, between the vector $\vec{A_0B_0}$ and the OX axis (Fig. 3.4B) and then construct the rotation matrix about the origin O as $R_z(\theta)$. Finally, the transformation matrix is computed as:

$$M(-x_0, -y_0, \theta) = T(-x_0, -y_0) \times R_z(\theta) \tag{3.14}$$

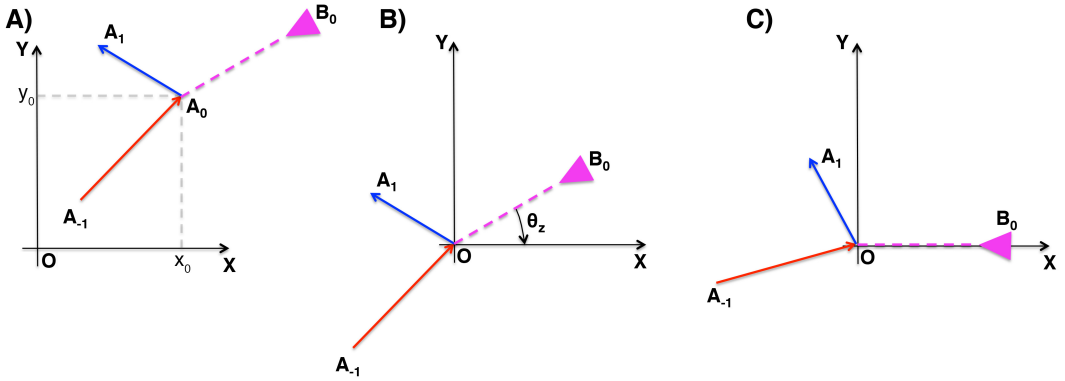

Figure 3.4: Schematic with the normalisation with respect to the position of the interacting cell in $2D$. Hypothetical representation of a colliding pair where one cell moves from A_{-1} to A_1, going through $\vec{A_{-1}A_0}$ (red arrow) and $\vec{A_0A_1}$ (blue arrow). Note that when the cell is at $A_0 = (x_0, y_0, z_0)$ while it's colliding partner is at B_0 (magenta arrow head). B) The origin of the coordinate system is translated to A_0 in order to obtain the angle of rotation, θ, about OZ by which the points are rotated to place the new position vector of the colliding partner, $\vec{A_0B_0}$ (magenta dotted line) in the XZ plane. C) Final configuration of the system with the two colliding cells facing each other along the OX axis. Note that the points are rotated accordingly to preserve the relative distances and orientations of the points.

The transformation in Equation 3.14 is then applied to points A_{-1} and A_1 independently. At this stage, the cells are arranged such that the two colliding partners are parallel to the OX axis, facing each other (Fig. 3.4C). Note that this transformation ensures that the distances between the three consecutive time points and their relative orientation are preserved after the normalisation [160].

3.6.3 Statistical analysis of hemocyte kinematics

To determine the significance of the tangential and normal acceleration components, we performed a one-sample t-test on our sample of colliding cells ($n = 20$ colliding cells). Furthermore, a binomial test was performed on the unit vectors of the cell velocities to determine if cells are migrating away from the collisions (after their lamella broke contact)($n = 20$ for both control and dia^5 mutant hemocytes). Any left or right biases are eliminated by mapping the direction of travel to the interval $[-\pi/2, \pi/2]$, with $-\pi/2$ representing that cells are migrating in opposite directions and $\pi/2$ means that cells are going towards each other (Figure 3.5). Finally a binomial test was also performed to assess if hemocytes the statistical significance of the direction in which hemocytes migrate [165].

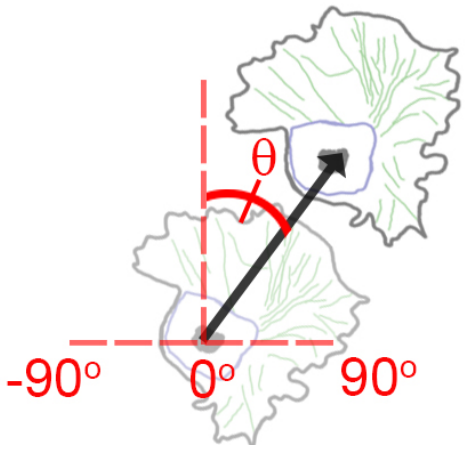

Figure 3.5: Schematic highlighting the method used to map the direction of travel to the interval $[-\pi/2, \pi/2]$**.** Figure recreated from [6].

To quantify the duration of collisions, the time between lamella and microtubule alignment, and between microtubule alignment and lamellae separation was measured for control and mutant hemocytes. To assess if there are any differences between control and mutant hemocytes a two-sample t-test was also performed ($n = 11$ for control collisions, $n = 5$ for zip^1 and $n = 11$ for dia^5 collisions).

To determine the cessation of forward movement during CIL, the ratio between the distance between nuclei and initial point of contact, D_t, and at the time of cell separation, $D_{t+\Delta t}$ was computed (Figure 3.6). A ratio of 1 means that cells continue to move towards each other, while a ratio greater than 1 would suggest hemocytes

started to migrate away prior to lamellar separation. The significance of this ratio was assessed using a two-sample t-test with Welchś correction for $n = 8$ control, $n = 5$ *zip*^{1}, and $n = 7$ *dia*^{5} hemocytes.

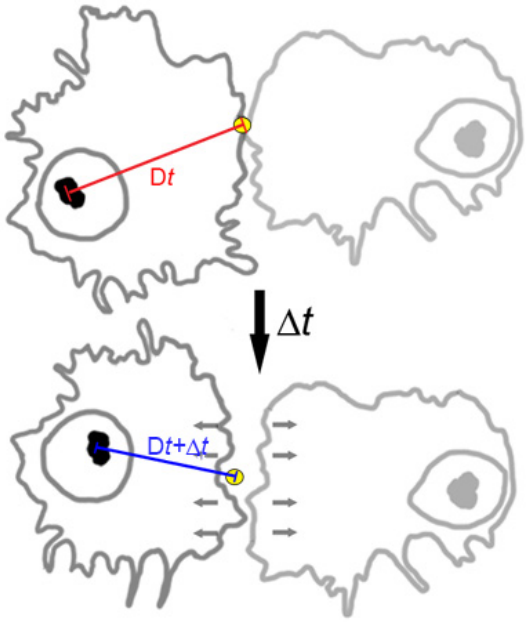

Figure 3.6: Schematic summarising the assay used to determine the cessation of forward motion during CIL. Note that D_t represents the distance between the nucleus and the site of cell contact. Figure recreated from [6].

3.7 Quantification of Hemocyte Dispersal

To measure the patterning dynamics of control and *dia*^{5} hemocytes cells were labelled with UAS-LifeAct-GFP and UAS-RedStinger and then imaged them for 90 minutes. The average position of hemocytes throughout the duration of the dispersal process was quantified from binary time-lapse images as described in [5]. Furthermore, hemocyte dispersion was measured by the nearest neighbour distance at stage 16 of the development and a Mann-Whitney test was performed to assess the statistical significance for both control and *dia*^{5} embryos ($n = 324$ cells from 9 control embryos and $n = 309$ cells from 9 *dia*^{5} embryos).

Hemocyte migration dynamics were characterised by automatically tracking their movement for 20 minutes in control and *dia*^{5} embryos, respectively. To quantify their wandering nature, the maximum distance they travelled from the starting

position was computed. A Mann-Whitney test was used to test if there were any significant differences between the two genotypes ($n = 48$ embryos for each genotype).

An alternative characterisation of migration of control and *dia*^{5} mutant hemocytes was performed by measuring the mean cell displacement was used to compute cell speed at 1 minute intervals ($n = 20$ cells for both genotypes) and the directional ratio over 6 minute period (the longest time hemocytes migrated for before colliding), at minute intervals ($n = 8$ cells for both genotypes).

3.7.1 Simulations of Hemocyte patterning

Hemocyte dispersal was modelled by our collaborators, Dr. John Robert Davis and Prof. Graham A. Dunn, at King's College London using the 2D kinematic model described in [5] where the collision sensitivity, ψ, was allowed to have any value between $[0, 1.25]$. By allowing ψ to vary, the repulsion was randomised as cells were free to choose how much to take into account the direction of their colliding partners.

3.8 Microscopy and image analysis

3.8.1 Image acquisition

Embryos were mounted as previously described by [5] and time-lapse images acquired every 5 s (for retrograde flow analysis) or 10 s (for kinematic and co-localisation analyses) using a spinning disk microscope.

For the kinematic analysis, hemocytes were labelled with nuclear and microtubule markers and time-lapse images were acquired at 10 s/frame. Nuclei were automatically tracked using Volocity (PerkinElmer) software. Microtubule alignment was used as a marker of a CIL event, and cells that had not collided with another cell for 4 min before and after the microtubule alignment were included in the analysis.

Time-lapse of freely moving or colliding hemocytes containing actin labelled with either LifeAct-GFP or Moesin-Cherry were acquired at 5 s/frame (when imaging actin alone) or at 10 s/frame (when imaging actin with other fluorescent probes).

For collision analysis, cells were chosen such that the cells collided once over the duration of the time course. Furthermore, to increase the accuracy of the FLUPS analysis, cells were manually segmented. All the image acquisition and cell tracking was performed by Dr. John Robert Davis.

3.8.2 Stress fibre formation

To analyse the formation of the actin stress fibre coupling colliding cells, the mean intensity of UAS-LifeAct-GFP over the entire time course of a collision was measured in paired cells within $n = 4$ paired cells.

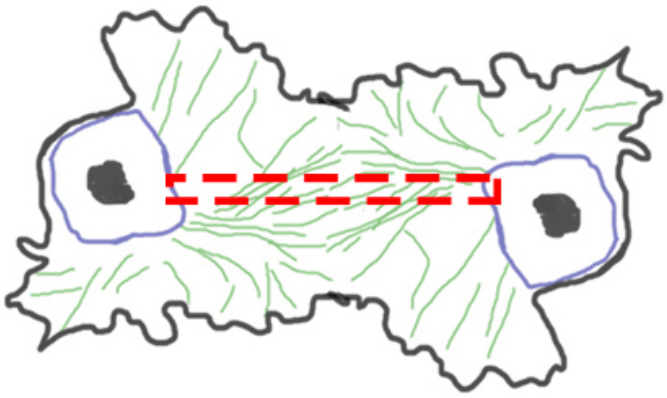

Figure 3.7: Schematic explaining the quantification of stress fibre coupling colliding cells. Red dotted rectangle represents the area over which the UAS-LifeAct-GFP intensity was measured. Figure recreated from [6].

To eliminate any variation in intensity caused by variable levels of fluorescence within different cells, the mean intensity was normalised to the average intensity within a region of $2.7 \times 23.4 \mu m$ which is representative for the area of the region spanned by the actin fibre across both cells (Figure 3.7).

To compare actin and Myosin II accumulation along the actin fibre during collisions the mean fluorescence intensity of UAS-GFP-Zip and UAS-LifeAct-GFP was measured within a region $2.7 \times 11.7 \mu m$ which corresponded to the size of the actin fibre within one colliding hemocyte (Figure 3.8) ($n = 4$ cells).

To investigate the fibre formation during CIL a region perpendicular to the site of initial cell cell contact measuring $8.1 \times 11.7 \mu m$ within the lamella of colliding cells was manually cropped. This region was further divided into 3 smaller rectan-

Figure 3.8: Schematic highlighting the area used to quantify actin and Myosin II fluorescent intensity during collisions. Figure recreated from [6].

gular regions, each measuring $2.7 \times 11.7 \mu m$. To quantify the fibre formation the ratio between the average fluorescence intensity of UAS-LifeAct-GFP within the central rectangular region (which contains the actin fibre) and the two adjacent regions at the time-point just before lamellae separation was computed (Figure 3.9). Finally a two-sample t-test was performed to test the significance of this ratio using $n = 10$ control, $n = 7$ for zip^1 and $n = 10$ for dia^5.

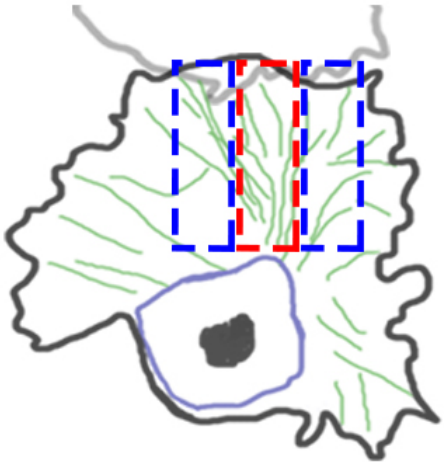

Figure 3.9: Schematic highlighting the regions of the lamellae used to quantify stress fibre formation. Figure recreated from [6]

To investigate the recruitment of actin fibres the central region of the lamella (corresponding to the corridor of low retrograde flow that develops during collisions) kymography of a region parallel to the site of cell-cell contact was performed.

This region was segmented from the lamella of one colliding partner, close to the cell body (3.10).

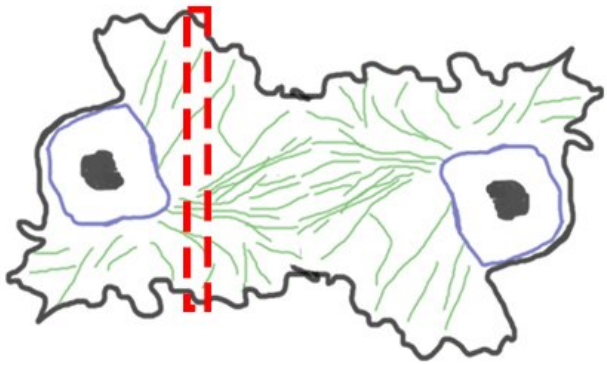

Figure 3.10: Quantification of actin fibres recruitment. Schematic highlighting the region used to quantify the recruitment of actin fibres from the periphery of the lamella to the region where the actin cable is developing. Figure recreated from [6]

3.8.3 Extension-retraction analysis

To analyse lamellar activity of either freely moving or colliding cells, binary time-lapse images as created by ImageJ were used. To highlight regions of lamellar activity consecutive frames were subtracted. Current frame was subtracted from previous one to obtain regions of lamellar retraction and current frame was subtracted from the subsequent one to obtain regions of lamellar extension.

Subsequently the area of the extension and retraction regions was measured, respectively. Because movies had different duration, each area of activity was normalised by the average activity over the length of the movie. This normalisation allowed for comparison between lamellar activity at the cell front versus rear. Furthermore, to investigate the formation of new protrusions versus cell separation, the area of the extension and retraction at the cell front and back was first measured and then normalised to the average extension or retraction area computed over the whole time course ($n = 8$ cells).

Kymographs of the region perpendicular to the leading edge in hemocytes expressing UAS-LifeAct-GFP were generated to quantify lamellar retraction rate. Subsequently the distance over time within 5 seconds intervals was measured to

quantify the average retraction rate over 3 minutes in freely moving cells and at the instantaneous retraction rate immediately after the time of cell separation. A two-sample t-test with Welch's correction was then used to test for the significance of the results for $n = 6$ control collisions and $n = 5$ control freely moving; $n = 6$ colliding zip^1 hemocytes, $n = 6$ zip^1 freely moving cells; $n = 8$ dia^5 colliding hemocytes and $n = 5$ freely moving dia^5 mutant cells.

3.8.4 Myosin II dynamics

To quantify the dynamics of Myosin II particles in freely moving cells Myosin II puncta labelled with UAS-GFP-Zip were manually tracked over a 40 seconds time interval. Subsequently their horizontal displacement was computed and a Mann-Whitney test was performed to test the significance of the results for $n = 72$ particles within freely moving cells and $n = 74$ particles within colliding hemocytes. .

3.9 Fluorescent pseudo-speckle microscopy (FLUPS)

Speckle microscopy has been used to measure lamellipodial actin retrograde flow and kinetics of actin polymerisation *in vitro* [90]. However, using true speckles to track the actin retrograde flow *in vivo* presents serious experimental challenges at the moment. Most importantly, it is very difficult to obtain the precise concentration of fluorescent actin required to get monomer resolution of the network because of the unknown concentration of free monomers inside the cytoskeleton of an *in vivo* cell. Therefore, correlative methods have to be employed to measure actin network dynamics *in vivo* [90, 85].

For the present work, the retrograde flow velocity was measured using fluorescence pseudospeckle (FLUPS) microscopy introduced by [7]. This method has been previously used to quantify the motion of the actin network in growth cones *in vitro*. FLUPS uses an adapted particle velocimetry approach based on 2D cross-correlation algorithms to compare a region of interest in an image (i.e. source image) with a subframe of a subsequent image (i.e. search image). To approximate the retrograde flow displacements, this algorithm tracks the motion of actin bundles and fluorescence intensity fluctuations within in the actin network [166].

For the movies used in this work, most of the prominent actin structures are about $1\mu m$, so FLUPS extracts squares of $1\mu m$ edge length separated by $0.5\mu m$ from the source image. The size of these squares limits the the resolution of FLUPS. Furthermore, the size of the search image is chosen such that it spans the maximum expected displacement of the actin structures during the acquisition time (in the present work a search image of approximately $2.5\mu m$ edge length is used for an acquisition rate of 5 s) (Figure 3.11).

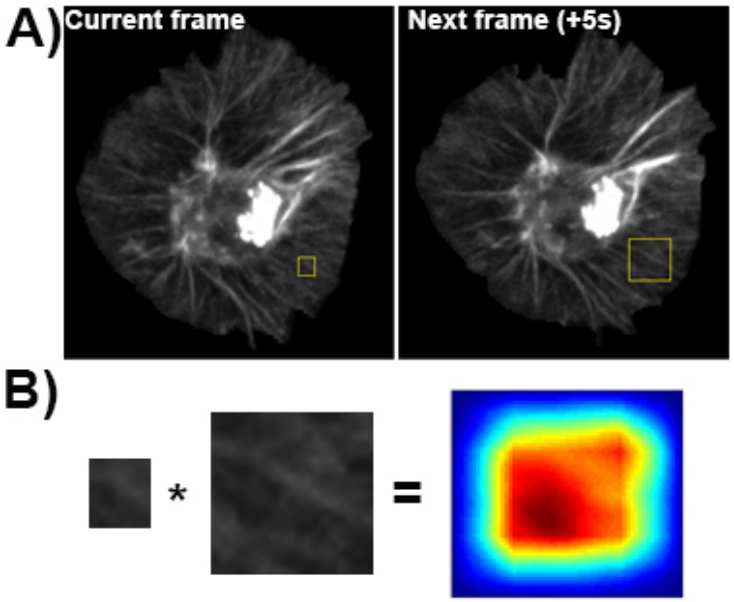

Figure 3.11: Example of a FLUPS cross-correlation map. A) Stills with a freely moving hemocyte the actin cytoskeleton was labelled using LifeAct-GFP. Note that yellow rectangle highlights an example source (left panel) and search area (right panel). B) Example of a cross-correlation map used to compute the displacement of the actin cytoskeleton over 5 seconds. Scale bar = $5\mu m$.

To compute the displacement of the actin network, a cross-correlation coefficient is computed using Equation 3.15 between the source image A and a subset of the search image B with equal size to A. To cover the whole search image, a different cross-correlation coefficient is computed between source image A and a sub-image of search image B shifted by 1 pixel. Once a cross-correlation map between a source and search image is obtained, the displacement of the actin network is determined by finding the maximum coefficient within this map. Finally, the algorithm (Figure 3.12) automatically stores the location of the source image, the

displacement and the cross-correlation values, which are used for post-processing of the results [166].

$$c = \frac{\sum_m \sum_n \left(A_{mn} - \bar{A}\right)\left(B_{mn} - \bar{B}\right)}{\sqrt{\left[\sum_m \sum_n \left(A_{mn} - \bar{A}\right)^2\right]\left[\sum_m \sum_n \left(B_{mn} - \bar{B}\right)^2\right]}}, \tag{3.15}$$

where c is the cross-correlation coefficient between images A and B, n, m are the position indices of each image point, and $\bar{A}$, $\bar{B}$ represent the average intensity of A and B, respectively. Note that c is already normalised to vary between -1 and 1, with -1 meaning complete anti-correlation, 0 no correlation, and 1 complete correlation.

FLUPS is a correlative method that imposes a vector field (flow displacements) on a pre-determined grid. Some of these values might represent false displacements of the actin network artificially introduced by the tracking algorithm. To remove these anomalous data, only displacements obtained with a cross-correlation coefficient above a certain threshold, c_0, are kept. The value of this threshold is determined based on the quality of the image being analysed. For the current work it is set to $c_0 = 0.5$. Because the retrograde flow has always been reported to be directed centripetally, from the leading edge towards the cell body, all vectors that point within $\pm 45^\circ$ were removed from the measurements (these vectors were usually introduced by edge artefacts). Finally, a spatial convolution with a Gaussian kernel with a variance of $1\mu m$ and temporal convolution with temporal kernel of 25 s were employed to interpolate the measured retrograde flow displacements to cover the pixels between grid points [166]. The spatio-temporal interpolation also ensures that the movement of larger structures, i.e. structures that cover more than one search image, is adequately captured. However, the algorithm needs to be used with caution as it can generate erroneous tracks if the movemement of these large structures is happening along a constant direction because the tracking will not be able to pick up any structural variation between consecutive frames. The complete algorithm for FLUPS, including the filtering and interpolation of measured retrograde flow displacements has been implemented in Matlab [163] (Figure 3.12).

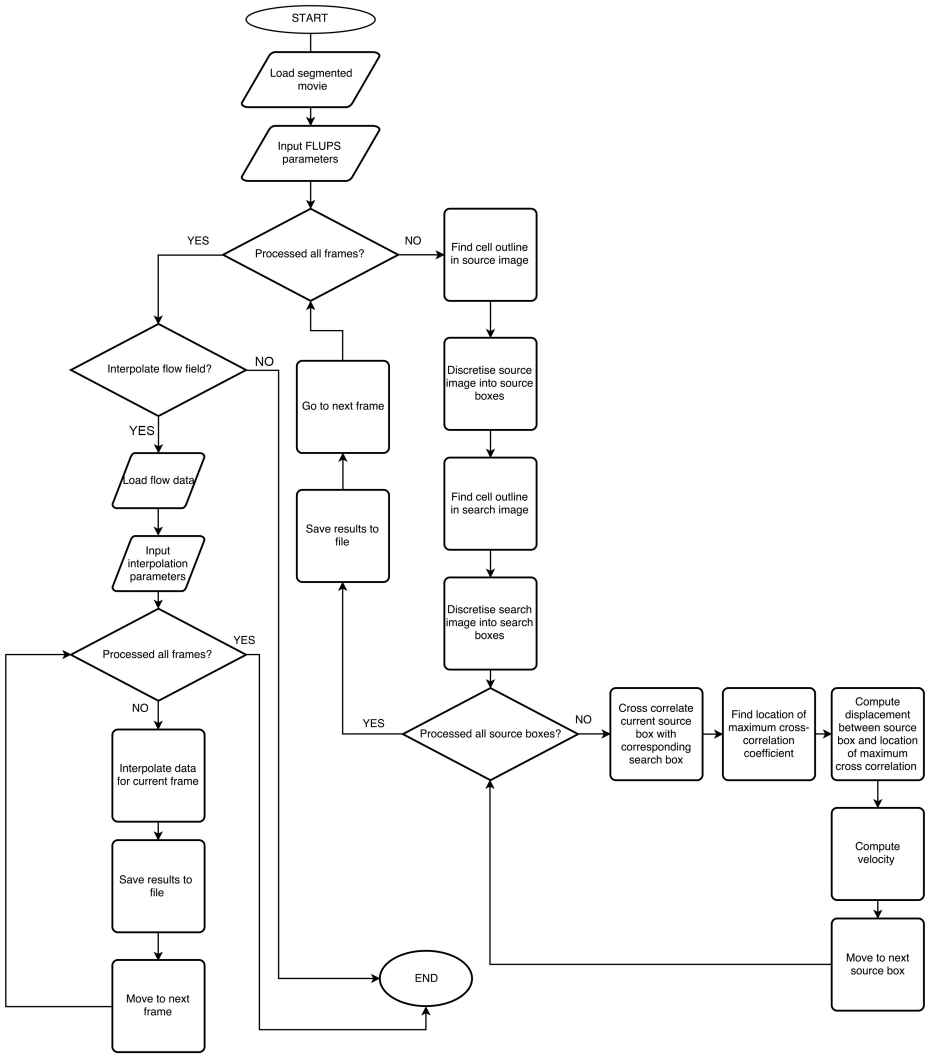

Figure 3.12: Flowchart describing the FLUPS algorithm.

3.9.1 Quantification of actin retrograde flow

To quantify retrograde flow rates in lamellae of freely moving cells, the cell body was manually segmented and data points within this region were discarded. To compare the flow rate in freely moving hemocytes, the mean flow speed within the lamella over a period of 3-4 minute in control, zip^1 mutant, dia^5 mutant and zip^1 rescued hemocytes ($n = 6,7,6,4$, respectively) and tested the statistical significance of the results using a two-sample t-test.

To compute the average change in flow speed and direction (Equations 3.16 and 3.17), only data from the region of the cell outline that was common between successive frames was used.

$$\Delta v_{ij}(t) = |\vec{v}(i,j,t+1)| - |\vec{v}(i,j,t)| \tag{3.16}$$

$$\Delta\theta_{ij}(t) = \tan^{-1}\frac{v_y(i,j,t+1)}{v_x(i,j,t+1)} - \tan^{-1}\frac{v_y(i,j,t)}{v_x(i,j,t)} \tag{3.17}$$

where $\vec{v}(i,j,t)$ represents the velocity of the retrograde flow at the location $(x = i\Delta x, y = j\Delta y)$ inside the cell at time t and (v_x, v_y) are the (x,y) components of the velocity, respectively.

This quantification has two main error sources. First, hemocytes are changing shape as they migrate which means that new regions of the lamella are constantly being extended or retracted. As a consequence, the above quantification will register a very large change in retrograde flow within those regions. To avoid this, only the area that was common between two successive frames was used for computations. Second, as the lamellae overlap, the resolution of the retrograde flow is lost. If the overlap region is too large it might bias the results introducing large artefactual changes in instantaneous flow speed and/or direction. To correct for this artefact, very large changes were discarded from future computations ($n = 4$ colliding pairs for control and *dia*^{5} mutant hemocytes).

3.9.2 Quantification of actin retrograde flow during collisions

To investigate the flow rates and changes in retrograde flow dynamics during collisions, I used a manually cropped rectangular region of $8.1 \times 11.7\mu m$, perpendicular to the site of initial cell contact, from the lamella of each colliding partner, similar to the one showed in Figure 3.8 ($n = 8$ for control and *dia*^{5} mutant hemocytes). When cropping, the area of lamellae overlap was carefully avoided as the pseudo-speckle algorithm was unable to differentiate the overlapped colliding actin networks.

I computed the cross-correlation between the instantaneous changes in flow speed and direction (Equations 3.18 and 3.19) within the cropped region to investigate the relationship between the flow rates across colliding partners.

$$cc_v = \sum_{i=-\infty}^{\infty} \Delta v^*{}_1[i]\Delta v_2[i+j] \tag{3.18}$$

where Δv_1, Δv_2 represent the changes in speed of the actin flow within each colliding partner, computed as in Equation 3.16 and $\Delta v^*{}_1$ is the complex conjugate of v_1.

$$cc_\theta = \sum_{i=-\infty}^{\infty} \Delta \theta^*{}_1[i]\Delta \theta_2[i+j] \tag{3.19}$$

where $\Delta\theta_1$, $\Delta\theta_2$ represent the changes in direction of the actin flow within each colliding partner, computed as in Equation 3.17 and $\Delta\theta^*{}_1$ is the complex conjugate of θ_1 ($n = 4$ colliding pairs for both control and *dia*^{5} mutant hemocytes). Furthermore, to investigate the spatial distribution of the observed changes, the cropped regions was split into 3 regions of the same length (i.e. $8.1 \times 3.9\mu m$) which represented the back, middle, and front of the lamella. Subsequently, the average retrograde flow rate and mean change in direction between the 3 smaller boxes were computed ($n = 8$ cells).

To investigate the relationship between the Zyxin labelled adhesion and the actin retrograde flow I computed the mean retrograde flow rate within a cropped area of the lamella that excluded the region of overlap ($8.1 \times 11.7\mu m$), perpendicular to the site of initial cell contact. Subsequently, the size of this region was extended to ($8.1 \times 16.3\mu m$) in order to include the the site of lamellae overlap where the adhesion was located and measured the maximum intensity of Zyxin within this region during the collision.

3.10 Elasticity theory of actin networks

The cytoskeleton of a cell is not just a diluted solution of rigidly cross-linked filaments, but a complicated composite material usually made from several entangled polymer networks, which are far from chemical equilibrium and contain numerous cross-linkers (section 2.1 and [167]). Nevertheless, linear viscoelasticity theory [168] serves as a very good first approximation for the relation between how the

network deforms and what could be the corresponding cytoskeletal stresses causing these deformations allowing us to investigate the mechanical response of the actin network to different stimuli.

In its simple form, linear elastic theory relates a one-dimensional deformation of the material, u to stress as [168]:

$$\sigma = Eu, \tag{3.20}$$

where E is the Young's modulus of the material, a measure of material stiffness. In this ideal case, the stress will grow continuously as the deformation increases. In the other extreme of a pure viscous deformation, there are materials in which the stress relaxes immediately. In this case, the stress depends linearly on how fast the material deforms, i.e. the strain rate $\dot{u} = du/dt$ [168].

$$\sigma = \eta \dot{u}, \tag{3.21}$$

with η the steady state viscosity. Linear viscoelasticity theory tries to combine these two extreme cases; in most cases this is done by approximating the time dependent stress with a model function obtained from a combination of ideal mechanical elements, such as a spring and/or a dashpot [168, 166]. If the deformation of the material is already known, then a qualitative picture of the material can be obtained by using the Boltzmann superposition principle [168]. Using this approximation, the stress at any time can be calculated as the sum of the stresses recorded from all previous times as:

$$\sigma(t) = \int_{-\infty}^{t} E(t-\tau) \frac{du}{d\tau} d\tau, \tag{3.22}$$

where $E(t)$ and $u(t)$ are the time dependent relaxation modulus and deformation, and τ is the lag in time, used to sum up the complete history of the deformation.

For 2 or 3 dimensional problems the description of the relaxation modulus is significantly more complicated than for ideal 1D cases. Nevertheless, Hooke's law (3.20) can be extended to higher dimensions by considering the stress and strains as

tensors. In this case, the strain tensor, u_{ij} can be computed at each point inside the material as:

$$u_{ij} = \frac{1}{2}\left(\frac{\partial u_i}{\partial x_j} + \frac{\partial u_j}{\partial x_i} + \frac{\partial u_i}{\partial x_j}\frac{\partial u_j}{\partial x_i}\right). \tag{3.23}$$

For small deformations, $\vec{u}$, the strain tensor can be linearised by neglecting the last term in Equation 3.23: $u_{ij} = 1/2\left(\partial u_i/\partial x_j + \partial u_j/\partial x_i\right)$. Using this formulation for the strain tensor, the 2D Hooke's law becomes:

$$\sigma_{ij} = C_{ijkl}u_{kl}, \tag{3.24}$$

where Einstein summation is assumed and C_{ijkl} is a fourth order tensor connecting the stress and strain. However, if the material under consideration is homogeneous and isotropic, then using the symmetry of the system, C_{ijkl} can be reduced to only two non-zero quantities called Lamé coefficients, λ, and μ, and Equation 3.24 becomes [168]:

$$\sigma_{ij} = \lambda u_{kk}\delta_{ij} + 2\mu u_{ij}, \tag{3.25}$$

where δ_{ij} is the Kronecker Delta. This relation can be further simplified by expressing the Lamé coefficients as a function of the bulk elastic properties of the network, Young's modulus E and Poisson ration ν [168].

$$\sigma_{ij} = \frac{E}{1+\nu}\left(u_{ij} + \frac{\nu}{1-2\nu}u_{kk}\delta_{ij}\right), \tag{3.26}$$

where the first term describes the effects of pure shearing, and the second term provides information about compression. Combining Equations 3.25 with 3.24 and recalling the stress in a viscoelastic material can be computed using Equation 3.21, the relation between stress and strain for a 2D deformation, $\vec{u}$, becomes:

$$\sigma_{ij}(t) = \int_{-\infty}^{t} \frac{E(t-\tau)}{1+\nu}\left(\frac{du_{ij}}{d\tau} + \frac{\nu}{1-2\nu}\frac{du_{kk}}{d\tau}\delta_{ij}\right)d\tau, \tag{3.27}$$

where $E(t)$ and ν are generally determined using rheological techniques. Fi-

nally, once the time dependent stress is obtained, the 2D force which causes the respective stress distribution can be computed using Eq. 3.28, if the system is in equilibrium [7].

$$f_i^{int} = -\frac{\partial \sigma_{ik}}{\partial x_k}, \tag{3.28}$$

To sum up, this model assumes that the actin cytoskeleton can be treated as a homogeneous, isotropic viscoelastic material modelled as combination of elastic (springs) and viscous (dash-pots) elements all operating together. The viscoelastic part of the model serves to model the dissipative nature of the cytoskeleton together with it's time dependent straining, while the elastic part is used to simulate the structural strength of the actin network. Furthermore, the model assumes that the deformations have a limited lifetime after which previous deformations don't directly contribute to the present state. Finally, because the lamellae are relatively thin, the model treats the actin network as a 2D system.

3.11 Stress model for actin retrograde flow

To compute the stress developed inside the cytoskeleton of both freely moving and colliding cells the actin network was assumed to behave as a linearly viscoelastic material (see section 3.10). This model requires several material properties of the actin network, time dependent elastic modulus, relaxation time, viscosity, Poisson ratio, Young's modulus, to be measured which is very challenging for *in vivo* systems. To overcome this hurdle, elastic properties of growth cones measured by Betz and colleagues [7], were assumed because retrograde flow rates were very similar in both systems. Furthermore, assuming that the cytoskeleton can be represented as a Kelvin-Voigt material, i.e. a viscous element in series with a parallel group formed by an elastic and a viscous elements (Figure 3.13), lead to a compact equation showed below to describe the time-dependent elastic modulus, $E(t)$ [7].

$$E(t) = \frac{a_1 b_1 - a_2}{b_1^2} e^{-\frac{t}{b_1}} + \frac{a_2}{b_1}\delta(t), \tag{3.29}$$

where $b_1 = \tau_R = 2.4 \pm 0.5s$ is the relaxation time, $a_1 = \eta = 4.8 \pm 1.2Pa.s$ repre-

sents the viscosity, and $E = \frac{a_1^2}{a_1 b_1 - a_2} = 112 \pm 21 Pa$ is the assumed Young's modulus. When calculating the time-dependent stress profile for freely moving or colliding hemocytes, it can be assumed that the strain rate, $\dot{u} = \frac{du}{dt}$, is constant during the time interval between two consecutive recorded frames, Δt [7]. Also, the actin network is able to remember its previous loading only for a limited period of time, T_0, which in this case was chosen as $T_0 = 40s$.

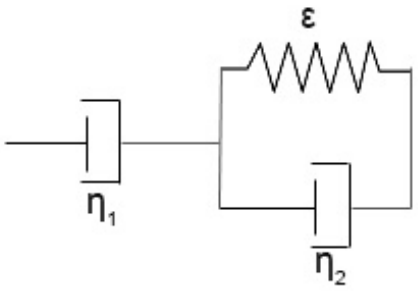

Figure 3.13: Schematic with extended Kelvin-Voight model. A Kelvin-Voight model was used to fit experimental measurements to determine the elastic properties of the cytoskeleton. The measurements and subsequent computation of the elastic and viscous parameters were conducted in [7].

Under these approximations, Eq. 3.27 can be discretised into a sum of $n = T_0/\Delta t$ consecutive parts of length Δt. For the most recent time interval Equation 3.27 was analytically integrated and to give the following expression for the cytoskeletal stress (see [7] for a detailed derivation):

$$\sigma_{ij}(\Delta t)_{[0,\Delta t]} = \frac{1}{1+\nu}\left(\frac{\Delta u_{ij}}{\Delta t} + \frac{\nu}{1-2\nu}\frac{\Delta u_{kk}}{\Delta t}\delta_{ij}\right)\left(\frac{a_1 b_1 - a_2}{b_1}\left(1 - e^{-\frac{\Delta t}{b_1}}\right) + \frac{a_2}{2b_1}\right) \tag{3.30}$$

Furthermore, the accumulated stress between $[-n\Delta t, -(n-1)\Delta t]$ is calculated using (see [7] for a detailed derivation):

$$\sigma_{ij}(\Delta t)_{[-n\Delta t,-(n-1)\Delta t]} = \frac{1}{1+\nu}\left[\left(\frac{du_{ij}}{d\tau}\right)_n + \frac{\nu}{1-2\nu}\left(\frac{du_{kk}}{d\tau}\right)_n \delta_{ij}\right]\frac{a_1 b_1 - a_2}{b_1} e^{\left(-\frac{\Delta t}{b_1}\right)n}\left(1 - e^{-\frac{\Delta t}{b_1}}\right) \tag{3.31}$$

Note that to compute the stresses, I only used the region of the cells that was

common over 40 seconds period. Furthermore, during collisions, I assumed that the two overlapping lamellae are behaving as a continuous material. To verify that the observed redistribution of stresses is not due to this artefact, I computed the stresses within the lamella of a single cell segmented from a collision.

3.12 Laser ablation of actin networks

Hemocytes were labelled with UAS-LifeAct-GFP and UAS-RedStinger and imaged on an inverted 780 Zeiss LSM multi-photon confocal with a time interval of $1s$. Cells were imaged for $5-10s$ and then ablated with a two-photon laser tuned to $730nm$ and focused in a $0.4\mu m \times 1.5\mu m$ region, either at the edge or within the actin network for freely moving cells or at the region of lamella overlap along the actin fibre for colliding cells. Hemocytes were then imaged for $60s$ with only $1.1s$ elapsing between frames surrounding the ablation. For mock ablation of colliding cells, the same protocol was performed as mentioned, except the laser was switched off.

3.12.1 Elastic force model for lamellar recoil

Lamellar recoil rate is a good approximation for the tension developed within the actin cytoskeleton (see section 2.1). To measure the recoil rate following an ablation experiment, kymography along the centre of the region of abscission was performed and subsequently the displacement of lamellae was tracked for 12 seconds. To simplify the measurement, binary images as produced by ImageJ were used. A two-sample t-test with Welch's correction was then employed to test the statistical significance of the difference between the initial recoil rates for $n = 17$ cells for collision and within the lamella of freely moving hemocytes regimes and $n = 10$ for the lamella edge of freely moving hemocytes.

Furthermore, these laser abscission experiments were used to directly assess the intra-cellular stresses developed within the lamella of freely moving and colliding hemocytes. To calculate the strain, $u(t)$, the initial deformation, Δl, was divided by the length of the lamella, l, which was measured directly from kymograhps as shown in Figure 3.14. To quantify the retraction rate, a fast exponential relaxation

overlayed onto a constant retrograde flow was fitted as showed in Equation 3.32. Subsequently, one-dimensional Hooke's law was used to calculate the force developed within the lamellae as: $F = E \times u_0 \times A$, where the same elastic modulus as in section 3.11 was assumed. The cross-sectional area was estimated as, $A = 4\mu m^2$ from an electron microscopy image showed in Figure 3.15.

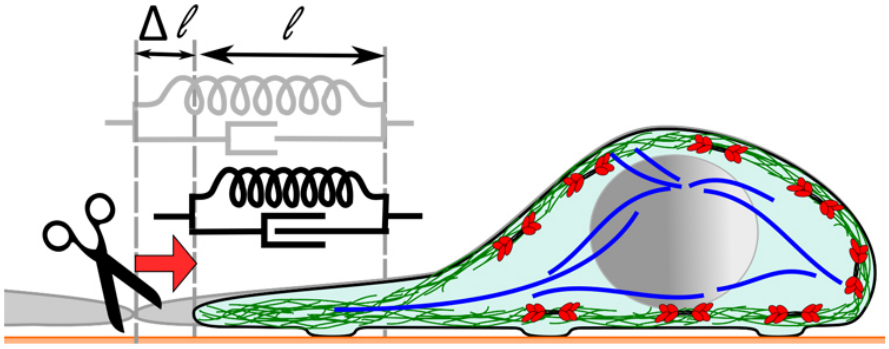

Figure 3.14: Schematic with the mechanical model highlighting the elastic and dissipative element. Note that the strain is computed as $\Delta l/l$, where l is the length of the lamella prior to deformation. Figure recreated from [6]

$$u(t) = u_0 e^{-\omega t} + vt + o, \tag{3.32}$$

where u_0 is the initial strain relaxation that was assumed to be dominated by tension, ω is the relaxation frequency, v is the constant retrograde flow speed, and o is an arbitrary offset.

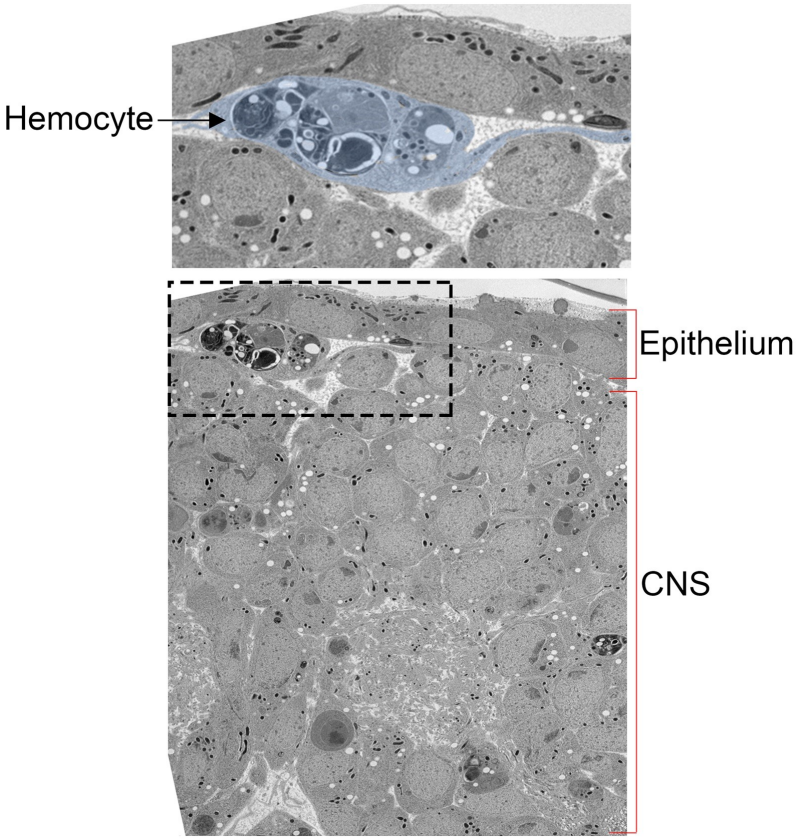

Figure 3.15: Electron micrograph of a hemocyte within the ventral hemocoel. Still showing a hemocyte squeezing between the epithelium and CNS in a space where the height is insignificant compared with the width suggesting that the space can be approximated as 2D for modelling purposes. Note that the topology of the space was maintained by high pressure freezing to avoid fixation artefacts induced by standard methods.

Chapter 4

Cellular Kinematics

In this chapter I present one application of CSPACC for studying cellular collisions in a 2D environment. The chapter begins with an in-depth analysis of hemocyte kinematics during contact inhibition. Following from this, the main main cytoskeletal events that coincide with the observed kinematic changes are investigated. This section on hemocyte kinematics ends with a short discussion about the implications of these findings.

4.1 Contributions

I developed and implemented the platform for quantifying hemocytes migration during CIL. Furthermore, I developed the subsequent analysis of cell tracks and kinematics data together with Dr. John Robert Davis. John was responsible for designing the experimental procedure, performing the experiments and the imaging required for building the library of freely moving and colliding cells.

4.2 Hemocytes CIL is a precisely coordinated process

It is now accepted that hemocytes rely on contact inhibition for their even dispersal during embryogenesis (Figure 4.1A; Movie 1, and Section 2.2.3). In this section, I will show how their contact inhibition dynamics can be investigated by analysing changes in cell acceleration during the response normalised to the time of microtubule alignment (Figure 4.1B; Movie 2). In previous work conducted by Stramer and collegues it was shown that as hemocytes collided, their microtubule

cytoskeleton reorganised into thick bundles growing from a region around the cell body towards the site of lamellae overlap [12]. This remodelling resulted in two microtubule bundles perfectly aligned between the two colliding cells which lasted only as long as cells were in contact [12]. These results suggested that microtubule alignment is a hallmark of CIL and also a very good temporal indicator of when changes in hemocyte motility are occurring during this process.

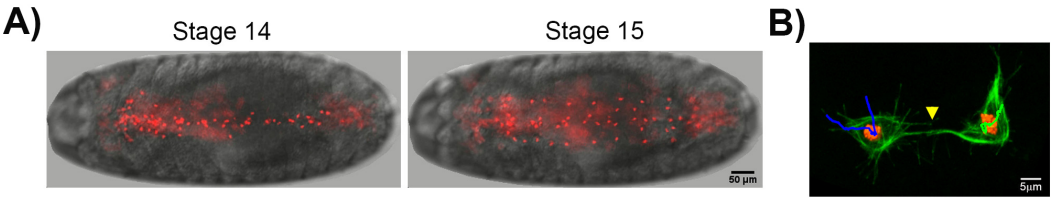

Figure 4.1: Hemocytes contact inhibition. A) Hemocyte dispersal during embryogenesis. Cells are labeled using a nuclear marker (red) and imaged as they migrate beneath the ventral surface of a *Drosophila* embryo (bright-field) at developmental stages 14 and 15. B) Automatic tracking (red) of colliding hemocytes while registering collisions with microtubules (green). Arrowhead shows the time point of microtubule alignment, which allows for temporal registration of CIL collision events in subsequent kinematic analysis. Figure reproduced from [6].

Before commencing with the kinematic analysis, an adequate abstraction of the cell as a geometric point had to be found. Previous work by Davis and collegues showed that tracking the centroid of the cell body or the centroid of the nucleus resulted in very similar tracks [5]. From a computational perspective, being able to track the centroid of the nucleus instead of having to continuously detect the cell body and determine its centroid greatly simplified the subsequent analysis as it reduced both the time taken and tracking errors that might have occurred from inaccurate detection of the cell body. Furthermore, the nuclei have a more regular shape relative to the cell body which is continuously remodelled and as such there are slight variations the position of it's centroid that might not necessarily be correlated to whole cell movement. Nevertheless, tracking the centroid of the nucleus is by no means perfect as the nucleus itself is free to move. However, the nuclear movement is not significant at the temporal resolution used for this work. Furthermore, [5] reported that for freely moving and colliding hemocytes there is little difference be-

tween tracking the whole cell body or tracking the nucleus. Therefore, to increase our accuracy and to minimise the time spent for tracking, in this work the position of the centroid of the nucleus was used to track the gross migration of hemocytes during CIL.

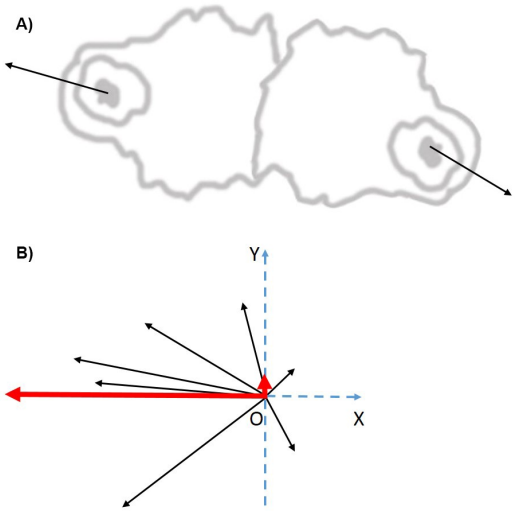

Figure 4.2: Schematic with highlighting acceleration vectors statistics. A) Schematic with two colliding hemocytes highlighting the relative orientation of the acceleration vectors at the time of microtubule alignment. B) Schematic with a collection of acceleration vectors from a series of collisions highlighting the *OX* and *OY* components of the resultant acceleration vectors(Red arrows). Note the small resultant acceleration in the *OY* direction signifying no directionality bias along that axis.

Since its initial discovery, it was long speculated that colliding partners are affecting each others kinematics during CIL. Furthermore, a major component of the response is the cessation of movement in the direction of the contact which was attributed to the cells inability to use each other as a substrate [9]. To investigate these effects of the colliding partner during the response, I studied the instantaneous acceleration of hemocytes, normalised to the position of the incoming partner, over the whole time course of their CIL response. Furthermore, the alignment of the microtubule cytoskeletons was used as a temporal registrar for collisions and as such I chose this time point to represent the zero time point of the kinematics analysis. It is important to note that the alignment of the microtubule cytoskeletons happens after the initial cell-cell interaction. However, previous kinematic study of hemocytes

collisions has identified the microtubule alignment as a crucial step in hemocytes CIL with cells showing a significant negative acceleration around that time [5].

Mathematically, the normalisation I used is equivalent to connecting the two colliding cells by a vector and then making this vector parallel to the *OX* axis (see section 3.6.2 for more details on the normalisation procedure). Performing this normalisation allowed me to investigate the kinematic changes that occur during the response in much greater detail than before. The main question I was interested in answering was if cells are passively avoiding each other or there is indeed an active process at play during CIL. Translated in statistical terms, this hypothesis implies that the tangential acceleration upon collision (i.e. the *OX* component of the acceleration vector) should be significantly negative, while the normal acceleration (i.e. the *OY* component of the acceleration vector) should show no statistical significance, irrespective of the temporal scale at which it is computed [126, 5].

4.3 Hemocytes undergo three synchronised kinematic phases during CIL

Using the normalisation procedure introduced in Section 3.6.2 to compute the acceleration of colliding hemocytes (note that only head on collisions were analysed as hemocytes colliding with the rear of another hemocyte or static cells did not undergo CIL as it will become clear later in this chapter) highlighted that cells consistently progress through a defined sequence of events (Figure 4.3). Three minutes prior to the microtubule alignment, they show a random distribution of the acceleration vectors (Figure 4.1A) suggesting that cells are free to move in any direction. Surprisingly, after just one minute, their behaviour changed and the resultant acceleration vector became positive (Figure 4.3A) indicating that cells are beginning to speed up towards each other around that time (later in this chapter it will become clear that the forward acceleration coincides with the moment when the lamellae of the two colliding cells first come in contact). This behaviour did not last long and acceleration vectors resumed to a random distribution within the following minute (Figure 4.3A). Nevertheless, the most striking event was a sudden back accelera-

tion upon microtubule alignment which suggested that colliding cells are slowing down and/or turning around (Figure 4.3A). This change in acceleration was significant at both 60*s* and 20*s* time intervals (Figure 4.3B), indicating both that microtubule alignment is playing an active role during the response and that hemocytes are precisely controlling their motility during CIL. Subsequently, cell acceleration immediately returned to a random distribution (Figure 4.3). After approximately two minutes from the MT alignment, a second back acceleration event took place (Figure 4.3A) suggesting that cells are actively changing their migratory behaviour while they are engaging in a collision.

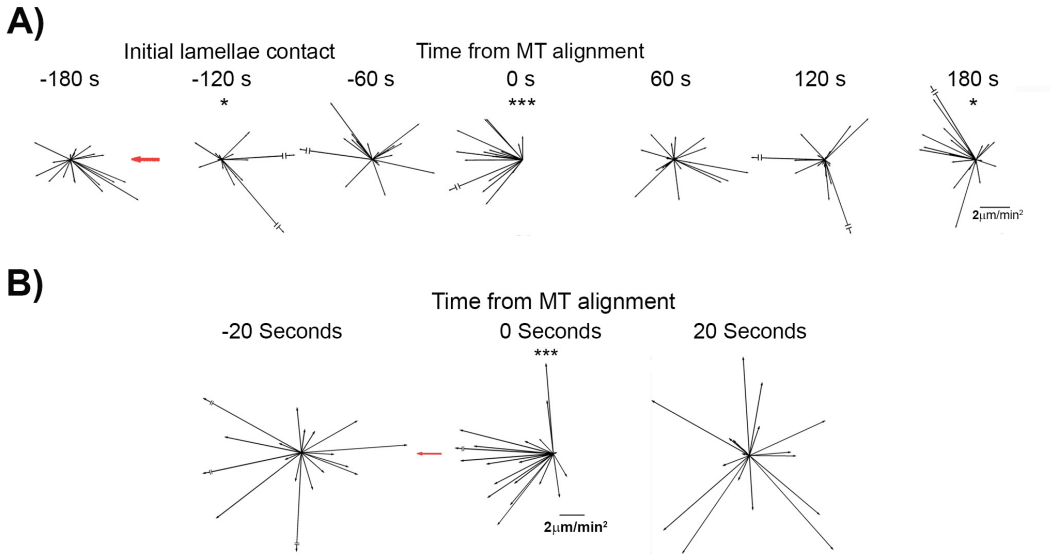

Figure 4.3: Hemocyte acceleration during CIL. A) Time course of hemocyte accelerations computed at 60*s* intervals (black arrows) surrounding a collision event. Note that acceleration vectors were computed with respect to the position of the colliding partner (red arrow). Interstingly, the only time points that show a bias along the *OX* axis are at $-120s$, $0s$, and $180s$, respectively. $*p < 0.05$, $***p < 0.001$. B) Time course of hemocyte accelerations computed at $20s$ intervals (black arrows). Note that acceleration vectors were computed with respect to the location of the colliding partner (red arrow). The only significant acceleration was at $0s$, upon microtubule alignment. $***p < 0.001$. Figure reproduced from [6].

To elucidate if the observed kinematic changes are due to the cells actively modulating their speed, the inter-nuclear distance of colliding hemocytes was quantified during their full CIL response. This data revealed that 2 minutes prior to the

microtubule alignment, the cells suddenly started to speed up towards each other as it was suggested by the increased slope of the inter-nuclear distance over time (Figure 4.4A). This increase in speed was further confirmed by analysing the nuclear displacement rates (Figure 4.4B) which showed a similar trend. Furthermore, immediately upon microtubule alignment, another change in the slope of the graph of the inter-nuclear distance over time took place (Figure 4.4A) and a slow down in nuclear displacement rates (Figure 4.4B) which confirmed that hemocytes were actively slowing down during a collision event. Finally, approximately 120s later, the nuclei clearly started to move apart (Figure 4.4A) as the internuclear distance begun to increase.

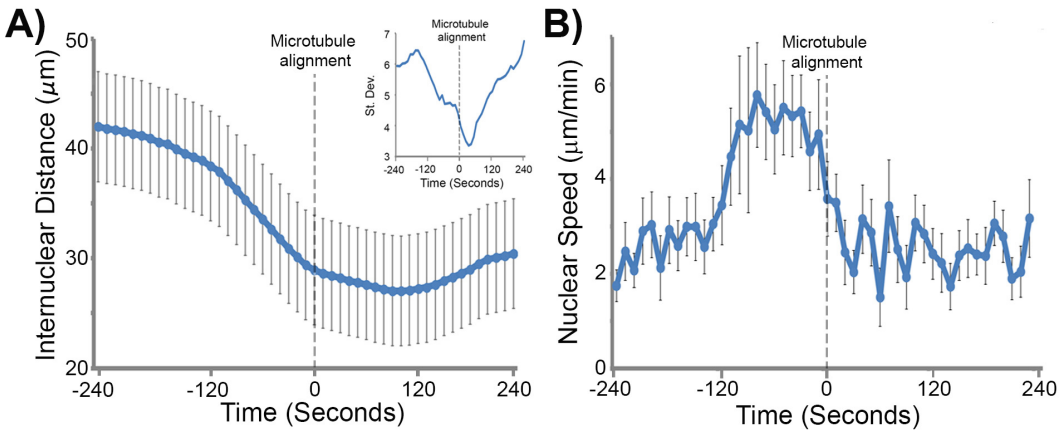

Figure 4.4: Hemocytes CIL involves precisely controlled kinematics steps. A) Graph with the inter-nuclear distance of colliding hemocytes during their CIL response. Note the three changes in slope occurring at $-120s$, $0s$, and $120s$, respectively. Error bars represent SD. (Inset) Plot with the standard deviation of the inter-nuclear distance over time. Note the sudden decrease in SD at $-120s$ indicating that cells behaviour is starting to be regulated. A further reduction in SD is observed upon microtubule alignment, suggesting that microtubules are crucial for controlling the distance between cells during CIL. B) Graph with the nuclear displacement rate during CIL. Note the two subsequent increase and decrease in speed occurring at $-120s$ and upon microtubule alignment, respectively. Error bars represent SD. Figure reproduced from [6].

Hemocytes clearly progressed through a defined sequence of events as they collided appearing to modulate their movement in accordance to each stage. Further analysis of the standard deviation of the inter-nuclear distance over time also highlighted different kinematic stages during CIL, indicated by clear changes in variance as cells transition through these phases (Figure 4.4A inset). These data suggest

that hemocyte CIL is differentially regulated throughout the response. The distinct kinematic stages highlighted by the acceleration analysis can also be visualised by inspecting the average velocity vector of each colliding partner (Movie 3). In addition, visual analysis of the average velocity vector over time further supports the idea that hemocyte contact inhibition response involves different stages, suggesting multiple points of regulation where colliding partners synchronously change their behaviour.

4.4 Actin and microtubule networks determine hemocyte kinematics during CIL

Previous work conducted by Stramer and collegues showed that prior to microtubule contact, the lamellae of colliding cells are the first to come in contact [12]. Building on this observation, I next wanted to investigate if this lamellar overlap could be determining the kinematic changes identified by the acceleration analysis.

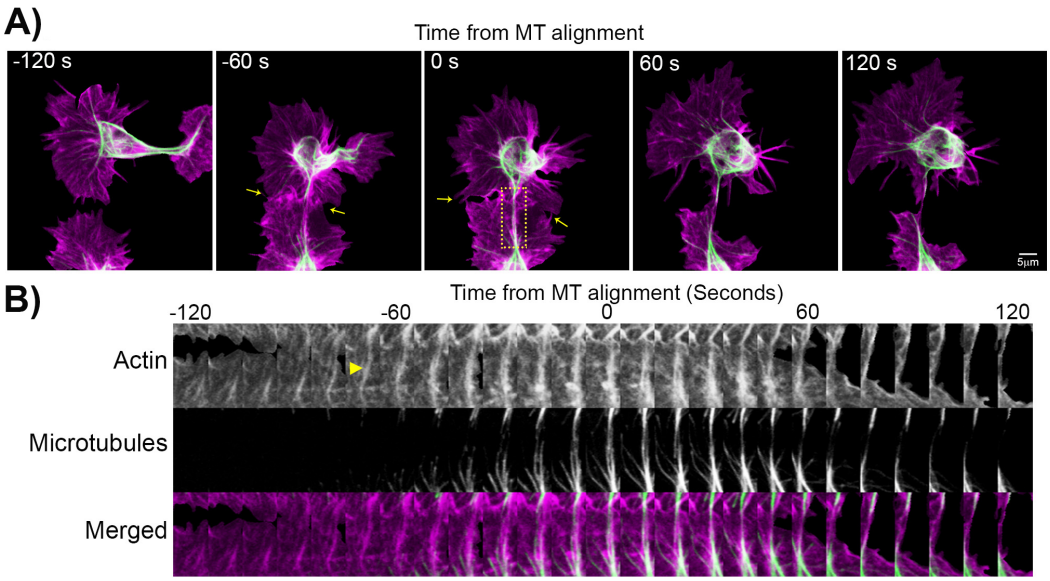

Figure 4.5: Dynamics of actin and microtubules cytoskeleton during CIL. A) Time-lapse sequence of colliding hemocytes where we labeled F-actin (magenta) and microtubules (green). Arrows highlight the region of lamellar overlap. B) Kymograph of the highlighted region in (A) showing the formation of the actin fibre and subsequent microtubule bundle development and alignment. Arrowhead represents time of actin fibre initiation. Figure reproduced from [6].

Analysing a time-lapse sequence of colliding hemocytes I observed that lamellae contact takes place 105 ± 22 seconds prior to microtubule alignment (Figure 4.5; Movie 4) which coincided with the forward acceleration phase (Figure 4.3A). Even more surprising, following lamellae contact, an actin fibre started to develop almost instantaneously between the two colliding cells and subsequently appeared to connect them (Movie 4).

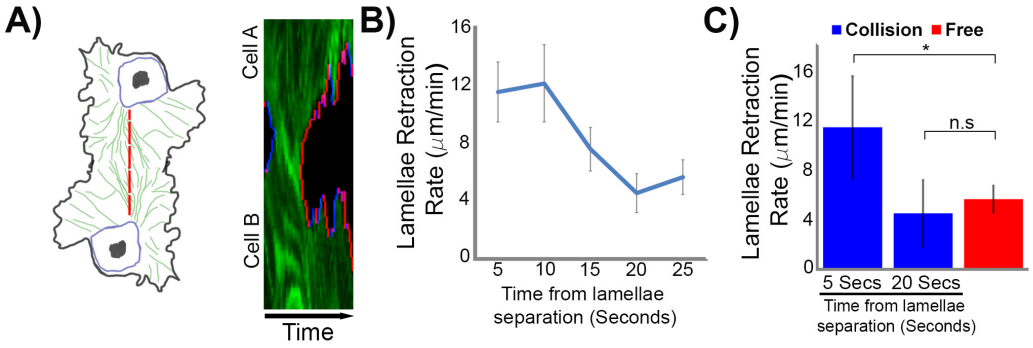

Figure 4.6: Lamellar retraction rates increases during CIL. A) Kymograph of lamellar activity (red region represent lamellar retraction and blue extension) during the CIL response. The kymograph was computed only for the region along the actin fibre (dotted, red line in schematic). Note the sudden simultaneous retraction event upon cell separation. B) Quantification of the rate of lamellar retraction over time. Error bars represent SEM. C) Comparison of the the average retraction rates in non-colliding hemocytes with the lamella retraction rates at 5 and 20s after cell separation. Error bars represent SD. $*p < 0.05$. Figure reproduced from [6].

In the previous section I showed that microtubule alignment correlates with a sudden change in acceleration from a random distribution to a back acceleration. To investigate if there could be a connection between the development of the actin fibre and microtubule cytoskeleton time-lapse analysis was performed where actin and MTs were visualised together. Visual inspection of these movies revealed that microtubules are actually using this actin fibre as guides during their alignment (Figure 4.5B) suggesting that there is some sort of coupling between the two structures.

Until this point, only head on collisions have been scrutinised which opened up the question if lamellar interaction is indeed required for hemocyte CIL. Analysis of cells colliding with the rear of another hemocyte (Movie 5) or with the lamella of a static cell (Movie 6) did not result in the formation of an actin fibre nor the subse-

quent repulsion observed when hemocytes collided head on suggesting that direct interaction of the lamellar networks is crucial for initiating the response. Nevertheless, it is still unclear what is the exact mechanism by which this is achieved.

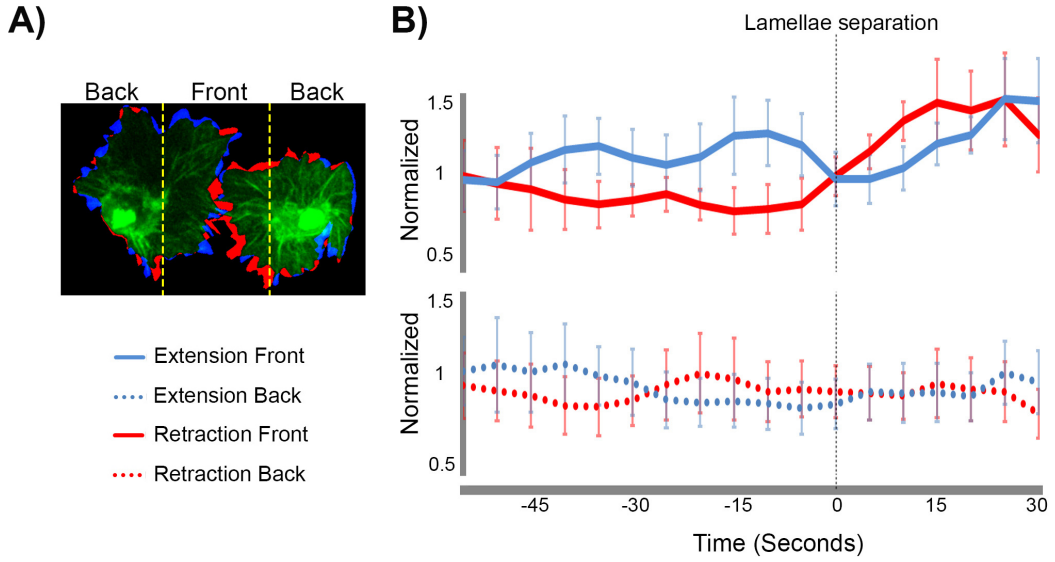

Figure 4.7: Lamellar retraction precedes the formation of new protrusions during CIL. A) Example of a pair of colliding hemocytes showing regions of lamellar retraction (red) and extension (blue). The lamellae of colliding cells was divided into two regions, front and back. The former represents the region of the cells facing each other, while the latter contains the regions of the cells facing away from colliding partner. B) Average area of lamellar extension and retraction for the regions highlighted in (A). Note that retraction of the leading edge occurs prior to the development of new protrusions away from the colliding partner. Error bars represent SEM. Figure reproduced from [6].

The acceleration time-course suggested that following the sudden, drastic reduction in movement, hemocytes begin to actively migrate away from each other. Analysis of the separation phase between colliding hemocytes revealed that the synchronised cellular behaviour in not limited to the initial phases, but instead persisted throughout the response. In fact, prior to the separation phase, lamellar retraction rates (computed as described in Section 3.8.3) simultaneously spiked to two to three times the speed of retraction events in freely moving cells (Figure 4.6). This sudden separation event took place $32 \pm 22s$ after microtubule alignment, which coincided with the initiation of movement away of the two colliding cells. To investigate the order of these events, lamellar extension-retraction maps were computed as de-

scribed in Section 3.8.3. This analysis revealed that lamellar retraction actually took place prior to the cells developing new protrusions away from the colliding partner (Figure 4.7A). Time series plots of the average area of lamellar extension and retraction confirmed that retraction of the leading edge occurred prior to the development of new protrusions away from the colliding partner (Figure 4.7B). These data suggest that rapid lamellar retraction initiates cell repolarisation as opposed to cells passively reacting to their colliding partners.

4.5 Discussion

In this chapter I showed that hemocyte contact inhibition of locomotion involves a sequence of three kinematics phases that are differentially regulated. To conduct this analysis, cells trajectories were normalised to the position of the incoming partner. Several studies have suggested that this normalisation is best for identifying if the two colliding partners influence each other during CIL [126, 10, 5]. Unlike previous methods, I normalised the full time course recorded with respect to a common temporal origin (i.e. time of microtubule alignment) which allows for a much more accurate description of instantaneous cell motion over time. To perform this analysis, I developed a Matlab based kinematics platform that allows users to 1) normalise tracks to any reference point, 2) compute different global and instantaneous statistical measures for velocity and acceleration vectors, and 3) visualise vector time series. Furthermore, CSPACC has a modular implementation which allows users to easily extend it's functionality by simply writing additional modules and linking them with the existent code.

A limitation of the current implementation is that it only analyses instantaneous measurements of motion, ignoring any global quantities such as mean squared displacement, similarity of cell tracks (e.g. are tracks of different cell types comming from the same statistical distribution?), or persistence of motion [169].

The accuracy of cell speed and acceleration magnitude performed by CSPACC is limited by the temporal resolution of the tracks (see Section 3.2) and as such requires careful acquisition if multiple tracks are to be compared. With this in mind,

CSPACC is robust enough to distinguish random fluctuations from actual changes in cell movement, a feature that was crucial for investigating cell kinematics during CIL.

In the early years after its discovery, there was speculation about the sequential nature of CIL [9]. However, until now there was no quantitative evidence that contact inhibition comprises of a series of successive events whereby cells rapidly change their migratory behaviour to progress through a defined series of events. The observed changes in kinematics are very sudden, especially the back acceleration event which occurs within a 20 seconds window surrounding the time of microtubule alignment. These results confirm that hemocytes CIL is a precisely regulated process as it was previously suggested by [5]. Interestingly, each of these steps coincided with different cytoskeletal dynamics, whereby the actin network appeared to undergo tremendous reorganisation in both colliding partners.

The alignment of the microtubule cytoskeletons is a crucial step for the process [12, 5]. It is clear that the actin and microtube networks are somehow interacting to control hemocyte motility during CIL. However, mainly because of experimental challenges, there are no studies trying to address how is the interaction between the actin and microtubules cytoskeletons affecting the CIL. It could be that the microtubule cytoskeleton is guided by the newly developed actin cable towards the site of cell-cell contact. However, this hypothesis needs to be put under scrutiny. In addition, most of the previous work investigated the role of the two cytoskeletal components separately during the process. Out of this work has emerged that disrupting the stability of microtubules in fibrolasts [147, 11] or hemocytes [12] resulted in a loss of ability to contact inhibit even if the cell lamellae still overlapped. In the case of hemocytes, they are not able to migrate away from each other at the end of the process [12]. This suggest that a stable microtubule cytoskeleton is necessary to ensure cells separate and repolarise. However, at this stage I do not have enough information to address what is the role of microtubules during CIL.

Different cell types display relatively different contact inhibition behaviours (see section 2.2). The sudden acceleration changes and synchronised lamellar dy-

namics reveal that hemocytes are undergoing a type 1 response, where cell-cell contact is followed by a sudden lamellar contraction and subsequent repolarization and migration away from the colliding partner. Surprisingly, their CIL response is very similar to the one observed by M. Abercrombie for chick heart fibroblasts [9]. It would be interesting to test if other cells, especially ones that undergo a type 1 contact inhibition, are progressing through the same kinematic phases. If this is the case, then we may be able to exploit different cell types to investigate how each kinematic phase is controlled.

Chapter 5

Actin Dynamics During Hemocyte CIL

This chapter begins with a description of the experiments and analysis I carried out to quantify the actin retrograde flow dynamics in freely moving hemocytes. Next, the main molecular motors driving the actin flow *in vivo* are identified. Subsequently the actin retrograde flow during collisions are described in detail as well as other cytoskeletal changes that occur during CIL. Additionally, I investigate if the actin networks are becoming mechanically coupled during CIL and analyse the nature of this coupling. Finally I examine the role of Myosin II contraction and *Diaphanous* during contact inhibition.

5.1 Contributions

This work has been conducted working closely together with our collaborators at King's College London, especially Dr. John Robert Davis. I was responsible for further developing the pseudo-speckle method for measuring the actin retrograde flow introduced by Betz and colleagues [170]. In addition, I created all the post processing tools for the analysing the dynamics of the flow. All the experiments and time-lapse movies were acquired by our collaborators. John was responsible for quantifying the flow of Myosin II and cell migration of control, zip^1, and dia^5 mutant hemocytes. We were both involved in the quantification of the cytoskeletal dynamics for all genotypes used. I would like to mention Fuad Mosis and James

Thachery who were the front line soldiers for the manual segmentation of the majority of the movies used in this chapter.

5.2 Actin network dynamics in freely moving hemocytes

Hemocyte CIL involves three distinct, yet precisely coordinated phases (see section 4.2 and 4.3). As the time of lamellae overlap corresponded with initial kinematic response, i.e. forward acceleration, I next examined actin dynamics during CIL. To this aim, I adapted a pseudo-speckle tracking technique (FLUPS) [170] to measure the precise velocity (i.e. speed and direction) of the actin flow within hemocytes *in vivo* (Figure 5.1). The main advantage of using pseudo-speckle tracking over more advanced tools like speckle microscopy is that it allows for the quantification of the actin retrograde flow with sufficient detail even at long time scales (e.g. several minutes) which allowed for the full response to be observed.

For this analysis the actin network within freely moving hemocytes was labeled using LifeAct-GFP and time-lapse movies were recorded at a rate of 5 seconds per frame. To improve the accuracy of the FLUPS analysis, movies were manually segmented to ensure that only the cell of interest was present in every frame.

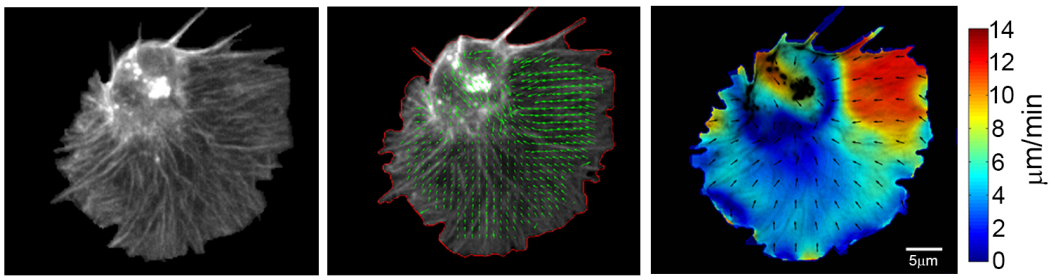

Figure 5.1: Quantification of actin retrograde flow within the lamella of freely moving hemocytes. A) Still of a freely moving hemocyte containing labelled F-actin. B) Quantification of the actin retrograde flow direction within freely moving cells. C) Example of a heatmap highlighting the magnitude of the actin retrograde flow and direction. Figure recreated from [6].

Visual inspection of these time-lapse movies revealed that hemocytes have a very rich and dynamic lamellae, with regions of high and low retrograde flow con-

tinuously appearing and disappearing within the lamella as the network is displaced in centripetal direction (i.e. from the edge of the cell towards the cell body) (Figure 5.1 and Movie 7). To obtain a quantitative description of the retrograde flow within hemocytes, I computed the average flow rate over the whole recorded time course. This analysis revealed that migrating hemocytes have on average a flow rate of $3.2 \pm 1.8 \mu m/min$ ($n = 6$ cells). Direct comparison of mean retrograde flow rates together with visual inspection of the flow in neuronal growth cones *in vitro* [7] showed that the two networks are similar (average values of the retrograde flow within NG108-15 growth cones was $1.46 \pm 0.6 \mu m/min$ [7]). This suggests that the two cell-types could have quantitatively similar physical properties.

5.2.1 Myosin II contraction drives actin retrograde flow *in vivo*

Previous studies showed that the retrograde flow dynamics in slowly migrating cells is generated by a combination of actin polymerisation and Myosin II contraction (see section 2.1.4 for a detailed review on the topic). Before assessing the exact contribution of Myosin II motors to the observed flow dynamics in hemocytes, first the movement of Myosin II puncta within the lamella of freely moving hemocytes was quantified.

Time-lapse movies of freely moving hemocytes acquired with at a temporal resolution of 10 seconds per frame where Myosin II and the actin cytoskeleton were fluorescently labelled revealed that hemocytes lamella contained many Myosin particles constantly flowing throughout the network (Figure 5.2). Manual tracking of Myosin II fluorescent particles indicated that Myosin II flows with a similar speed to the actin network. This quantification was limited by the resolution of the time-lapse movies. Thus, Myosin II particles were tracked until they disappeared or got incorporated into larger structures which resulted in tracks of different lengths. Nevertheless, normalising the tracks to a common origin, revealed that particles were actually flowing with the actin network, in a retrograde direction (Figure 5.2A - 5.2C; Movie 8). The presence of Myosin II throughout the network and the similarity between its movement and the movement of retrograde flow suggests that Myosin II contraction is playing a role for the retrograde flow *in vivo*.

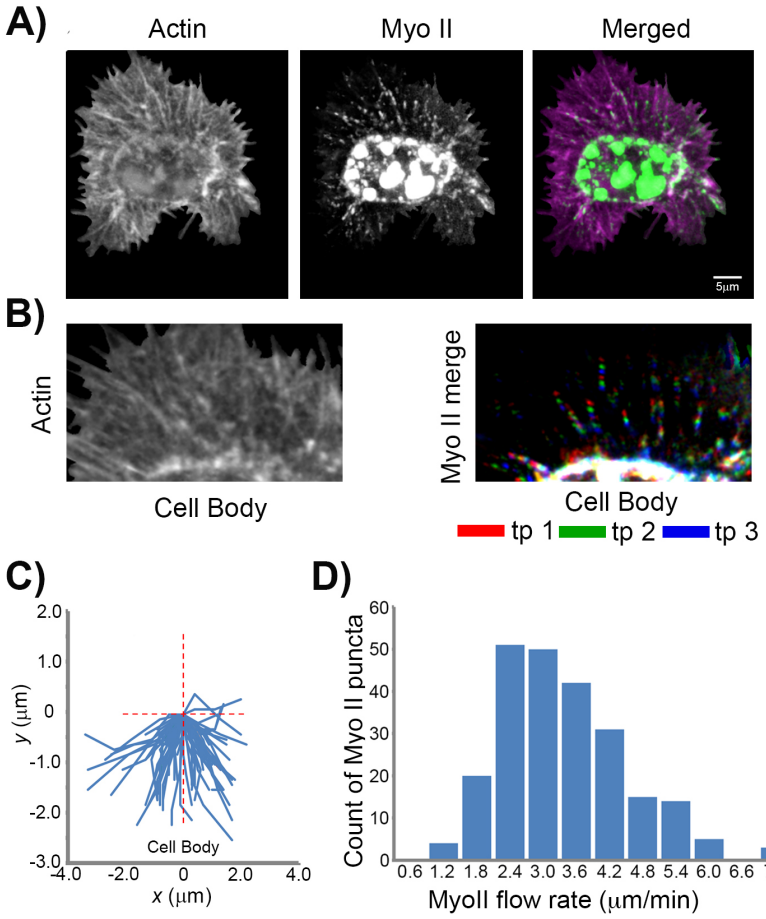

Figure 5.2: Myosin-II particles follow the retrograde movement of the actin network. A) Example of a hemocyte containing labeled F-actin (magenta) and Myosin II (green). B) Left panel shows the lamella of frely moving hemocyte containing labeled F-actin. Right panel shows several tracks of Myosin II particles within the lamella. Note the retrograde movement of the Myosin II particles as highlighted by the temporal color coding where we labeled the first time point red, the second in green, and the third time point in blue. C) Quantification of Myosin II tracks in freely moving cells. D) Distribution of Myosin II particle speeds within the lamella of freely moving cells. Note the mean particle speed of $3.4 \pm 0.6 \mu m/min$. Figure recreated from [6].

To verify this hypothesis I analysed the actin retrograde flow in a situation where Myosin II contraction was inhibited. Therefore, hemocytes in *myosin II heavy chain* mutant embryos (called Zipper [Zip] in the fly) were analysed. To confirm that these mutant embryos have very little residual levels of *myosin II heavy chain* the migratory behaviour of hemocytes during the development of these embryos was first scrutinised. This analysis revealed that *Drosophila* zygotic mutant

embryos (zip^1) showed significant defects which appeared at later stages of development, approximately around the time when these time-lapse movies were acquired (Figure 5.3). These data suggest that hemocytes require *myosin II heavy chain* for their normal migration during development dispersal.

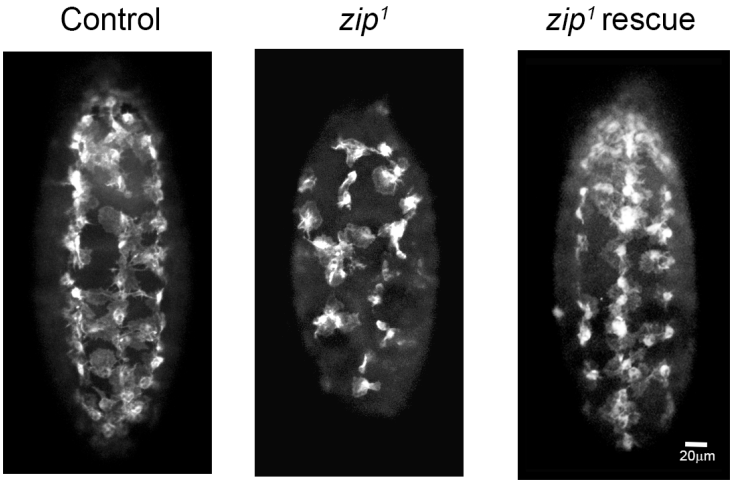

Figure 5.3: Migration of *zip*^{1} mutant hemocytes during development. Left panel shows a still image of hemocyte dispersal along the ventral surface of Stage 15 control embryos. Middle panel contains still image of hemocyte dispersal of zip^1 mutant cells. Note the disruption in the pattern when compared with the control embryos at the same developmental stage. Right panel shows the rescue of the dispersal by expression of GFP-tagged Myosin II specifically in *myosin II* mutants. Figure recreated from [6].

Analysis of the actin retrograde flow in freely moving *myosin II heavy chain* mutants revealed a significant reduction in the retrograde flow rates from approximately $3-4\mu m/min$ in control cells to $1.5\pm1.0\mu m/min$ in these mutant cells (Figure 5.4A; Movie 8). Furthermore, analysis of the distribution of retrograde flow speed revealed that zip^1 mutant cells displayed a much higher probability for low flow values and almost no flow speed above $3.5\mu m/min$ (Figure 5.4A). Qualitative analysis of time-lapse movies of freely moving zip^1 mutant hemocytes showed that the retrograde flow dynamics was severely affected, displaying a global reduction in flow and disappearance of the ”weather”-like pattern that I observed in control cells (Figure 5.1; Movie 9). These results suggest that Myosin II contraction is required to drive the retrograde flow in hemocytes. Surprisingly, quantification of the actin retrograde flow dynamics in zip^1 mutant hemocytes specifically express-

ing GFP-tagged Myosin II recovered similar flow dynamics as control cells where the network recovered it's pattern (as indicated by careful visual inspection of both control and Myosin II rescue cells). Further quantification of the retrograde flow rate within these cells also revealed a recovery of the average flow rates to the values recorded for control cells as compared to the average flow rates measured for freely moving cells (Figure 5.4A). I also quantified the distribution of retrograde flow values within the entire lamella of hemocytes rescued for Myosin II. This analysis revealed a reduction in the probability of low retrograde flow speed values and a shift in the distribution towards speeds more common in control cells (Figure 5.4B). These strongly support the hypothesis that Myosin II activity is required for retrograde flow dynamics within hemocytes.

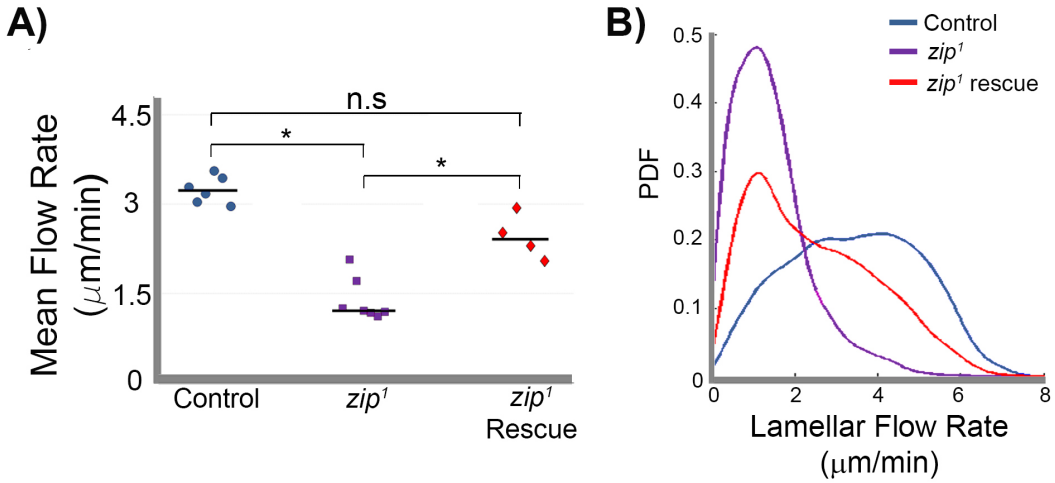

Figure 5.4: Myosin II contraction drives retrograde flow in hemocytes. A) Quantification of the mean retrograde flow across the lamella of freely moving cells for control, zip^1 mutant, and zip^1 mutant rescue hemocytes. $*p < 0.05$. B) Probability density function (PDF) of the retrograde flow speed in freely moving control, zip^1 mutant, and zip^1 mutant rescue hemocytes. Note the increased distribution of higher flow rates caused by expression of GFP-tagged Myosin II in zip^1 mutant cells. Figure recreated from [6].

5.3 Global reorganisation of the actin networks during CIL

Previous studies suggest that the actin cytoskeleton is playing a role during CIL (section 2.2.2). Thus I next wanted to investigate this hypothesis by extending the

pseudo-speckle analysis to colliding hemocytes. For this experiment, time-lapse movies of colliding pairs where the actin network was labelled using LifeAct-GFP were acquired at 5 seconds per frame. Quantification of the actin retrograde flow dynamics in these movies revealed that in contrast to freely moving cells which display a consistent retrograde flow dynamics, in colliding hemocytes the actin networks are undergoing significant reorganisation during the CIL response. (Figure 5.5; Movie 9). Visual inspection of colliding hemocytes consistently highlighted the development of a prominent actin bundle between the cell body and the point of contact in both colliding cells immediately after their lamellae first come in contact. This actin fibre persists for the entire duration of the collision (Figure 5.5 top panels; Movie 9).

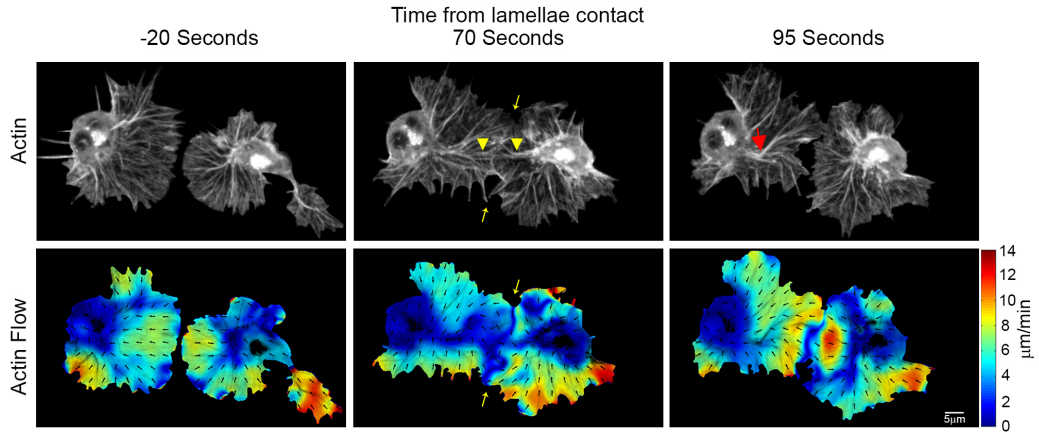

Figure 5.5: Reogranisation of the actin network during CIL. Top panels contain still images from a time-lapse movie of colliding hemocytes with labeled F-actin. Notice the development of an actin fibre between the cell body and the point of contact in both colliding partners (arrowheads). This fibre subsequently deforms and finally breaks upon lamellar separation (red arrow). Bottom panels highlight the dynamics of the actin flow measured using our FLUPS platform. The algorithm is not able to distinguish between the two lamellae in the overlap region (highlighted by yellow arrows) which results in a decreased actin retrograde flow speed. Figure recreated from [6].

Quantification of the actin retrograde flow speed as measured by the pseudo-speckle program I developed revealed that as the lamellae were coming in contact, a corridor of low retrograde flow started to develop in both cells simultaneously (Figure 5.5 and 5.7A). Interestingly, this decrease in the actin flow magnitude lasted throughout the response (Figure 5.5 and 5.6; Movie 9). Further quantification of the

mean retrograde flow rate normalised to the maximum flow rate recorded during the response also revealed that as cells were coming in contact, the retrograde flow rate decreased to a minimum value of about half that prior to collision (Figure 5.6). Even more surprisingly, around the time of lamellae separation there was a sudden increase in retrograde flow rate to a local maximum of approximately 1.5 times the value recorded prior to initial lamellar contact. This increase in flow speed lasted for about 20 seconds, similar to the duration of the lamellar recoil (Figure 4.6). Furthermore, the retrograde flow speed continued to increase as cells were migrating away from each other, approximately $15-20$ seconds after the lamellae disengaged. Interestingly, this time frame coincided with the time interval during which cells were repolarising (Figure 4.3 and 4.4).

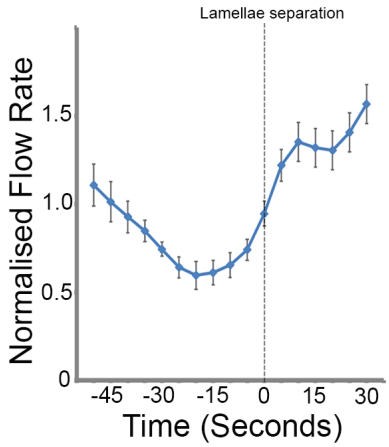

Figure 5.6: Actin retrograde flow speed increases during collisions. Quantification of the retrograde flow rates within the lamella of colliding hemocytes. Note the reduction in retrograde flow upon lamellae contact and the subsequent rapid increase in flow speed around the time when lamellae separate. Figure recreated from [6].

I next wanted to investigate if there were other changes in retrograde flow dynamics occurring during CIL as visual inspection of time-lapse movies suggested that a global reorganisation was taking place. To this aim, I quantified the instantaneous changes in retrograde flow speed and direction for the full response (see section 3.9 for the details of this quantification). Analysis of the instantaneous change in flow speed confirmed that as cells were colliding, the retrograde flow slowed down up to the point of lamellar separation when there was a sudden in-

crease in retrograde flow which persisted for approximately 30 seconds, as cells were repolarising and beginning to migrate away from each other (Figure 5.6 and 5.7B; Movie 10).

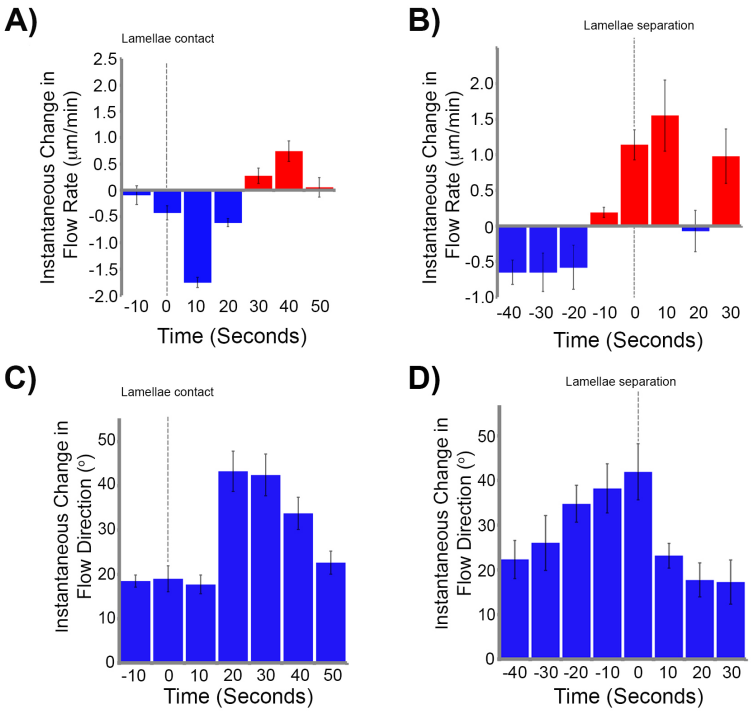

Figure 5.7: Actin networks rapidly reorganise during CIL. A) and B) Instantaneous changes in actin retrograde flow speed quantified from lamellar contact A) and lamellae separation B). C) and D) Instantaneous changes in the direction of the actin retrograde flow computed from lamellar contact C) and lamellae separation D). Error bars represent SD. Figure recreated from [6].

Furthermore, analysis of the change in direction revealed that as the cells were colliding, the actin networks underwent a sudden change in the direction in which they were flowing, from a retrograde motion to flowing perpendicularly to the low flow corridor as indicated by the instantaneous changes in retrograde flow direction and visual inspection of the actin flow heat maps (Figure 5.7C and 5.7D; Movie 11). These data suggest that the CIL response is not a simple passive reaction to the presence of the colliding partner, but a a much more complicated active process, that involves a dramatic global reorganisation of the actin networks within both colliding partners.

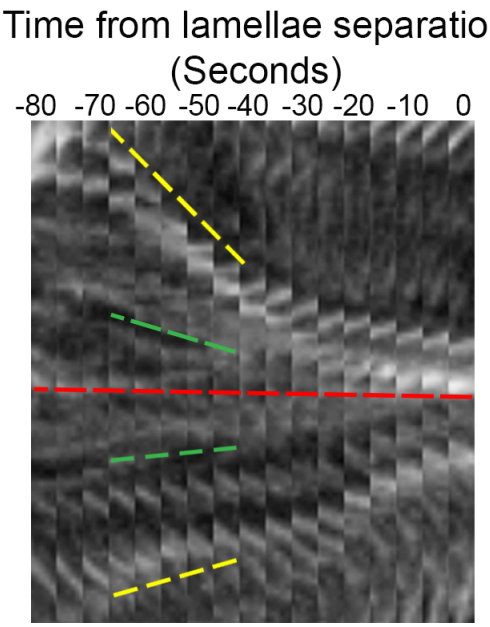

Figure 5.8: Actin fibres are recruited from the periphery to the centre of the lamella during CIL. Kymograph of the region perpendicular to the actin fibre highlighting the recruitment of preexisting F-actin within the lamella. Note the increase in the rate of recruitment at the periphery (yellow dashed lines) compared with those closer to the centre of the lamella (green dashed lines). Figure recreated from [6].

Kymography of the actin cytoskeloton revealed that as cells were colliding, an actin fibre started to develop between the two colliding partners (Figure 5.8). I next set to investigate if the sudden changes in retrograde flow were contributing to the development of the actin fibre. Kymography of the lamellar region perpendicular to this actin fibre revealed that the development of the actin fibre appeared to be aided by the change in retrograde flow direction as pre-existing fibres appeared to be recruited to the low flow corridor (Figure 5.8). Surprisingly, measurement of the rate of recruitment of pre-existing actin fibres to the actin cable developing between colliding cells revealed that rate of actin fibres recruitment was higher towards the periphery of the lamella compared to the region closer to the centre (Figure 5.8). Further quantification of the fluorescent intensity in the central region of the lamella (where the fibre was developing) revealed that the actin fibre only persisted as the cells were in contact. This analysis showed that as soon as the hemocyte lamellae separated, the actin fibre deformed and subsequently disappeared as the actin flow

rapidly returned to a centripetal flow (Figure 5.5 5.8 and Movie 9). Furthermore, the changes in retrograde flow speed and direction coincided with the development of the actin fibre between colliding cells. Surprisingly, the actin fibre developed inside the low retrograde flow, growing perpendicular to the leading edge of the cells (Figure 5.5 and 5.9). These data suggest that the initial contact between lamellae triggers a network wide reorganisation, including the development of an actin fibre that appears to link the two colliding partners as they engage in a collision.

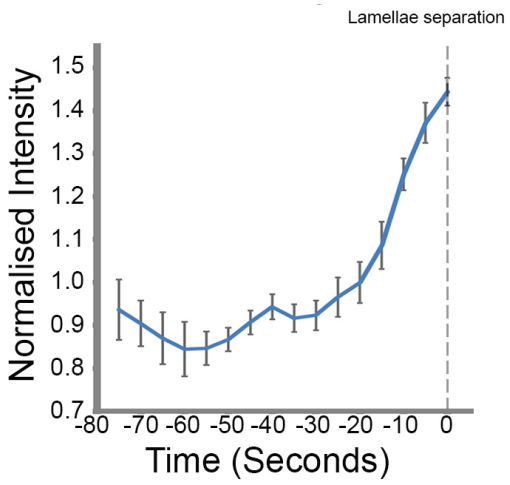

Figure 5.9: An actin stress fibre develops between colliding cells during CIL. Quantification of F-actin intensity within a corridor corresponding to the region of actin fibre formation during CIL. Figure recreated from [6].

A major aspect of hemocyte contact inhibition is the alignment of the microtubule cytoskeletons as cells are undergoing a collision. I also investigated if the reorganisation of the actin networks is somehow contributing to this alignment. Kymography of the region surrounding the actin fibre in time-lapse movies where both the microtubule and actin cytoskeletons were labelled using different fluorescent markers revealed that the microtubule bundles also developed within the low retrograde flow corridor (Figure 5.10; Movie 12) which happened simultaneously in both colliding cells. Additionally, the microtubules appeared to use the recently developed actin fibre as tracks to guide them towards the site of cell-cell contact (Figure 4.5 and 5.10). These data suggest that immediately upon lamellar contact, colliding hemocytes are somehow beginning to coordinate their cytoskeletal dynamics, which results in a synchronous global reorganisation of the actin and micortubule

networks.

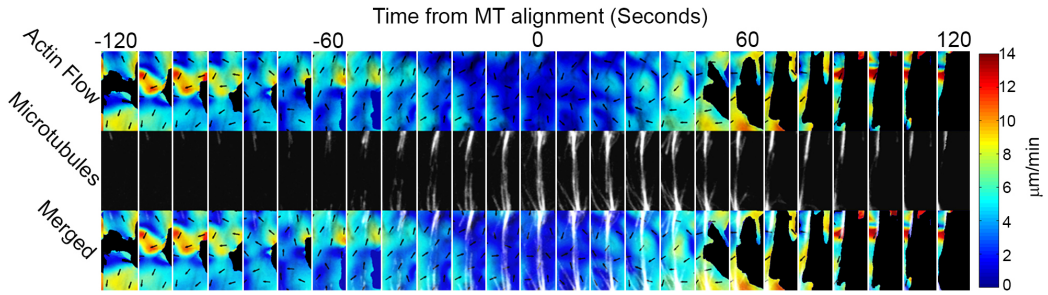

Figure 5.10: Microtubule bundle develops within the low retrograde flow corridor. Kymograph of the region surrounding the actin fibre showing the dynamics of the actin retrograde flow and the formation of the microtubule bundle (pseudocoloured white). Figure recreated from [6].

5.3.1 Actin networks are mechanically coupled during CIL

The results presented so far suggested that the two lamellae networks are becoming coupled during the CIL response. To test this hypothesis, I analysed the cross-correlation between the instantaneous changes in flow velocity (*i.e.* speed and direction). The cross-correlation was computed as described in section 3.8.4 where the instantaneous changes in flow speed and direction were sampled only in a region surrounding the actin fibre. I performed this quantification with reference to both the time when the two cells lamellae first overlapped and when their lamellae first separated. This analysis showed an increase in the mean correlation coefficient compared to the values recorded prior to the collision for the changes in retrograde flow speed immediately after the lamellae overlapped (Figure 5.11A). The increased correlation lasted throughout the response, although it slightly decreased as cells were in contact. Surprisingly, there was another spike in the mean correlation between changes in flow speed at the time of cells separation, followed by a sharp decrease in correlation as the cells were breaking from the collision (Figure 5.11B). Analysis of the correlation between instantaneous changes in retrograde flow direction revealed a similar trend, with the mean correlation coefficient increasing as the cells were colliding. Nevertheless, the correlation of the changes in flow direction spiked approximately 20 seconds after the lamellar overlap (Figure 5.11C) and persisted throughout the response, even after the cells were not in

contact any more (Figure 5.11D). These data suggest that hemocytes lamellae are becoming mechanically coupled during CIL, where the initial lamellae contact triggers the global reorganisation of the networks.

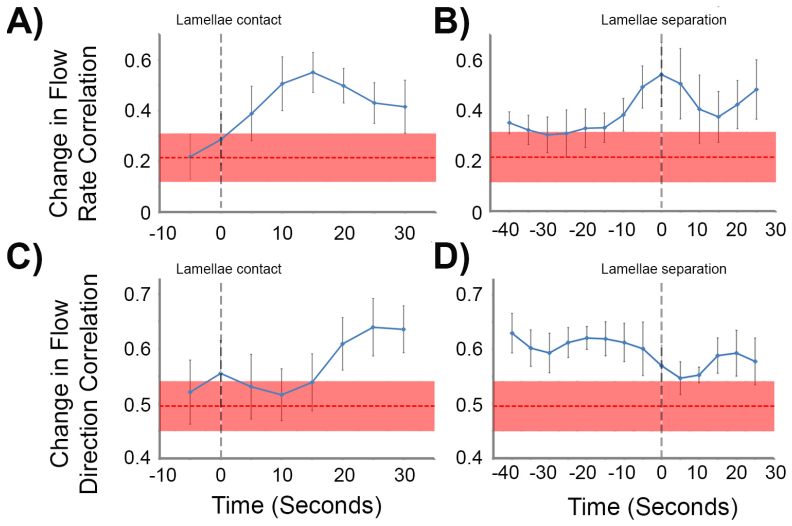

Figure 5.11: Coupling of actin networks between colliding cells. Cross-correlation of the instantaneous changes in actin retrograde flow rate (A and B) and flow direction (C and D) computed with respect to lamellae contact (A and C) and lamellae separation (B and D). Error bars represent SEM. Red dotted lines correspond to the mean cross-correlation between colliding cells prior to lamellae contact. Note that the shaded region represents the SEM. Figure recreated from [6].

5.4 An inter-cellular actin clutch coordinates the actin networks during CIL

In the previous section I showed that the actin network is undergoing tremendous reorganisation during the hemocyte CIL response. This reorganisation is accompanied, and even contributed to the formation of an actin fibre that spans colliding hemocytes. Nevertheless, these events all take place after the initial lamellae contact. Therefore, I set to investigate if this initial contact could be responsible for the observed behaviour of the actin network.

In a number of previous studies, it was reported that cells undergoing CIL first form an inter-cellular adhesion as they are coming in contact [138, 16, 17, 18, 19, 20, 21]. To assess what is happening at this crucial time of initial cell contact, we

expressed mCherry-Zyxin in colliding hemocytes as Zyxin was reported to be a marker of both cell-matrix and cell-cell adhesions [171].

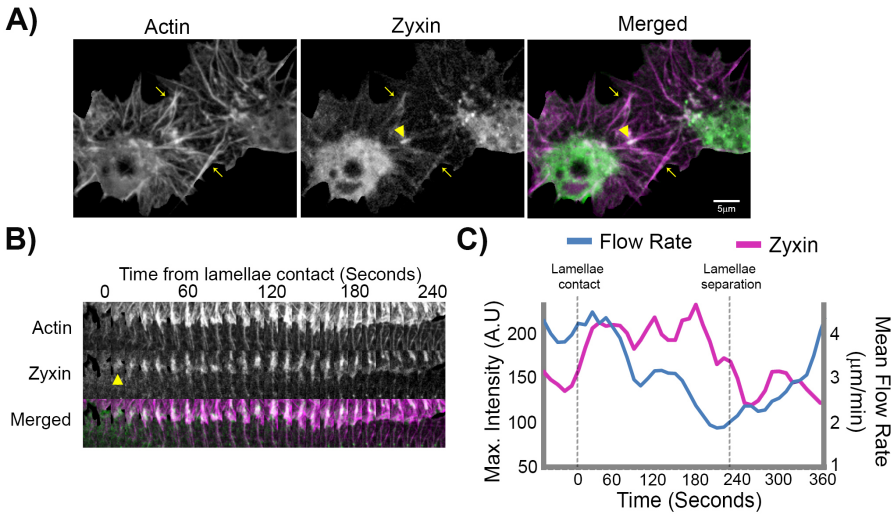

Figure 5.12: An inter-cellular adhesion develops between colliding hemocytes. A) Still image of a collision between hemocytes expressing mCherry-Zyxin (green) and labeled F-actin (magenta), which highlights the inter-cellular adhesion at the point of initial contact (arrowhead). Arrows highlight region of lamellar overlap. B) Kymograph of Zyxin and actin dynamics un the region of the actin fibre. Note the punctum of Zyxin (highlighted by the arrowhead) forms in line with the actin fibre and persists for the duration of the time in contact. C) Quantification of the maximum intensity of Zyxin and average actin flow rate during the collision. Figure recreated from [6].

To investigate if hemocytes are engaging in an inter-cellular adhesion during CIL, time-lapse movies with Zyxin and actin labelled were acquired at a rate of 10 seconds per frame. Colocalization of Zyxin-labelled adhesions and actin revealed that a punctum of Zyxin formed immediately upon lamellar overlap at the site of initial cell-cell contact (Figure 5.12). This Zyxin punctum did not form while cells were not in contact, suggesting that Zyxin is labelling an inter-cellular adhesion rather than a cell-ECM adhesion (Movie 13). Furthermore, kymography of the region surrounding the actin fibre in these movies showed that this punctum persisted for the entire duration of the response (Figure 5.12B; Movie 13). Further quantification of the maximum intensity levels of Zyxin fluorescence and the mean actin retrograde flow rate in a region surrounding the actin fibre from these time-lapse movies revealed that as the lamellae overlapped, there retrograde flow rate started

to decrease while the Zyxin levels stayed almost constant. As the cells separated, the retrograde flow rate increased while the Zyxin level dropped sharply (Figure 5.12C).

Further quantification of the actin retrograde flow within the lamella of colliding cells where Zyxin was also labelled revealed that the corridor of low retrograde flow was developing immediately after the appearance of the Zyxin puncta (Figure 5.13). These data suggest that the punctum of Zyxin is actually labeling a transient inter-cellular adhesion that is modulating the dynamics of the actin network through a mechanism similar to the integrin-based actin clutch encountered in migrating cells *in vitro* [103]. It could be that as the cells are coming in contact, they engage an inter-cellular adhesion which then restricts the movement of the actin network causing a reduction in the retrograde flow rate. Pseudo-speckle microscopy cannot be used to quantify the rates of actin polymerisation, therefore, I could not objectively assess if actin polymerisation is affected by the inter-cellular adhesion. However, visual inspection of colliding hemocytes suggests that the polymerisation machinery is not affected by the contact (Movie 9), but more work is required to confirm this observation.

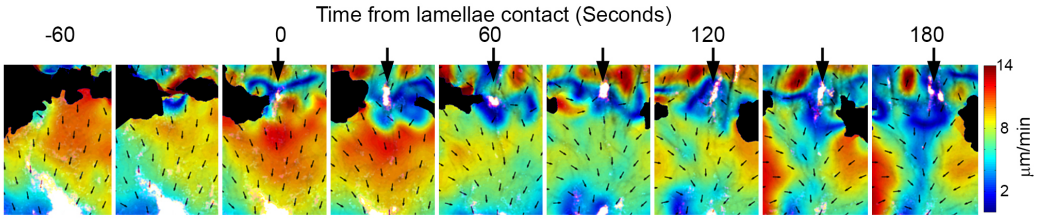

Figure 5.13: Low retrograde flow corridor develops in line with the inter-cellular adhesion. Comparison between the actin retrograde flow dynamics and the Zyxin localisation (pseudocoloured white). Note how the region of low retrograde flow develops right after the appearance of the Zyxin puncta at the site of cell contact (arrow). Figure recreated from [6].

In the previous section I showed that as hemocytes were colliding, the microtubule appeared to be using the developing actin fibre as tracks to direct their growth towards the edge of the cell. Microtubules are known to also target cell-matrix adhesions, actively contributing to their disassembly [37], however it is still unclear what role they play in disassembly of cell-cell adhesions. Thus, to investigate if mi-

crotubules are directed towards the cite of cell-cell contact, time-lapse movies with both Zyxin and microtubules fluorescently labelled were recorded at a frame of 10 seconds per frame.

Kymography of the region surrounding the microtubule bundle revealed that microtubules were polymerising toward the site of adhesion and appeared to target the Zyxin puncta (Figure 5.14A; Movie 14). Further analysis of the maximum intensity of Zyxin and microtubules at the region where the inter-cellular adhesion formed revealed that the microtubule intensity increased approximately until the cells separated when a sharp drop in intensity was observed. Furthermore, the intensity of Zyxin started to increase immediately after the initial contact and then decreased as the cells separated (Figure 5.14B). These data provide further support for the targeting of the inter-cellular adhesion by microtubules.

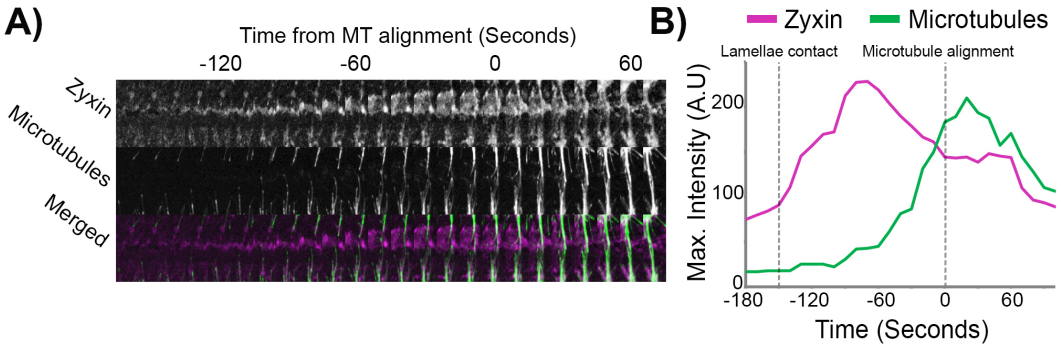

Figure 5.14: Microtubules target the inter-cellular adhesion during CIL. A) Kymograph of Zyxin and microtubule dynamics in the region of the actin fibre. Note the development of the microtubule bundle towards the Zyxin puncta. B) Maximum intensity of Zyxin and microtubules at the inter-cellular adhesion in the region highlighted in A). Figure recreated from [6].

5.5 CIL requires Myosin II contraction and stress fibre development

5.5.1 Myosin II contraction is crucial for the CIL behaviour

In section 5.2.1 I showed that Myosin II contraction is required for generating the retrograde flow dynamics within hemocytes. In addition, Mysoin II contraction is also crucial for normal hemocyte migration during *Drosophila* embryo

development, with mutant hemocytes lacking Myosin II resulting in an aberrant developmental pattern. Next I wanted to investigate the role played by Mysoin II contraction during hemocyte contact inhibition.

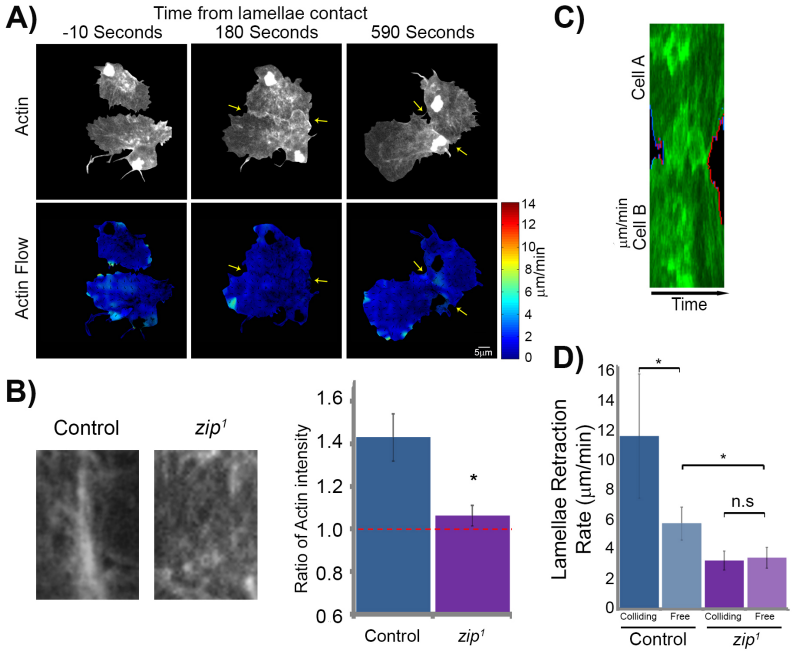

Figure 5.15: Myosin II mutant (*zip*^{1}) collisions. A) Top panels are still images from a time-lapse movie of hemocytes containing labeled F-actin during a collision. Bottom panels are heatmaps obtained using FLUPS showing no substantial changes in the retrograde flow. Arrows highlight the region of lamellar overlap. B) Quantification of actin fibre formation in control and *myosin II* mutant hemocytes during CIL. The graph represents the relative increase in the actin intensity within the region encompassing the actin fibre with respect to the surrounding regions of the actin network (see section 3.8.2 for further details on the method). C) Kymograph of lamellar activity in colliding partners in a region perpendicular to the point of cell contact (red regions highlight lamellar retraction, blue regions highlight lamellar extension). D) Quantification of the speed of lamellar retration in *myosin II* mutants at the time of separation. Note that the retraction rate in *zip*^{1} mutant cells was no different from the values encountered in freely moving cells. Error bars represent SD. $*p < 0.05$. Control retraction rates are taken from Figure 4.6. Figure recreated from [6].

To investigate the contribution of Myosin II to the CIL response, time-lapse movies of colliding hemocytes where both the actin network and Myosin II were fluorescently labelled were acquired at a frame rate of 10 seconds per frame. Visual inspection of these time-lapse movies and further quantification of the actin retrograde flow within the lamellae of *myosin II* mutant hemocytes during CIL revealed

that in contrast to control cells (Figure 5.5), *zip*^{1} mutants failed to reorganise their actin networks (Figure 5.15A; Movie 15).

Quantification of the actin intensity in the region of the *zip*^{1} mutant hemocytes lamella located approximately where the actin fibre developed within control cells, showed that mutant cells were also unable to develop an actin fibre (Figure 5.16B). Furthermore, measurement of the lamellar retraction rates using extension/retraction assay developed in this work (see section 3.7 for more details) revealed that *myosin II* mutant cells did not display increased lamellar retraction rates upon separation (Figure 5.15C and 5.15D). These data suggest that hemocytes require Myosin II to reorganise their actin cytoskeleton as they are undergoing a collision.

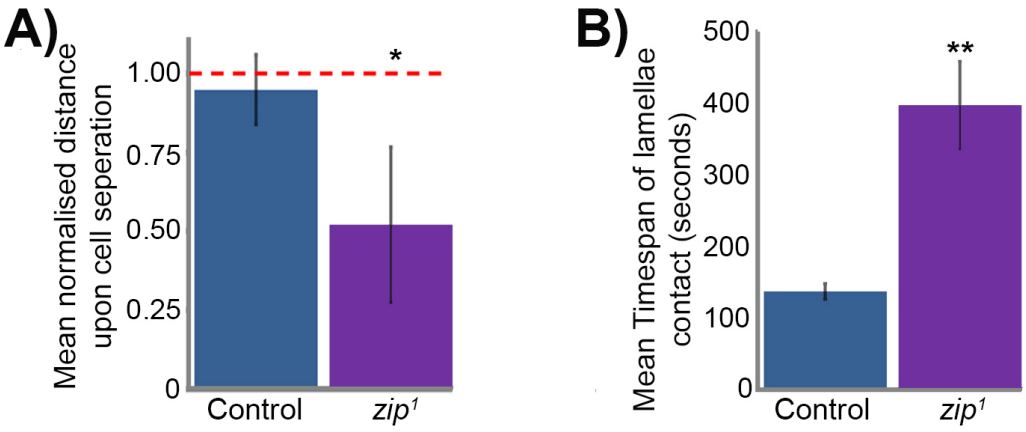

Figure 5.16: *zip*^{1} fail to inhibit their forward movement during CIL. A) Quantification of the cessation of forward movement during CIL revealed that *zip*^{1} mutants failed to inhibit their forward movement in comparison with control cells. Error bars represent SD. $*p < 0.05$. B) Graph of mean time of lamellae contact revealed that *zip*^{1} mutants maintained cell-cell contacts for a longer duration than control cells. Error bars represent SD. $**p < 0.01$. Figure recreated from [6].

An important part of the contact inhibition response is the cessation of forward movement upon contact. Evidence provided in this chapter suggests that *myosin II* mutant hemocytes move slowly overall and are unable to evenly disperse throughout the embryo (Section 5.2.1). These cells also displayed abnormal lamellar dynamics during CIL. Therefore, I next wanted to interrogate if these mutants also have any defects in their migration during the CIL response. To this aim, a cessation assay was developed to measure if cells stopped their forward movement after the

initial lamellae contact (see section 3.6.3 for details on how this quantification is performed). This analysis highlighted that *zip*^{1} mutant cells failed to arrest their forward motion upon contact, even more so, the cells continued to move forward which resulted in an increased time in contact (Figure 5.16). These data suggest that adequate levels of cellular contraction are required for a normal CIL response to take place.

5.5.2 An actin stress fibre couples hemocytes during CIL

Myosin II is required for a normal hemocyte CIL response (section 5.5.1). Thus, I wanted to further characterise the role of Myosin II during the response.

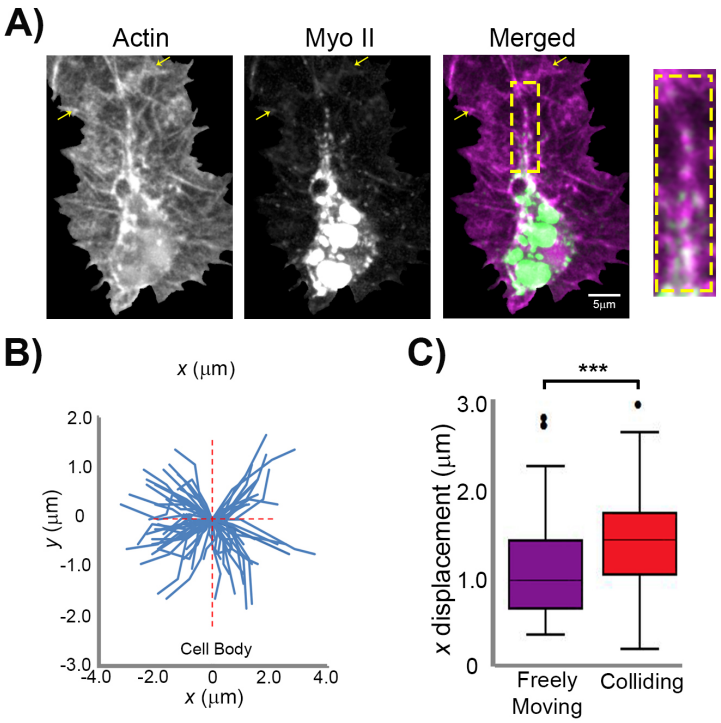

Figure 5.17: Myosin II dynamics during CIL. A) Still image of a collision between hemocytes containing labelled actin and Myosin II. Note the puncta of Myosin II along the actin fibre (inset). Arrows highlight the region of lamellae overlap. B) Quantification of Myosin II tracks for 40s upon lamellae overlap during CIL. C) Quatification of the lateral displacement of Myosin II particles from the tracks in Figure 5.2B and 5.17B. Notice the increase in horizontal displacement of Myosin II particles toward the actin fibre during collisions. $***p < 0.001$. Figures recreated from [6].

To this aim, time-lapse movies of colliding hemocytes where actin and Myosin II were fluorescently labelled were acquired at a temporal resolution of 10 seconds

per frame. Visual inspection of these movies revealed that after the initial lamellar contact, Myosin II puncta started to decorate the actin fibre that was developing between colliding partners (Figure 5.17A). Further quantification of the movement of these Myosin II particles by manually tracking these particles and then measuring their lateral displacement (see section 3.8.4 for more details on the quantification) showed that Myosin II particles also changed their flowing direction. Surprisingly, they reoriented to flow perpendicularly to the actin fibre, in a similar fashion to the actin retrograde flow (Figure 5.17B and 5.17C). Furthermore, as the cells separated, Myosin II puncta returned to moving in a retrograde fashion with the actin network (Movie 16). These data suggest that there is a strong connection between the flow of the actin network and the flow of Myosin II motors during CIL. Furthermore, visual inspection of the time-lapse movies of colliding hemocytes where both actin and Myosin II were fluorescently labelled revealed a defined accumulation pattern of Myosin II to the actin fibre. Quantification of the actin and Myosin II intensity within a region surrounding the actin fibre showed that as hemocytes are colliding, Myosin II accumulation follows the formation of the actin fibre (Figure 5.18). Furthermore, dividing the region surrounding the actin fibre into two sub-regions and subsequently measuring the intensity of Myosin II fluorescence in these two sub-regions revealed that Myosin II accumulation takes place from the back of the network, following the fibre as it develops towards the leading edge (Figure 5.17; Movie 16). Further quantification of Myosin II fluorescence in the region surrounding the actin fibre also revealed that Myosin II particles were decorating the actin fibre in a period pattern at $\sim 1.4\mu m$ apart (Figure 5.18A). Similar patterning of Myosin II along actin fibres has been reported for stress fibres *in vitro* [76]. Furthermore, analysis of the intensity of Myosin II puncta overlaid onto the quantification of the actin retrograde flow within a region of the lamella surrounding the fibre showed that as the actin fibre started to develop, Myosin II begun to accumulate in the center of the low retrograde flow corridor (Figure 5.18B). Kymography of the region surrounding the actin fibre also revealed that Myosin II accumulates along the actin fibre developing between colliding cells (Figure 5.18C).

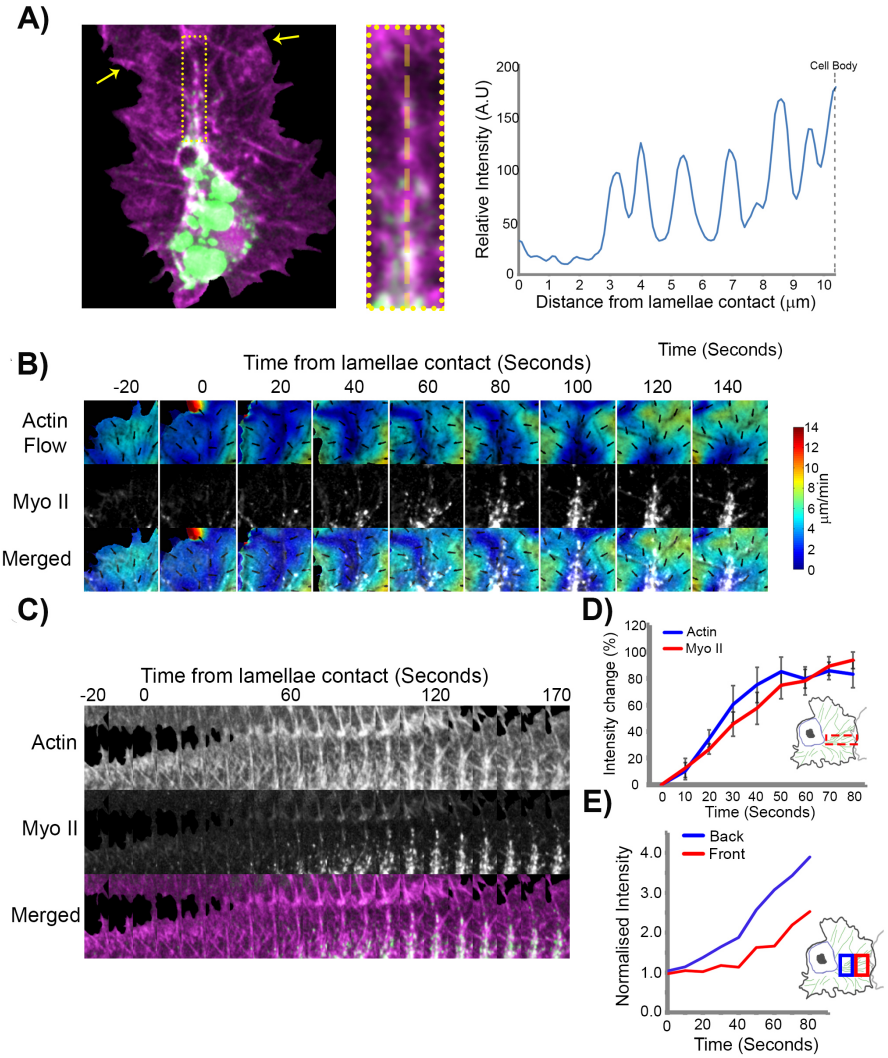

Figure 5.18: Myosin II decorates the actin fibre developing between colliding cells. A) Still image of a colliding hemocyte containing labeled F-actin (magenta) and Myosin II (green). Yellow arrows highlight the region of lamellar ovelap. The inset shows the region of the actin fibre used for the line scan analysis. Note the repeating peaks of Myosin II intensity along the fibre. B) Analysis of the actin retrograde flow dynamics in comparison with Myosin II localisation (pseudocoloured white) highlighting that actin reorganisation stars prior to Myosin II acumulation along the fibre. C) Kymograph of the region surrounding the actin fibre in 5.17A highlighting Myosin II accumulation during CIL. D) Quantification of the increase in actin acnd Myosin II intensity in the region corresponding to the actin fibre relative to values prior to lamellae contact. Error bars represent SEM. E) Quantification of Myosin II intensity in regions corresponding to the back versus the front of the actin fibre during a collision. Figure recreated from [6].

Further quantification of the actin and Myosin II fluorescence intensity in a region spanning the actin fibre revealed a synchronous increase in intensity compared

to values prior to lamellae contact (Figure 5.18D). Furthermore, quantification of Myosin II intensity in regions corresponding to the back and the front of the actin fibre showed that Myosin II accumulation starts at the back of the fibre, from the region surrounding the cell body (Figure 5.18E). These data suggest that the actin fibre that was developing was actually a stress-fibre like structure that coupled the two colliding hemocytes.

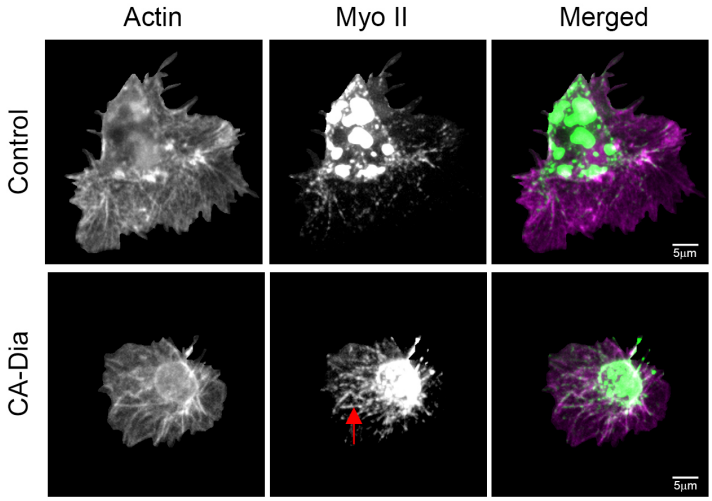

Figure 5.19: Expression of constitutively active Diaphanous affects cell area and Myosin-II localisation. Still images of control and constitutively active Diaphanous expressing hemocytes with labeled F-actin (magenta) and Myosin II (green). Note the decrease in area of hemocytes containing constitutively active Diaphanous and the enhanced Myosin II localisation within the lamella (arrow). Figure recreated from [6].

To confirm if the actin fibre developing between the two colliding hemocytes was an actin stress fibre-like structure, the localisation of Diaphanous (Dia), a formin that was reported to be crucial for the development of stress fibres within cells *in vitro* [76], was also analysed during the CIL response. The first experiment performed was to investigate the effects of expressing constitutively active Dia within freely moving hemocytes. For this analysis, time-lapse movies of freely moving hemocytes containing GFP-tagged Myosin II and actin were acquired at 10 seconds per frame. Visual inspection of these movies revealed that expressing constitutively active Dia within freely moving hemocytes caused cells to spread less than control cells and Myosin II excessively accumulated within the lamella which

resulted in periods of severe contraction of the actin network (Figure 5.19; Movie 17). These observations suggest that hemocytes could activate Dia to increase cellular contraction and implicitly the tension generated within the actin cytoskeleton (Figure 5.19).

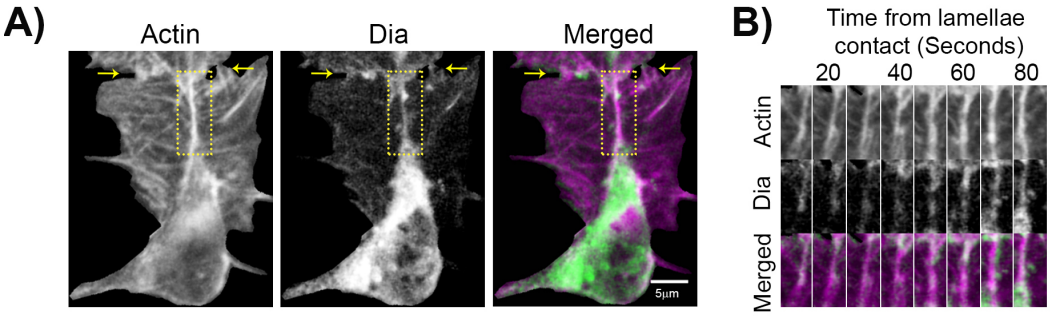

Figure 5.20: Diaphanous accumulation along the actin fibre. A) Still image of a collision between hemocytes containing labeled actin (magenta) and Diaphanous (green). Arrows highlight region of lamellae overlap. B) Kymograph of the region surrounding the actin fibre in A). Figure recreated from [6].

The increased cellular contraction displayed by freely moving hemocytes expressing constitutively active Dia and the development of the Myosin-II decorated actin fibre between colliding cells suggest that lamellar contraction is somehow involved in the CIL response. Thus, I next wanted to investigate the behaviour of Dia during hemocyte collisions. To this aim, a region surrounding the actin fibre, perpendicular to the leading edge, was analysed during CIL. Kymography of this region during the response for both actin and Dia channels revealed that Dia accumulated along the actin fibre (Figure 5.20). These results reveal that the actin fibre developing during CIL is indeed a stress-fibre like structure that couples the actin networks of colliding cells. Furthermore, stress-fibres are well both known force generating structures via the activation of Myosin-II driven contraction (see section 2.1.3) suggesting that during collisions force is developing and perhaps accumulating within the cytoskeleton of the two interacting hemocytes in order to guide their CIL response.

5.5.3 Importance of the actin stress fibre during CIL

During CIL, hemocytes are becoming coupled through a stress-fibre like structure that develops upon lamellar contact (see section 5.5.2). Therefore, I set to investigate what is the role of the actin stress-fibre during the contact inhibition response. To this aim I analysed the response in *diaphanous* (*dia*^{5}) mutants in both freely moving and colliding situations.

Diaphanous is suggested to be involved in the organisation of the actin cytoskeleton [172]. I next analysed the behaviour of freely moving *diaphanous* mutant hemocytes to investigate if these mutants have any defects in actin retrograde flow dynamics or other unexpected migration behaviour. For this analysis, time-lapse movies of *dia*^{5} mutant hemocytes expressing fluorescent actin and Dia were acquired at a resolution of 10 seconds per frame. The resulting movies were analysed using the pseudo-speckle program to quantify the dynamics of the retrograde flow within the lamella of these cells.

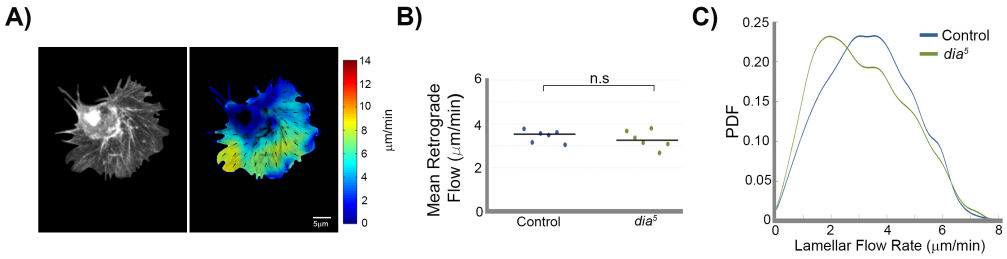

Figure 5.21: Analysis of freely moving *dia*^{5} mutant hemocytes. A) Left panel shows a still image of a freely moving hemocyte containing labeled F-actin. Right panel is an example heatmap with the actin retrograde flow field. B) Mean retrograde flow across the lamella of freely moving control and *diaphanous* mutant hemocytes. C) Probability density function (PDF) of the retrograde flow values within the lamella of freely moving control and *dia*^{5} mutant cells. Figure recreated from [6].

This revealed that freely moving *dia*^{5} mutants showed a qualitatively similar retrograde flow dynamics to control cells (Figure 5.21A; Movie 18). Further quantification of the average retrograde flow rate within the lamellae of these cells revealed no significant difference between the rates within mutant and control cells (Figure 5.21B). Analysis of the distribution of the retrograde flow speed highlighted the same trend, with no major differences between the distribution of the actin flow

speed between control and *dia*^{5} mutant hemocytes. These data suggest that although *Diaphanous* is missing, the actin retrograde flow behaviour is unchanged when compared with a wild-type situation.

As the actin network showed no aberrant behaviour within the lamella of freely moving *dia*^{5} mutant hemocytes, next I investigated if these mutants had any defects in cell migration. First the lamellar retraction rate was measured using the method introduced in section 3.8.3. This analysis revealed that there was no significant difference between the rate at which lamellae retract in freely moving *dia*^{5} mutant cells compared to control cells (Figure 5.22A). To assess if mutant cells experienced any defects in migration, the speed and directional ratio were quantified (see section 3.7 for further details). This analysis revealed that *diaphanous* mutant hemocytes were migrating with the same speed (Figure 5.22B) and displayed the same directional persistence (Figure 5.22C) as the control cells. These data suggest that *dia*^{5} mutant cell motility is not affected.

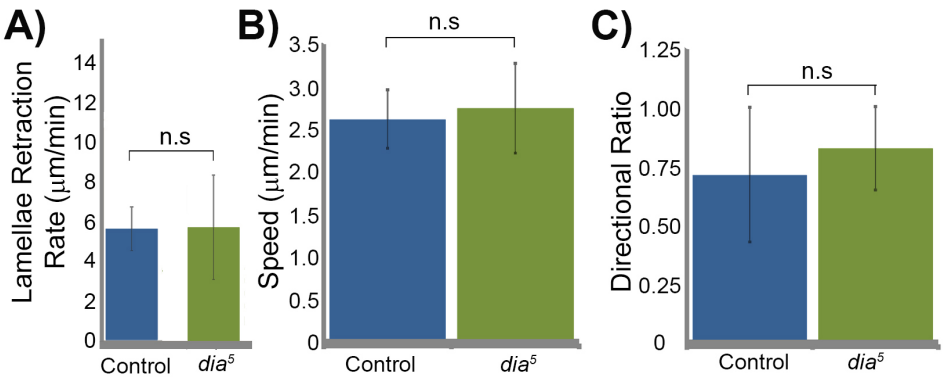

Figure 5.22: Quantification of *Diaphanous* mutant hemocytes migratory behaviour. A) Quantification of lamellar retraction rates for freely moving control and *diaphanous* mutant hemocytes. B) Quantification of cell speed in freely moving control and *diaphanous* mutant hemocytes. Error bars represent SEM. C) Quantification of the directional persistence of freely moving and *dia*^{5} mutant cells. Error bars represent SEM. Figure recreated from [6].

Visual inspection of time-lapse movies of *dia*^{5} mutant hemocytes undergoing a collision revealed a highly variable contact inhibition response (Movie 19). Surprisingly, quantification of the actin retrograde flow dynamics within the lamella of these cells showed a reduced capacity to coordinate they actin dynamics (Figure

5.23A).

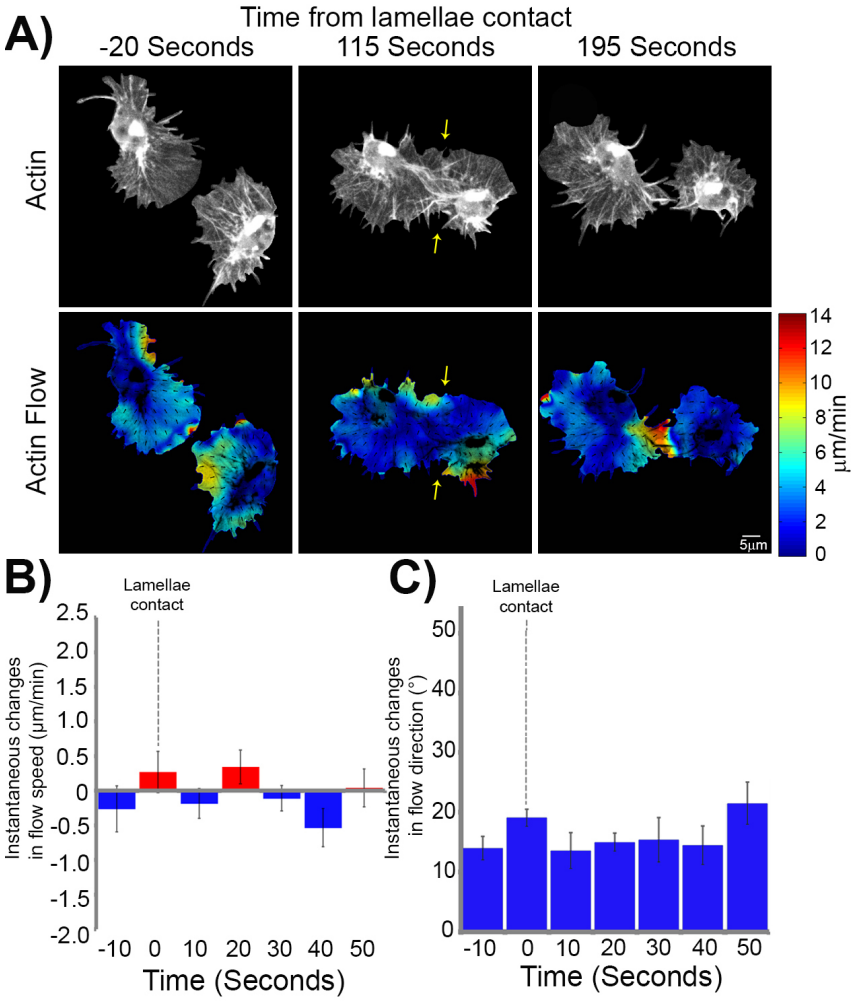

Figure 5.23: *dia*^{5} mutant hemocytes show aberrant CIL response. A) *diaphanous* mutant (*dia*^{5}) mutant collisions. Top panels show still images from a time-lapse movie of hemocytes containing labeled F-actin during a collision. Bottom panels are heatmaps obtained from the FLUPS analysis showing retrograde flow dynamics. Arrows highlight the region of lamellar overlap. B) Quantification of instantaneous changes in retrograde flow rate *dia*^{5} mutant hemocytes during CIL. Error bars represent SD. C) Quantification of the instantaneous changes in retrograde flow direction in *dia*^{5} mutant hemocytes during CIL. Error bars represent SD. Figure recreated from [6].

The same result was also highlighted by analysing instantaneous changes in flow speed and direction with reference to the time when lamellae first came in contact (Figure 5.23B and 5.23C). These data suggest that *dia*^{5} mutant hemocytes are not capable to reorganise their actin network upon contact.

Next I investigate if the failure to reorganise their actin network caused other

defects. Quantification of the actin stress fibre formation by measuring the actin intensity within a region surrounding the fibre showed that *dia*^{5} mutant hemocytes also failed to generate a stress fibre on average (Figure 5.24A). Furthermore, quantification of the mean distance upon separation as introduced in section 3.7 also revealed that mutant cells had a reduced capacity to cease their forward movement upon collision (Figure 5.24B) which resulted in an increase in the time spent in contact (Figure 5.24C). These data revealed that although the migration of freely moving mutant cells was not affected, *dia*^{5} mutant hemocytes display an aberrant behaviour during collisions which suggests that stress-fibre development is required for a normal CIL response.

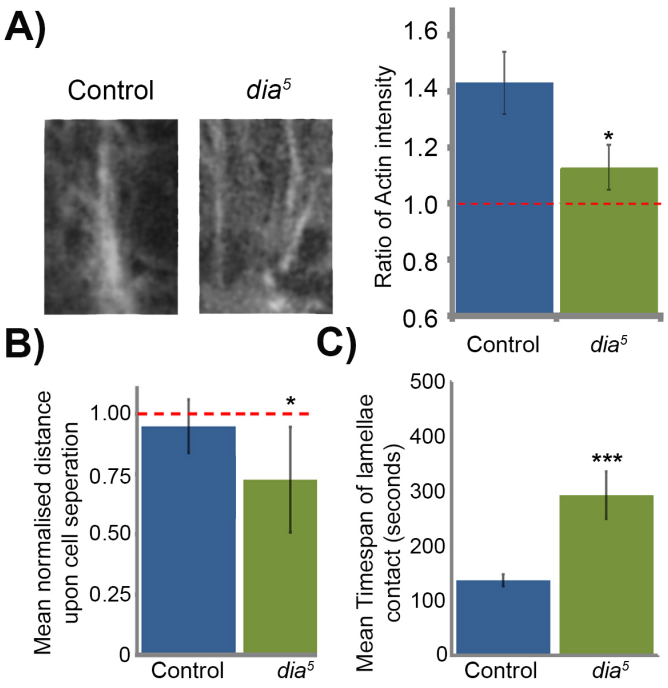

Figure 5.24: ***Diaphanous*** **mutant hemocytes aberrant behaviour during CIL.** A) Quantification of actin fibre formation in control and *dia*^{5} mutant hemocytes during contanct inhibition. The graph represents the relative increase in actin intensity within the region encompassing the actin fibre with respect to the surrounding regions of the actin network. B) Quantification of the cessation of forward movement during contact inhibition. Note the failure of *dia*^{5} to inhibit their forward movement in comparison to control cells. Error bars represent SD. $*p < 0.5$. C) Graph of the mean time of lamellae contact showing that *dia*^{5} mutants maintained cell-cell contacts for longer than control cells. Error bars represent SD. $**p < 0.01$. Figure recreated from [6].

Wild type hemocytes undergoing a collision became mechanically coupled by an inter-cellular adhesion developing immediately after lamellae contact.

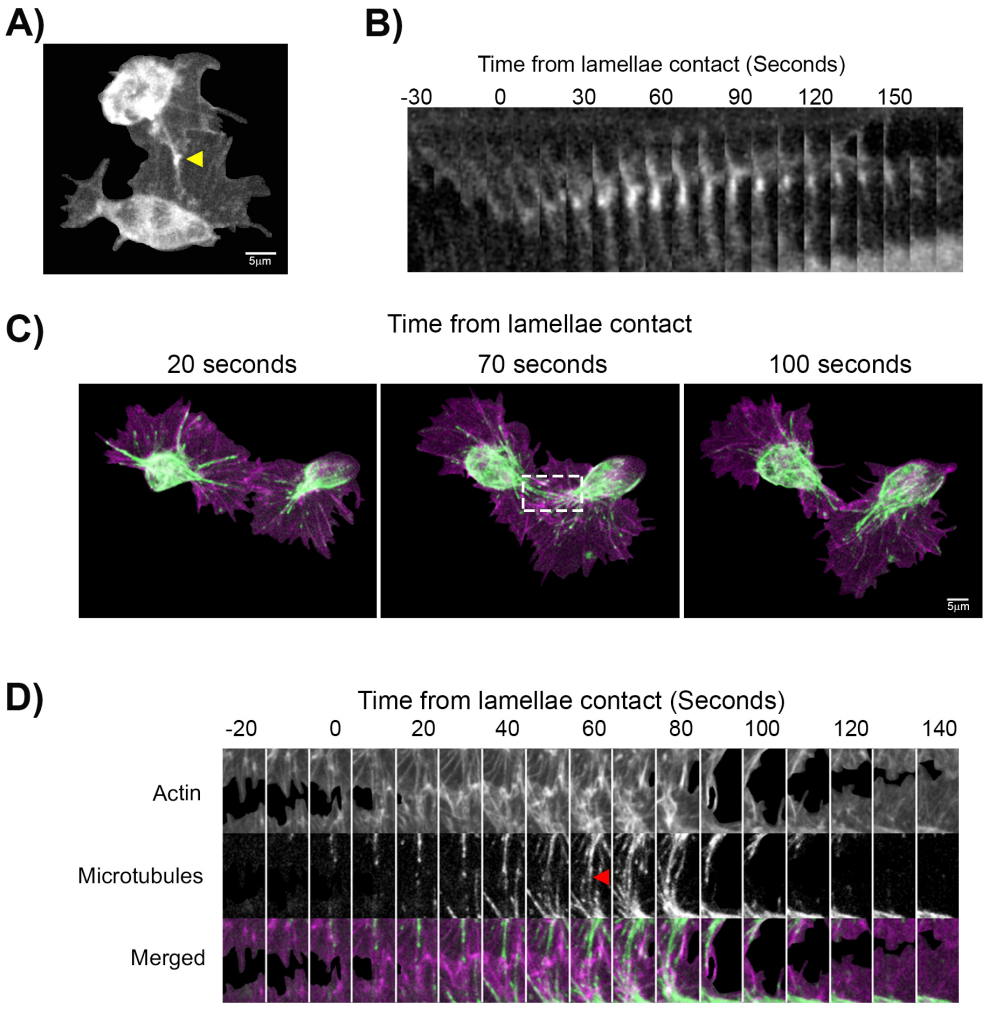

Figure 5.25: *Diaphanous* mutant hemocytes still form an intercellular adhesion, and align their microtubule networks during CIL. A) Localisation of Zyxin in *diaphanous* muntant hemocytes during a collision revealed that puncta of Zyxin (arrowhead) are forming at the site of cell-cell contact. B) Kymograph of Zyxin puncta during *diaphanous* mutant collision. Note the presence of Zyxin at the region of lamellae overlap throughout the time course of the response. C) A collision between *diaphanous* mutant hemocytes containing labeled F-actin (magenta) and microtubules (green). D) Kymograph of the region highlighted in (C) showing the alignment between the microtubule networks (arrowhead) in *diaphanous* mutant cells. Figure recreated from [6].

Interestingly, expressing Zyxin in *diaphanous* mutant hemocytes showed similar qualitative results as for control collisions, with a Zyxin labelled adhesion developing at the site of cell-cell contact. Kymography of a region surrounding the site

of cell-cell contact showed that the Zyxin puncta persisted throughout the response which confirms that a Zyxin labelled adhesion is developing at the cite of cell-cell contact (Figure 5.25 B) similar to control cells.

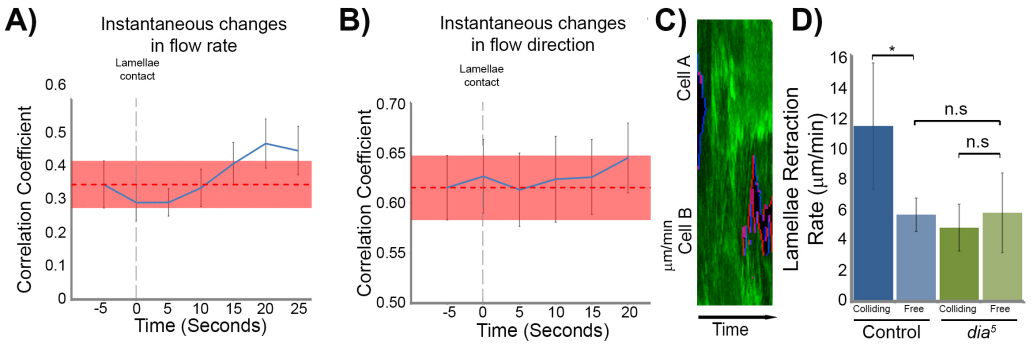

Figure 5.26: *Diphanous* mutant hemocytes fail to coordiante their cytoskeletal dynamics during CIL. A) Cross correlation of the instantaneous changes in flow rate in lamellae of colliding *diaphanous* mutant cells. Error bars represent SEM. Red dotted line represent the mean correlation between colliding cells immediately prior to cell-cell contact with the thickness representing the SEM. Note that unlike control cells (Figure 5.12), dia^5 mutant hemocytes do not show any increase in the correlation coefficient upon lamellae contact. B) Cross correlation of the instantaneous changes in flow direction in lamellae of colliding *diaphanous* mutant cells. Error bars represent SEM. Red dotted lines represent the mean correlation between colliding cells immediately prior to cell-cell contact with the thickness representing the SEM. Note that there is no increase in the correlation coefficient upon lamellae contact as observed in control cells (Figure 5.12). C) Kymograph of lamellar activity in colliding partners in a region perpendicular to the point of cell contact (red regions highlight lamellar retraction, blue regions highlight lamellar extension). D) Quantification of the speed of lamellar retration in *diaphanous* mutants at the time of separation. Note that the retraction rate in dia^5 mutant cells was no different from the values encountered in freely moving cells. Error bars represent SD. $*p < 0.05$. Control retraction rates are taken from Figure 4.7. Figure recreated from [6].

In control collisions, the microtubule bundles followed the developing actin stress fibres as they were growing towards the site of cell-cell contact. Visual inspection of time-lapse movies of dia^5 mutant collisions where both the actin and microtubules were fluorescently labelled revealed that to some extent microtubule bundles were still aligning between the two colliding partners (Figure 5.25C). Further kymography of the region surrounding the actin fibre in both colliding partners confirmed this observation (Figure 5.25D) suggesting that microtubule alignment

can still take place even in the absence of a fully developed actin stress fibre.

Analysis of the cross-correlation between instantaneous changes in speed and direction within a region of the lamella of colliding *dia*^{5} mutant hemocytes revealed that mutant cells did not show any increase in the mean correlation coefficient for either changes in flow speed or changes in flow direction compared to the values prior to the initial lamellar contact (Figure 5.26A and 5.26B). *Diaphanous* mutant hemocytes also failed to show any increase in lamellar retraction upon cell separation (Figure 5.26C and 5.26D). Kymography of the retraction/extension activity and subsequent quantification of the lamellar retraction rates (see section 3.8.3) for more details on the quantification) revealed that there was no distinction between the lamellar retraction rates of freely moving or colliding *dia*^{5} mutant cells. The measured values were significantly less than the ones obtained for colliding control cells which suggests that a certain level of lamellar tension is required for a normal CIL response. These data also show that although cells are able to eventually separate and migrate away from each other in the absence of the stress fibre, sudden lamellar retraction upon cell separation requires that the two colliding partners be coupled by a stress-fibre like structure.

5.6 Discussion

In this chapter I showed that the stereotyped sequence of kinematic steps coincides with significant global reorganisation of the actin cytoskeleton during the CIL response. I found that the process starts with the formation of an inter-cellular adhesion which coincides with the development of an actin stress fibre between the two cells. In control cells, a punctum of Zyxin appears when the two lamellae first come in contact and persists for the entire duration of the response (until cells break from contact). Furthermore, the formation of the Zyxin punctum coincides with the global reorganisation of the actin networks, most importantly the development of a low retrograde flow corridor and the formation of an actin stress-fibre like structure connecting the two colliding hemocytes. Furthermore, I showed that when Myosin II contraction is inhibited as in the zip1 mutant, hemocytes migration is affected,

the retrograde flow is severely affected, and cells do not undergo CIL. It would be interesting to investigate what happens with this inter-cellular adhesion in a situation when cell contractility is inhibited, such as in the zip1 mutant. Investigating the behaviour of this cell-cell adhesion, if it is even forming, could reveal more about the nature of the adhesion and the role it plays during the CIL response.

Previous studies of the role of actin during CIL had primarily focused on the cessation of ruffling at the leading edge following a collision. These studies suggested that as cells collide, they stop polymerising new actin filaments which leads to a paralysis of ruffling (see section 2.2). This aspect of contact inhibition is still unclear because, as Abercrombie observed, the cell-cell contact could impose additional mechanical and geometrical constrains that increase the strain at the leading edge leading to a cessation of ruffling [9].

The sudden and synchronised nature of the observed changes in retrograde flow suggest that the CIL response is not a simple passive reaction to the presence of the colliding partner, but a much more complex active process involving a dramatic global reorganisation of the actin networks across relatively large spatial and temporal scales. The orchestration of such a reorganisation event would involve very fast information transfer to and from the actin cytoskeleton over large distances. Considering how crowded the cytopasm is [31], it is unlikely that diffusion alone would not be fast enough to facilitate the rapid transport of information and matter that we observed during CIL. Therefore, the entire CIL process exploits the mechanical coupling and the subsequent changes in the geometry of the network to coordinate the response.

One interesting implication of the mechanical coupling of colliding cells is what happens with the two actin networks as the adhesion is established. Upon cell-cell contact, the actin networks begin to coordinate their dynamics which leads to synchronised instantaneous changes retrograde flow speed and direction until the cells separate (section 5.3). As the cells are in contact, they couple through a clutch-like mechanism that allows them to regulate the amount of force transmitted by engaging the actin cytoskeleton or not (see Section 2.1.4 and 2.1.5 for more details on

how the actin retrograde flow generates motile forces). Through this mechanism cells would engage their actin networks to start pulling on the other network instead of trasmitting the generated force to the substrate. Furthermore, I speculate that the adhesion connects the two distinct polymer meshworks into a single material. As a consequence, local changes taking place within the network can easily propagate throughout the network and coordinate across the two cells, facilitating the mechanotransduction of lamellar forces. It is possible that a similar mechanism is used by cells to orchestrate large scale cellular behaviours during embryogenesis, such as the coordination required for apical constriction during gastrulation [173].

Previous studies on the regulation of the retrograde flow have showed that as myosin II activity is inhibited and as such the retrograde flow rates slow down, the microtubules and leading edge extend at a greater rate suggesting that in control situations the microtubules are actually polymerising against the continuous actin flow being constantly pushed back or have their growth rate slowed down [87]. Furthermore, microtubules usually target cell-matrix adhesions, contributing to their disassembly either by increasing the local stress concentration [37, 79] or by delivering specific adhesion disassembly proteins [79]. In this section I showed that during collisions the retrograde flow is slowing down which facilitates the development of the microtubule bundle toward the site of cell-cell contact. It could be that microtubules play a similar role for cell-cell adhesions developed during CIL as they do for cell-matrix adhesions. If that is the case, then microtubules could be actively contributing to the disengagement of the inter-cellular clutch. As appealing as this might be, it is just a hypothesis for now and will require further investigations to resolve. However, these results clearly show that CIL is not just a passive reaction of the cell to the presence of the colliding partner, but a multifaceted process involving the active coordination of both actin and microtubules across multiple length and time scales.

In addition to the kinematics tools, I also adapted a pseudo-speckle technique to quantify the movement of the actin network *in vivo*. The basis of this tool have been independently established by Betz *et al* (2009) and Vallatton *et al* (2004) for mea-

suring the retrograde flow dynamics *in vitro*. My implementation comes equipped with several filtering and interpolation capabilities which confers it a greater degree of generality. The greatest limitations of this method compared to true speckle microscopy are three fold. First, being a grid based method limits its resolution to the size of the grid. The results are highly dependable on the size of the source and search regions of interest which means that the user is required to have some information about the behaviour of the network to ensure that accurate results are obtained. Second, as it employs correlations between successive frames to identify the movement of bright actin features, the method is unable to measure the displacement of the network for regions of the lamella that retract or extend from one frame to the next. This does not represent a major issue because hemocyte lamellar extension and retraction is not large over 5s intervals. Nevertheless, to correct for this, the resulting retrograde flow is interpolated from available data inside the cell.

Chapter 6

Lamellar Tension Orchestrates Hemocyte CIL

This chapter describes my investigations of whether the presence of Myosin II and the development of a stress fibre between colliding partners are causing an increase in the lamellar tension during CIL. I investigate the role of this tension for cellular collisions. Finally, in this chapter I explore the roles of contact inhibition during embryo development.

6.1 Contributions

My contribution was to develop the visco-elastic model for the stress redistribution and the subsequent analysis of the instantaneous changes in actin retrograde flow direction. I also developed the test to show that release of cellular tension is sufficient to induce the CIL response and I designed the assay for quantifying directional preferences in the motion of cells and conducted the kinematics and retrograde flow analysis for *dia*^{5} mutant cells.

I would like to mention both Dr John Robert Davis and Dr Timo Betz who have both contributed to the results I am presenting in this chapter. Specifically, Dr John Robert Davis conducted all the experiments (including imaging and laser abscission) and the simulations and subsequent analysis for the patterning experiments and contributed to various aspects of the data analysis and making of some parts of the figures.

Dr Timo Betz has been crucial in analysing the lamellar recoil and developing the elastic model for quantifying lamellar tension from the laser abscission experiment.

Finally, I would like to acknowledge the contribution of Fuad Mosis and James Thackery who manually segmented a large part of the movies used throughout this chapter.

6.2 Lamellar tension is increasing during CIL

As hemocytes were undergoing contact inhition, their actin cytoskeletons synchronously reorganise which leads to the development of an actin stress fibre-like structure between the two colliding partners. This actin stress-fibre like cable couples the two cells during the response (Figure 5.5 and 5.18). Furthermore, as cells separated there was also a sudden increase in lamellar retraction rates (Figure 4.6) which followed the global, synchronous reorganisation of the actin cytoskelton in both colliding partners. These data suggest that tension developed within the actin network during the hemocytes CIL response. Thus, next I directly tested this hypothesis. As it is well established that lamellar retraction rates are a good indicator of the preexisting tension in the lamellae [174], laser abscission of the actin cytoskeleton was performed and subsequently the lamellar recoil rates within a 12 seconds window after the ablation were analysed.

Prior to assessing the lamellar recoil during collisions, it was necessary to quantify the lamellar retraction rates within freely moving hemocytes. This analysis was required to establish a baseline for the lamellar tension. The leading edge was first ablated in freely moving cells where the actin cytoskeleton was fluorescently labelled. For these movies, one frame was acquired every second to ensure that the accuracy of the measured lamellar recoil rates is as high as possible. Kymography of the lamellar recoil upon laser abscission revealed that the lamella of freely moving hemocytes retracts with at a rate of $28.6 \pm 6.8 \mu m/min$. Quantification of the retraction rates upon ablation an actin fibre within the lamella of freely moving hemocytes indicated lamellar retraction rates of $33.2 \pm 4.3 \mu m/min$ which were sim-

ilar to the measured rates when ablating the lamellae edge (Figure 6.1A and 6.1B). Furthermore, this analysis also showed that the recoil rates were unidirectional, oriented towards the cell body (Figure 6.1 and Movie 20) which could be explained by the increased Myosin II contraction at the rear of the lamella [175, 176].

In contrast, laser abscission experiments for colliding hemocytes showed a completely different behaviour. When the region of lamellae overlap was ablated across the actin fibre linking the two cells the lamellae of both cells suddenly retracted. Quantification of this initial recoil rate showed that breaking of the cell-cell contact resulted in almost double the rate measured for freely moving cells, with the lamella retracting at a rate of $65.8 \pm 11.1 \mu m/min$. These data suggest that during CIL, lamellar tension stored within the actin network increased (Figure 6.1B and Movie 20) as the cells were becoming coupled by the actin stress-fibre.

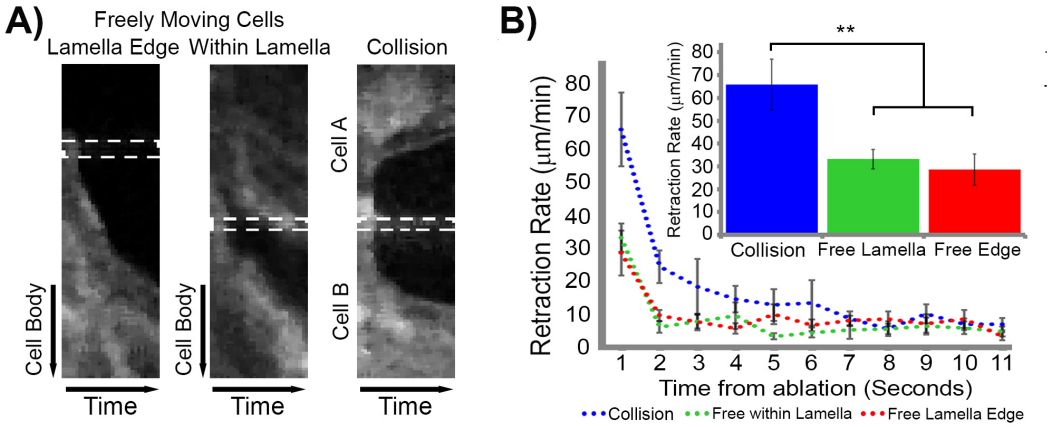

Figure 6.1: Lamellar recoil rates increase during CIL. A) Kymograph of lamellar recoil upon laser abscission of actin cytoskeleton in freely moving and colliding hemocytes. Dotted rectangle highlights the width of the ablation region. B) Quantification of lamellar recoil rate over time upon laser abscission. Error bars represent SEM. $** p < 0.01$. Figure recreated from [6].

Lamellar recoil rates are a good first approximation of the forces present in the lamella. However, to quantify the amount of tension stored within the actin cytoskeleton prior to the ablation, an adequate model is needed to link the measured strain rates to lamellar tension. Only the initial response is needed to determine the tension within the network after laser abscission, therefore the actin cytoskeleton can be considered to behave elastically as the time scale at which the lamellar

recoil rate was measured is of the order of seconds. To quantify the strain rate with the lamellar network after the laser abscission, the lamella edge was tracked for 12*seconds* after the abscission (see section 3.12 for details on strain rates and elastic forces).

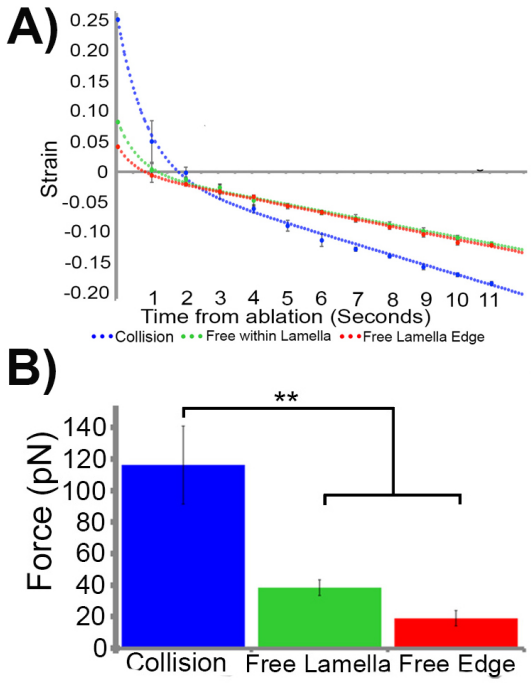

Figure 6.2: Lamellar tension increases during CIL. A) Quantification of lamellae strain over time upon laser abscission and modeled forces assuming that the actin network behaves elastically over short time scales. The elastic and dissipative mechanical properties in the lamellipodium are modeled by an exponential decay of the strain that is overlayed onto the constant retrograde flow. Note that zero strain represents the end of the exponential decay. Assuming mechanical properties similar to previously published lamellipodia we can estimate the tension. The strain, u is calculated by the ratio $\Delta l/l$. Error bars represent SEM $**p < 0.01$. B) Modelled lamellar tension immediately upon laser abscission assuming that the actin network behaves elastically over short time scales. Figure recreated from [6].

Subsequently, the measured strains were modelled using a fast exponentially decaying recoil, which was meant to recreate the sudden recoil upon laser abscission, overlayed onto a linear centripetal movement, which represented the constant pull of the actin retrograde flow. Applying this model to the experimental data revealed that the two actin cytoskeletons displayed a two-phase behaviour with a very sudden release followed by a linear response that continued throughout the duration

of the time-lapse movies (Figure 6.2A). Subsequently, using linear elasticity theory, the instantaneous strain rates were converted into lamellar tension by assuming that the actin cytoskeleton can be modelled as an elastic material (see section 3.10 for more details on the elasticity of actin networks) with the same elastic properties as the ones measured for neural growth cones *in vitro*. This assumption stemmed from the fact that hemocytes showed a qualitatively similar actin retrograde flow dynamics as ones reported for growth cones [170, 7]. This analysis revealed that immediately upon abscission of the lamellae there was a three-fold increase in tension when compared to the values obtained for freely moving cells (Figure 6.2B) which could explain the rapid exponential decay in the strain rates. These data provide direct support to the hypothesis that upon lamellar overlap, the actin cytoskeleton starts to ratchet up tension which gets released immediately as the two lamellae break contact.

6.3 Release of lamellar tension is sufficient to cause cell repulsion

During hemocyte contact inhibition, there was an increase of lamellar tension which followed initial lamellar overlap and lasted for the duration of the response. To investigate the role of forces developed within the actin network, I performed a kinematic analysis (see section 3.6 for more details on kinematics) of hemocytes immediately after laser ablation in three situations: the leading edge of freely moving cells, a mock ablation of collisions (see section 3.12 for further details), and ablation of the site of cell-cell contact. This analysis only measured cell velocity as it is the best indicator of the direction in which cells are migrating. To recreate the control situation, where velocity was computed with respect to position of the colliding partner, for this experiment the velocity was normalised with respect to the site of ablation, which also corresponds to the site of cell-cell contact in colliding hemocytes. This analysis revealed that immediately after the laser ablation was performed, colliding hemocytes started to move away from each other. Surprisingly, analysis of the response of freely moving cells and collisions where no ablation was

performed (i.e. mock collisions) did not show the same response. On the contrary, in these control situations, cells continued to move forward on average (Figure 6.3; Movie 21). These data show that release of lamelllar tension is sufficient to reverse the direction in which cells are moving, suggesting that forces are the main driver of CIL.

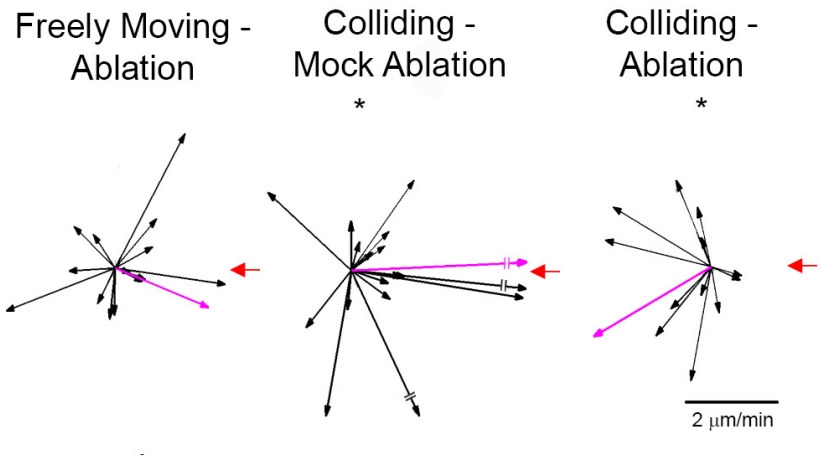

Figure 6.3: Release of lamellar tension is sufficient to induce CIL response. Hemocyte velocities in freely moving and colliding cells 60 seconds after laser abscission. The velocities were computed with respect to the position of the ablation site (red arrow). Magenta arrows represent the average direction of the sample. Note the significant forward movement after mock ablation, while ablation of the fibre during collisions led to significant rearward movement. $*p < 0.05$. Figure produced from [6].

6.4 Redistribution of lamellar stresses during CIL

During collisions Myosin II puncta propagated from the rear of the actin network towards the leading edge, decorating the actin fibre that developed between the two hemocytes (see section 5.5). As Myosin II motors are one of the main force generating mechanisms within the cytoskeleton, I next investigated if the lamellar tension also begins to build up from the rear of the network during CIL. To investigate the localisation of lamellar stresses (a proxy for lamellar tension), I adapted previously developed techniques for modelling the stresses developed within the actin cytoskeleton of migrating cells in *in vitro* [67, 7]. Briefly, if the rate at which the network is deforming over time (*i.e.* the actin retrograde flow rate) is known, then the stresses causing that deformation can be inferred by choosing a suitable

constitutive relation (i.e. a mathematical expression for how strain and stress are related) and elastic properties of the network. The former plays a key part in the validity of the model; however, because of the similarities between the measured actin network dynamics within hemocytes lamellae and growth cones *in vitro* (see section 5.2), I used the same constitutive relation as in [7] to map lamellar strain rates into stresses. This model assumed that at the temporal scales of interest for this study, the actin network behaved like a linear viscoelastic material (see section 2.1.7 and 3.10 for more details on viscoelasticity of actin networks) with the same viscoelastic properties as neuronal growth cones [7]. The choice of the model parameters is motivated by the pseudospeckle analysis of the actin retrograde flow which revealed that actin network within freely moving cells flows at a rate very similar to the ones measured for neuronal growth cones *in vitro* [170, 7]. Therefore, the first approximation I am making is that hemocytes cytoskeleton is as soft as growth cones over short second scales.

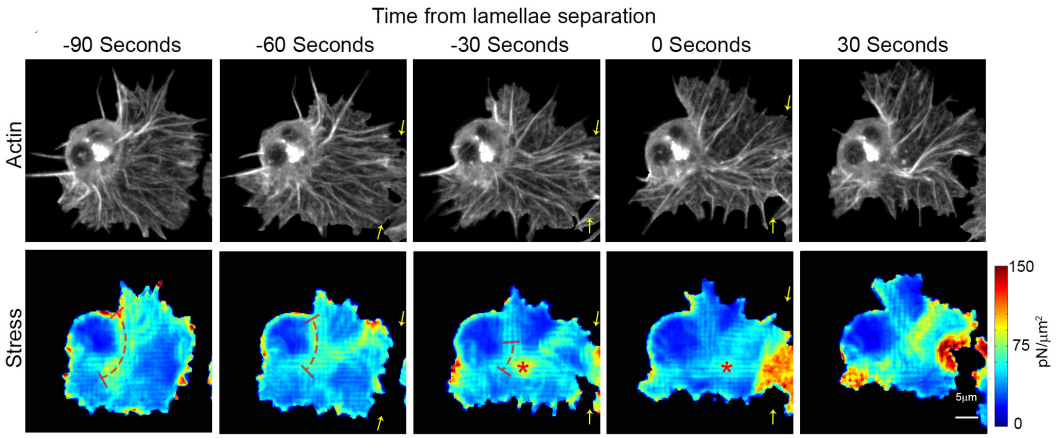

Figure 6.4: Localization of actin network stress during cell collision. Top panels are a time-lapse series of a hemocyte containing labeled F-actin undergoing a collision (adapted from Figure 5.5). Bottom panels are the modeled intracellular actin stresses. Note that stresses were only measured for regions of the lamella that persisted for a 40*s* period as deformation history is required in the analysis. Arrows highlight region of lamellae overlap. Dotted line highlights the redistribution of stresses around the cell body and asterisks the regions of high stress that colocalize with the actin fiber. Figure recreated from [6].

Furthermore, I considering that over long time scales, *e.g.* minutes, the actin network behaves like a fluid with the history of the deformation being lost after 40*s*.

I also assumed that the actin network has a Poisson's ratio of ~ 0.5 that confers the deformation a directional bias which is higher in the direction of the higher elongation. Finally, the cross-correlation between the instantaneous changes in actin retrograde flow observed during collisions, suggests that as the two cells are in contact, they behave like a single viscoelastic material which allowed for the model to be easily extended from single cells to colliding cells.

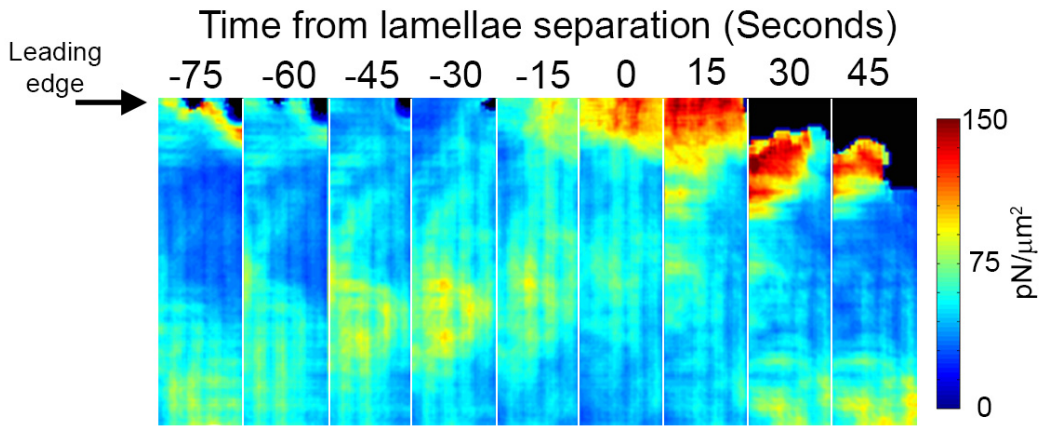

Figure 6.5: Lamellar stress propagation during CIL. Kymograph of lamellar stresses over the region that colocalized with the actin fiber. Note the redistribution of stress from the back of the network to the front. Figure recreated from [6].

Using solely these assumptions and the measured retrograde flow rates I was able to simulate the amount of stress present within the network. Kymography of heat maps summarising the magnitude of the lamellar stress developed during the response showed that most of the stress was localised around the cell body, at the rear of the lamella (Figure 6.4; Movie 22). Subsequently, as hemocytes were engaging in a collision, the stress started to propagate towards the site of cell-cell contact, along the low retrograde flow corridor from the base of the actin stress-fibre to more distal regions of it (Figure 6.5; Movie 22). Myosin is accumulating from the cell body towards the site of cell-cell contact (Figure 5.18) and as this is happening, more myosin starts to colocalize in the region of low retrograde flow and contracts, causing the observed increase in lamellar stresses starting from the rear of the cell. Furthermore, as cells separated, there was a second redistribution of the stress where lamellar stress propagated from the lamella to the region surrounding

the cell body (Figure 6.4; Movie 22).

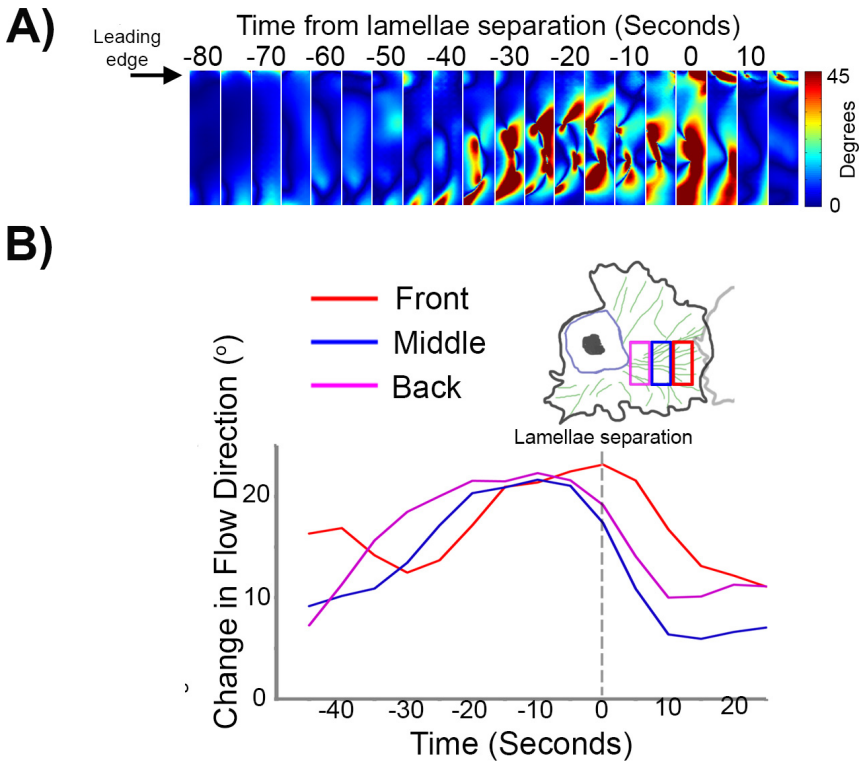

Figure 6.6: Network deformation starts at the rear of the lamella. A) Kymograph of the instantaneous changes in actin flow direction in the region colocalizing with the actin fiber. B) Quantification of the mean change in flow direction of the actin network in three regions corresponding to the back, middle and front of the actin fiber. Note that the changes initially increase in the rear of the network. Figure recreated from [6].

These data show that during collisions, stress is indeed redistributing from the rear of the lamella to the site of cell-cell contact which suggests that the cytoskeletal changes are propagating from the rear of the network. Analysis of the instantaneous changes in the direction of the actin retrograde flow during collisions revealed that the rear of the network is the first region where changes in directions are recorded. These changes are subsequently propagating towards the leading edge of the cell (Figure 6.6). The reorganisation starting at the cell rear coincides with myosin accumulation from the region around the cell body (Figure 5.18). This accumulation of myosin suggests that there is an increased contraction in the low retrograde flow region which triggers the subsequent reorganisation of the actin network. Furthermore, these data revealed that there is a redistribution of the forces from the rear of

the network towards the region of cell-cell contact.

6.5 Hemocyte developmental dispersal requires a precisely controlled CIL response

Up until now I showed that hemocyte CIL is orchestrated by inter-cellular forces developed within the actin cytoskeleton as cells were undergoing a collision (chapter 5 and sections 6.2 - 6.4). The release of this tension is playing a role in inducing the movement of cells away from the collision during a normal CIL response.

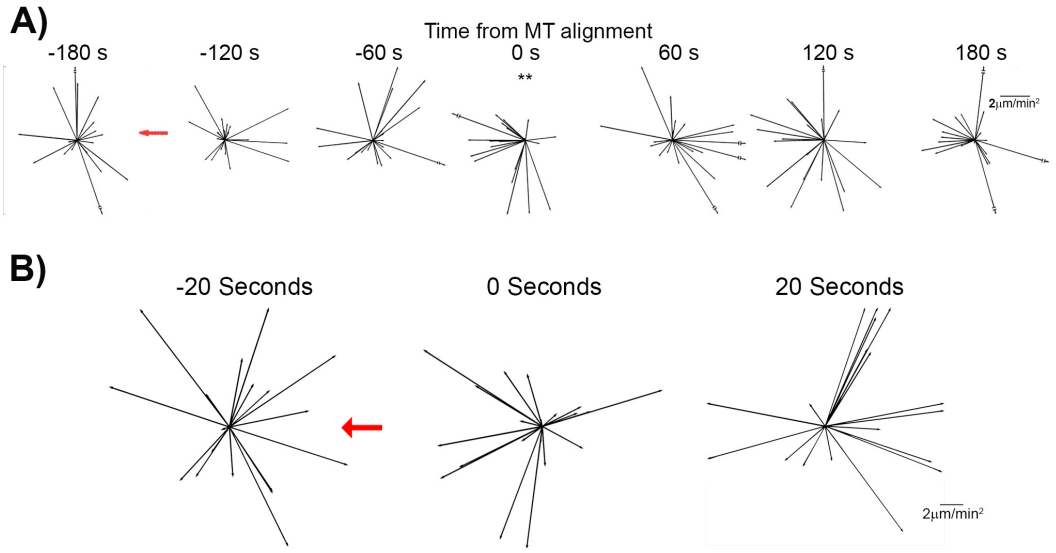

Figure 6.7: *Diaphanous* mutant hemocytes have an abnormal CIL kinematics. A) Time course of hemocyte acceleration in dia^5 mutants (black arrows) surrounding a collision event. The acceleration vectors are computed with reference to the colliding partner (red arrow). Note that all time points show random accelerations except for the time of microtubule alignment. $**p < 0.01$. B) Time course of dia^5 mutant hemocyte accelerations computed at $20s$ intervals (black arrows) surrounding a collision event. The acceleration is computed with respect to the location of the colliding partner (red arrow). Note that there is no significant back acceleration upon microtubule alignment. Figure recreated from [6].

Next I explored if CIL is required to be precisely coordinated during *Drosophila* development in order for hemocytes to acquire an even spacing within the embryo. Dia^5 mutant cells showed little coordination of their actin cytokeleton during CIL, therefore I set out to investigate if this also affected their migratory behaviour dur-

ing development. Analysis of the acceleration normalised to the direction of the incoming partner revealed that *dia*^{5} mutant cells do not undergo three distinct kinematic phases observed for control cells. Even if mutant cells showed a weak back acceleration upon microtubule alignment, this was only significant when computed at 60*s* (Figure 6.7), suggesting that *dia*^{5} repulsion is not as tightly controlled as for wild-type cells. To further investigate this observation, I quantified the movement of *dia*^{5} mutant cells after microtubule alignment. This analysis showed that mutant cells did not move away from their colliding partners. On the contrary, *diaphanous* mutant hemocytes continued to move forward (Figure 6.8) which resulted in an increase in the time they were in contact (Figure 5.26B).

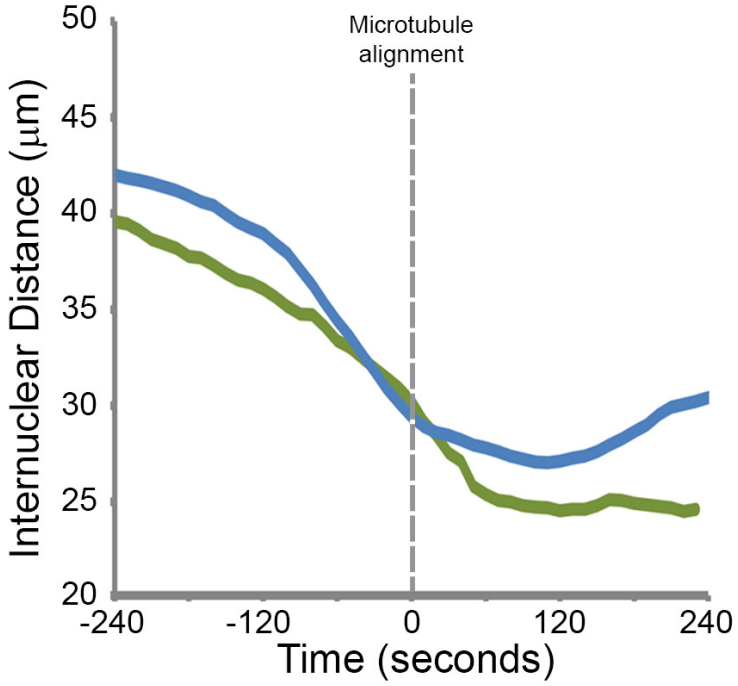

Figure 6.8: *Diaphanous* mutant cells fail to cease their forward motion upon collision. Analysis of the inter-nuclear distance over time during the CIL respons for control cells (blue line) and *diaphanous* mutant cells (green line). Note that unlike control cells, *dia*^{5} mutant cells have a reduced capacity to slow down upon microtubule alignment and subsequently separate. Control analysis was taken from Figure 4.4. Figure recreated from [6].

Kinematic analysis of wild-type cells showed that hemocytes migrate away from collisions 240*s* after the microtubule alignment. Naturally, as *dia*^{5} mutant hemocytes displayed aberrant cytoskeletal dynamics I investigated if their CIL kine-

matics was also affected. At the time when *diaphanous* mutant cells separated (approx 240*s* after lamellar overlap), cells did not show any significant directional preference with respect to their colliding partners. On the contrary, dia^5 mutant cells continued to move forward, completely ignoring the presence of their colliding partners (Figure 6.8).

These data suggest that dia^5 mutant cells failed to actively repel each other even if they retained some of the characteristics of a normal CIL response, such as partially developing an actin stress-fibre like structure during collisions (see sections 5.5.2 and 5.5.3). Furthermore, wild-type cells actively migrate away from the collisions 240*s* after the microtubule alignment (Figure 6.9A) (also the time when dia^5 separated) (Figure 6.8). However, dia^5 mutant cells did not show any significant directional preference with respect to their colliding partners (Figure 6.9). These data suggest that although dia^5 mutant cells retain some of the characteristic CIL features, they failed to actively repel each other.

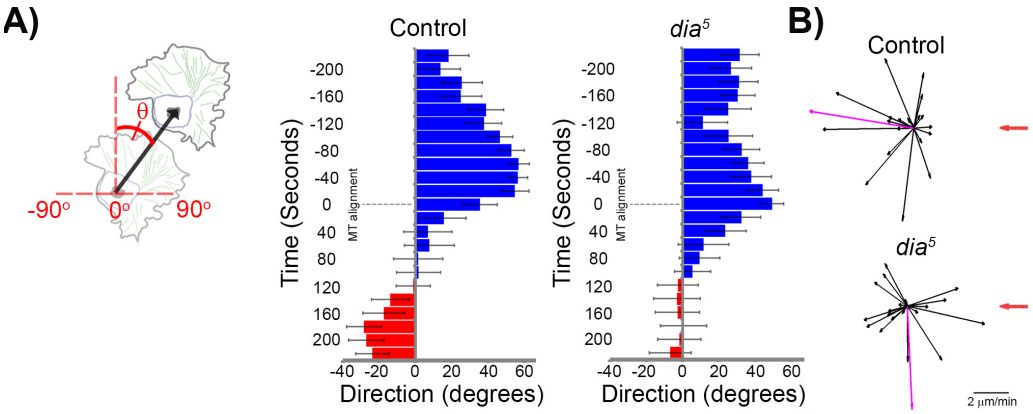

Figure 6.9: *Diaphanous* mutant hemocytes fail to migrate away from collisions. A) Quantification of the average cell direction during the CIL time course. Blue highlights forward movement and red movement away from the colliding partner. Error bars represent SD. B) Cell velocities at 240*s* after the microtubule alignment computed with respect to the colliding partner (red arrow). Magenta arrows show the resultant velocities for each genotype. Note that unlike control cells, dia^5 mutant hemocytes do not show a significant movement away from the colliding partner. $*p < 0.05$. Figure recreated from [6].

Previous results showed that hemocytes are capable of actively migrating away from collisions. However, it is still unclear if the inability of dia^5 to actively migrate from their colliding partners has any effects on their developmental dispersal,

specifically, their ability to make an evenly spaced pattern. To elucidate this question, first the average domains occupied by hemocytes during their migration were analysed. This analysis revealed that wild-type cells were moving within defined regions along the ventral surface of the embryo (Figure 6.10A), whilst *dia*^{5} mutant cells showed a more erratic movement. Although cells were capable of dispersing throughout the embryo, their final distribution is not uniform, with no clear domains forming along the entire ventral surface, by end of the stage 15 (Figure 6.10A and 6.10D; Movie 23).

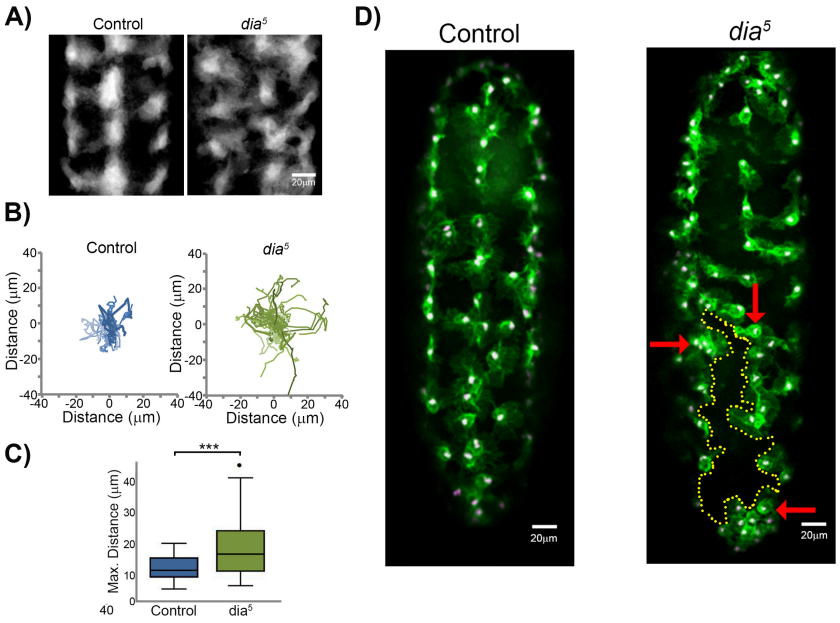

Figure 6.10: *Diaphanous* mutant hemocytes have an aberrant developmental dispersal. A) The average regions occupaied by hemocytes during their developmental dispersal revealed a disruption in the even spacing in *diaphanous* mutants. B) Tracks of hemocytes migrating over a 20*min* period after they have spread throughout the embryo. C) Quantification of the maximum distance hemocytes migrate from the tracks meansured in B). Note the increase in the distance traveled for *dia*^{5} mutants. $***p < 0.001$. D) (Left panel) Still image of wild-type hemocytes dispersed within the ventral surface of a Stage 15 *Drosophila* embryo containing labeled F-actin (green) and nuclei (magenta). (Right panel) Still image of *diaphanous* mutant hemocytes dispersed within the ventral surface of a Stage 15 *Drosophila* embryo containing labeled F-actin (green) and nuclei (magenta). Note the clumping of hemocytes (red arrows) with large regions devoid of cells (dotted line). Figure recreated from [6].

Further quantification of the maximum hemocyte displacement during the em-

bryonic stages of interest revealed that *dia*^{5} mutant cells migrated larger distances within the embryo than control cells (Figure 6.10C and 6.10D) suggesting that in the lack of coordination between the actin cytoskeletons of the two colliding cells allows them to be less constrained to move along the ventral surface of the embryo which results in an aberrant dispersal pattern.

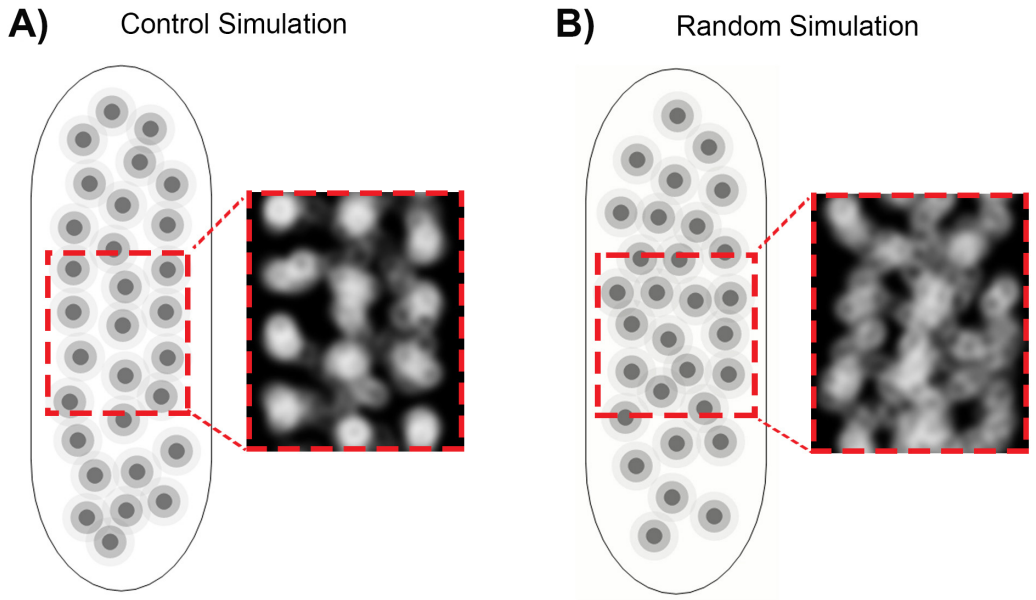

Figure 6.11: Hemocytes require CIL for their developmental dispersal. A) Still image of a control simulation (as generated in [5]) showing the even spacing of cells (left panel) which results in an evenly spaced domain map (right panel). B) Still image of a simulation in which the cells fail to consistently take into account the direction of the colliding partner during CIL. Note the aberrant spacing of cells (left panel), which results in a failure to acquire a defined domain map (right panel). Figure recreated from [6].

To further quantify the repulsion dynamics of *dia*^{5} mutant cells, the nearest neighbour distance was calculated for both control and mutant situations. This analysis revealed that *diaphanous* mutants had a reduced cell spacing as indicated by the decrease of the nearest neighbour distance (median = $17.5\mu m/min$ for controls and $15.8\mu m/min$ for *dia*^{5}, $p < 0.05$). These data provide further support for the hypothesis that precisely orchestrated repulsion dynamics are required for confining the migration of hemocytes to selected domains within the ventral side of the *Drosophila* embryo during development.

Previous mathematical modelling of hemocytes motile behaviour suggested that

CIL is essential for determining their normal dispersal [5]. In this model, the hemocytes were allowed to exist in two states: a freely moving state and a colliding state. In the freely moving state, cells follow a random walk, whilst in the collision state the cells care react to the presence of their colliding partner. Furthermore, the cells can switch between the two states based solely on the inter-nuclear distance (which was experimentally determined as $30\mu m$ [5]. Finally, to simulate the constant number of hemocytes on the ventral surface, the simulation used periodic boundary conditions. Using this simple two state model, [5] showed that perturbing the way in which cells are allowed to interact, i.e. reducing the sensitivity of a cell to it's colliding partner, resulted in an aberrant developmental pattern [5]. Therefore, simulations were next performed to investigate if the lack of directional preference with respect to their colliding partners upon separation observed for dia^5 mutant hemocytes could be related to the aberrant pattern previously observed. In contrast to previous studies [5], for the simulations created for the present work the sensitivity of the simulated cells to the direction of their colliding partners was randomised.

Analysis of the resulting dispersal patterning revealed when simulated hemocytes were allowed to randomly repel in the presence of another cell resulted in a similar aberrant domains (Figure 6.11; Movie 24) as the ones observed for dia^5 mutant cells. Further analysis of the spacing between the simulated cells lead to similar results where for cells that could randomly select values for ϕ between $[0,1]$. A median nearest neighbour distance of $23.8\mu m/min$ was measured as opposed to control simulations where the nearest neighbour spacing was $24.2\mu m/min$. The difference between the resulting cell spacing in both types of simulations, although small, was statistically significant ($p < 0.001$) suggesting that precisely coordinated collision dynamics is crucial for the normal developmental dispersal of hemocytes.

6.6 Discussion

In this chapter I have showed that the hemocyte contact inhibition response is controlled by the lamellar tension developed within the actin network during CIL. My current model suggests that as the two cells engage in a collision, their actin cy-

toskeletons become mechanically coupled by an inter-cellular adhesion which triggers a global reorganisation of the actin network that leads to a build up in lamellar tension during CIL. I speculate that it is the build-up of this force that causes the two cells to separate and subsequently repolarise to migrate away from the collision. Laser abscission experiments proved that release of lamellar tension is indeed sufficient to induce the contact inhibition response. This result suggests that intracellular forces developed as the cells are in contact could be a general conductor for orchestrating CIL. It would be interesting to investigate the dynamics of the retrograde flow and intra-cellular forces developed during the collision between other cell types.

The current model for contact inhibition postulates that as the two cells collide and adhere to each other, a signal is released at the site of cell-cell contact which then triggers the whole response. However, I showed that as hemocytes come in contact, they link with each other through a Zyxin-labelled adhesion that develops at the site of cell-cell contact. In the same time with the development of this adhesion, the actin cytoskeletons of the two colliding hemocytes undergo a global reorganisation, which happens synchronously in both cells. This global reorganisation takes place in short amount of time (see Section 4.3 and 5.3). During this time the actin retrograde flow rate significantly decreases leading to the development of a corridor of low retrograde flow. This behaviour was previously encountered in cells migrating in vitro and is consistent with an actin clutch-like structure coupling the two cells, similar to the ones developed between the cell and the ECM (see Section 2.1.5). Furthermore, within this corridor of slow retrograde flow, an actin stress-fibre forms which couples the two colliding cells. Finally, these changes in the retrograde flow and the actin network are accompanied by an increase in the intracellular tension. This increase in tension leads to a local concentration of stress propagating from the region surrounding the cell body (where most of the myosin II is found) to the site of contact. Furthermore, after the wave of stress reaches the site of cell-cell contact, a second reorganization event takes place when the actin retrograde flow rate suddenly spikes in both colliding partners and the local stress

redistributes back around the cell body. Around the same time, the cell-cell contact breaks, the leading edge collapses in both cells, the actin stress fibre disappears leading to the hemocytes starting to migrate away from the collision. Maybe as the intracellular forces increas, they reach a level so high that the actin cytoskeleton is unable to sustain leading to it suddenly "breaking". A similar behaviour has been reported for actin networks in vitro where densely cross-linked F-actin networks subjected to high stresses broke when the stress reached a certain threshold value [177]. Another possibility is that as the stress fibre starts to develop it induces a redistribution of myosin along the fibre which triggers a wave of contraction from the cell body to the leading edge. Eventually this myosin induced contraction causes a spike in lamellar tension that could lead to the break of the adhesion between the two colliding hemocytes. This spike in contraction could also trigger a wave of disassembly through the network, which might serve as a signal to start producing protrusions in it's wake, causing an asymmetry in the network that causes the cell to repolarise and migrate away from each other. It was previously shown that myosin can induce global network reorganisation by enhancing network disassembly [1]. It is still an open question on how myosin promotes disassembly which I believe would be a very interesting avenue of research in the future. These findings show that the whole CIL response requires a high degree of coordination both internally, between the actin and microtubule networks, and externally between the two colliding partners. These data suggest that, at least in hemocytes, the contact inhibition of locomotion response is mechanically controlled. The precise nature of the response together with the synchrony of the large scale changes I observed cannot be simply explained solely by the release of a signalling molecule at the site of cell-cell contact. If that would be the case, then this signalling molecule would need to start different signalling cascades that would affect both the actin and the microtubules cytoskeletons synchronously in both cells. Furthermore, all the changes I observed begin in the region surrounding the cell body, which means that signals have to travel from the leading edge to the cell body and then trigger the response. Finally, the sudden increase in retrograde flow coupled with the spike in intracellular force

and the collapse of the leading edge at the time when cells break from the contact, suggests that the signalling cascade would also need to amplify lamellar contraction, stop actin polymerisation at the leading edge, and simultaneously signal to the actin cytoskeleton to start polymerising away from the other cell. It is my opinion that this behaviour is too complex to be explained by the release of a signal. It is far more likely that all the changes I observed are triggered by mechanical stimuli that enable information to be coordinate and transmitted and interpreted across larger scales both inside and outside the cells. Such a mechanism was previously shown to induce global network reorganisation through increased myosin II mediated forces that enhanced network disassembly and promoted cellular movement[1]

There is still an important open question that needs to be addressed in the future: how are microtubules contributing to this response? One possible role might be to target the inter-cellular adhesion and stop it from forming into a stable adherens junction and as such allowing the two cells to separate. I speculate that in the absence of a viable mechanism for breaking the inter-cellular adhesion the cells would not be able to separate. It could be that the actin cytoskeleton provides the machinery for synchronizing the behaviour of the cells whilst the microtubules are aiding with the disengagement of this connection once the two actin networks have been synchronised. In a purely theoretical thought experiment, imagine that the cells are not capable of breaking the adhesion, the actin cytoskeleton could serve as a way of synchronising the behaviour of the cells across multiple scales, conferring the resulting tissue structural homogeneity.

To investigate the role of forces during contact inhibition we experimentally perturbed the collision by laser abscission and measured the resulting recoil rates. This experiment yielded a good estimate of the instantaneous strain existent in the network immediately prior to cell separation. Surprisingly, a simple strain model fits the data almost perfectly, suggesting that the recoil observed could indeed be explained by a combination of a rapid release of stress and a constant ”pull” from the retrograde flow. Further mathematical modelling of the elastic stress revealed that as the adhesion between cells breaks, there is a significant increase in lamellar

tension to about three times the values encountered in freely moving cells. For this model the actin cytoskeleton was assumed to behave like an elastic material. This is a reasonable assumption as several studies have already showed that actin networks both in solution and *in vitro* have elastic characteristics at a sub minute temporal resolution [1] which is a lot longer than acquisition rate used for this experiment. Furthermore, for this elastic model it was assumed that the actin network within hemocytes has the same elastic properties as for growth cones. It is important to note that this assumption only affects the absolute value of the force, not the difference between freely moving and colliding conditions.

As mentioned earlier, I also employed a linear viscoelastic model to convert the measured retrograde flow rates into intracellular stress, similar to other models that have been used to investigate the amount of tension present inside the actin cytoskeleton of different cell-types *in vitro* [67, 7]. As with the elastic case, this model also assumes that the actin network has the same properties as for growth cones. The justification for this assumption stems from the fact that both hemocytes and growth cones have very similar retrograde flow dynamics. Furthermore, changing the parameters of this model would not have any effects on the relative values of the stress. One potential fallacy of this model could be that I assumed that the two actin networks become mechanically coupled during contact inhibition and as such can be considered a single lamella. I made this assumption because immediately upon lamellar overlap, an inter-cellular actin clutch develops which couples the two cells and synchronises the dynamics of the two actin networks.

Finally, in this work I showed that contact inhibition is a positive migratory cue for hemocyte developmental patterning. Disruption of contact inhibition leads to aberrant patterning with cells failing to evenly distribute themselves along the ventral surface of the embryo. This observation confirms an earlier observation made by Davis and collegues where they showed that randomising the sensitivity of the cells to the presence of the colliding partner *in silico* generated aberrant dispersal patterns [5]. Furthermore, hemocytes are the main producer of proteins required for the basement membrane formation [154]. A role for this even dispersal pat-

tern might be to ensure that collagen is evenly distributed within the embryo as fast as possible as diffusion alone would be insufficient to allow for the basement membrane formation in time with other developmental events that take place at this developmental stage.

Chapter 7

Discussion

In this work I showed that hemocyte contact inhibition is precisely regulated, and that cellular behaviour upon collisions is not just a stochastic response to the contact with another cell involving a stereotypical sequence of events. Furthermore, both hemocyte collision and subsequent repulsion are differentially modulated by the actin and microtubule cytoskeletons. Changes in each of these networks are synchronised between the two colliding partners throughout the duration of the process. The orchestration of hemocyte CIL relies on a transient inter-cellular adhesion physically coupling the two colliding hemocytes via a clutch-like mechanism similar to the one employed by cells to sense the substrate on which they migrate on and to generate the traction stresses that allow them to move. In response to this mechanical coupling, the actin cytoskeleton ratchets up tension which ultimately leads to cells separating and subsequently repolarising. It is this inter-cellular clutch and the associated mechanical response that sets the scene for the precise orchestration of cellular behaviours during contact inhibition of locomotion (Figure 7.1).

An inter-cellular adhesion connecting the two colliding cells is a characteristic of contact inhibition in several cell types [138, 178, 20]. Recent work investigating the nature of these intercellular adhesions during CIL revealed that several cadherins, including E-cadherin and N-cadherin [137, 16, 19], and a wide range of accessory proteins involved in the formation of stable adherene junctions, such as β-catenin, p120, vinculin, and α-catenin, appear to be involved in CIL [137, 178]. For example, in *Xenopus* and zebrafish neural crest cells, repulsion was inhibited

by switching between the active cadherin isoforms. These studies showed that cells expressing E-cadherin remain in contact after they collide, whilst cells expressing N-cadherin undergo a repulsion event. These data suggest that different cadherin isoforms could be triggering different signalling cascades involving p120 and smallGTPases that lead to cells switching between a repulsive and adhering state [137]. Further evidence for the role played by adhesions during CIL came from studies investigating the Eph-ephrin signalling between prostate cancer cells and fibroblats [11, 22, 23, 179, 13]. These studies showed that prostate cancer cells *in vitro* can switch between a repulsive behaviour during homotypic collisions to a non-repulsive one during collisions with fibroblasts by tweaking their Eph-ephrin interactions. For example, during homotypic collisions the prostate cancer cells express EphA which promotes their repulsive behaviour. In contrast, during collisions between prostate cancer cells and fibroblasts, EphB signalling was active which suppress CIL [11, 22, 23, 179]. Clearly, the adhesion developing between colliding cells during CIL is detrimental for the whole response. Nevertheless, much remains to be said about its exact nature and how different cell types expressing different intercellular adhesions are capable of exhibiting the same repulsive behaviour. It would be interesting to investigate if there are any structural differences between the actin networks within these different cell types or if the adhesion complexes involved in CIL show different behaviour when subjected to mechanical forces. For example, it could be that different adhesion molecules can sustain higher stress before breaking which would lead to cells never migrating away from a collision as their actin cytoskeletons would be incapable of generating high enough intercellular forces to disengage the adhesions.

Another interesting aspect about the inter-cellular clutch connecting the two collidng hemocytes is that it appears very similar to the actin organisation between epithelial cells where a stress fibre develops perpendicularly to the leading edge. Furthermore, this alignment is preceded by an initial punctate adhesion developing between epithelial cells prior to their maturation into cadherin-based cell-cell junctions (known in the literature as focal adherens junctions [180]). This speculation

stems from the observation that development of focal ahderens junctions is both tension dependent [181] and involves a radial actin bundle perpendicular to the leading edge [182, 178]. Furthermore, cadherins were also observed to flow centripetally with the actin network in both astrocytes and fibroblasts [183] which could mean that an actin clutch-like mechanism involving cadherins is developing at cell-cell adhesions to facilitate their maturation into adherens junctions [99]. Based on these observations, it would be interesting to study what causes this difference in adhesion maturation where contact inhibiting cells exploit the inter-cellular adhesion to actively repel while in epithelial cells it leads to a stable connection. I believe it is interesting to investigate if the different contact inhibition responses observed between cells of the same or different cell types are a consequence of the different physical properties of the adhesion molecules and how they respond to tension.

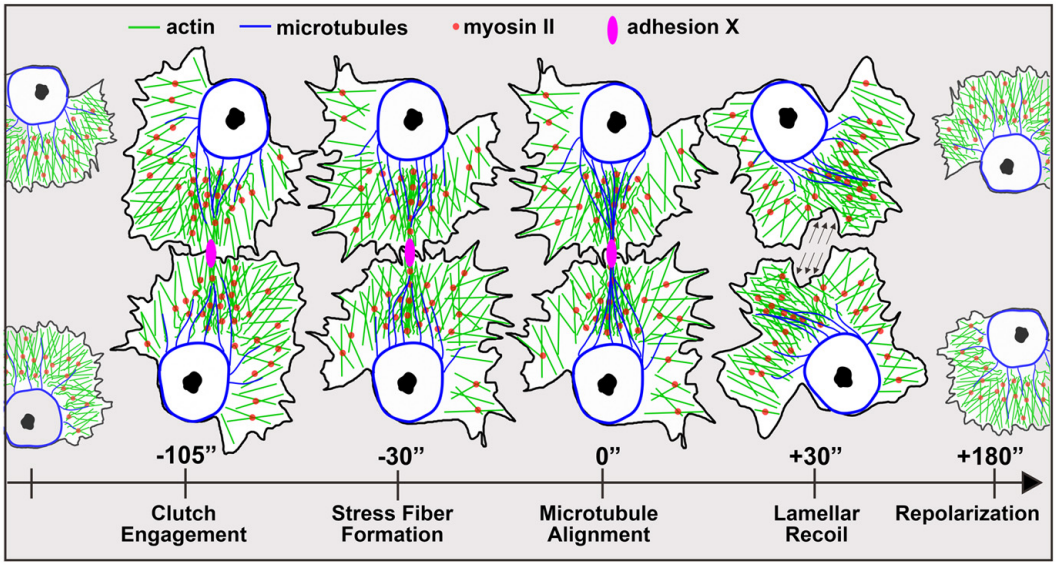

Figure 7.1: Schematic highlighting the main events taking place during hemocytes CIL.

Cell-cell junctions have been receiving a lot of attention in recent years, however there is to a lot of speculation about the existence of an inter-cellular clutch mechanism that would couple adjacent cells [99]. Furthermore, recent work on apical constriction during gastrulation also suggested that a ”clutch-like” adhesion together with acto-myosin contraction are directing the process [173]. In this work I showed that an inter-cellular adhesion serves a double role of coordinating the

inter-cellular responses and the intra-cellular dynamics leading to a synchronised response in colliding cells. I believe that as apical constriction, and possible any other process that requires a fast, coordinated response across large length scales such as rapid directional changes during white blood cell migration, could rely on a similar clutch-like mechanism for modulating and integrating the forces [184].

After the establishment of the inter-cellular adhesion, the actin networks are undergoing fast and synchronous reorganisation. This reorganisation begins immediately upon lamellar contact, with the development of a stress-fibre like structure between the two colliding cells. As the fibre is developing, the actin network is also slowing down creating a low flow corridor further facilitating the development of the fibre. Perhaps an even more surprising effect is the very sudden change in actin retrograde flow direction from a centripetal motion to perpendicular to the stress fibre. I hypothesise that this is possibly due to the high concentration of myosin II along the fibre which when activated contracts and ”pulls” the actin network towards the fibre. As the cells separate, the actin networks undergo another significant global reorganisation, with the retrograde flow rate suddenly and synchronously increasing in both cells as their lamella break from the contact. It would be interesting to investigate the interplay between network assembly and disassembly during CIL. In recent years it has emerged that the actin cytoskeleton behaves more like an active material, being constantly out of equilibrium (see section 2.1.7 for a short introduction to this topic). However, how much of the reorganisation I observed during CIL is due to an active remodelling of the network versus a passive response to the engagement of the inter-cellular actin clutch is still a topic under discussion.

Lamellar tension starts to increase immediately upon the engagement of the actin clutch. I have shown that upon the establishment of this adhesion, the actin networks start to ratchet up tension which could be causing the forward acceleration I observed upon lamellar overlap. Chick heart fibroblasts show a similar forward acceleration during collisions [9] which suggests that there is some degree of generality of the response, at least among cells undergoing a Type 1 CIL where cells undergo a lamellar contraction event upon cell-cell contact and subsequently repel

each other. This increase in intracellular tension might also directly contribute to the formation of the transient actin stress-fibre that spans the two colliding cells as it has been shown for other cell types [76]. I believe that the main role of this stress fibre is to act as a mechanosensor, creating a haptic feedback mechanism that allows cells to ”pull” on each other during the response. Until now there have been no similar mechanisms reported for cell-cell interaction. However, a similar mechanism is thought to be involved in substrate sensing, where cells are able to modulate their mechanics based on the stiffness of the extracellular matrix [185]. Furthermore, this stress fibre is embedded in the actin network and as such could cause network wide reorganisation while it is contracting similar to the ”contractile treadmilling” observed toward regions of actomyosin contraction in fibroblasts [186]. From a mechanics point of view, it is still unclear how this reorganisation of the cytoskeleton takes place during CIL. I suspect that the initial mechanical input serves as an activator for further signalling which might enhance actin kinetics and/or redistribute cross-linkers, essentially changing the physical properties of the network. Alternatively, it is possible that when the cells lamellae collide, an intercellular adhesion forms which releases a signal at the site of cell-cell contact that triggers the activation of different signalling cascades involving smallGTPases such as RHO, RAC, and CDC42 and terminating with the repolarisation of the cells. For example, RAC1 activity is inhibited while RHOA is activated in colliding neural crest cells. Several studies showed that the inhibition of RAC1 activity leads to the activation of RHOA via the PCP signalling cascade which in terms activates the cotraction of protrusions through a RHOA-ROCK signalling cascade that leads to cells repolarising and migrating away from each other [137, 4, 142, 187].

In parallel to the reorganisation of the actin cytoskeleton, and possibly helped by it, the microtubules also polymerise into the region of low retrograde flow. In several cell-types it was suggested that the actin network is somehow connected to microtubules, with MTs undergoing frequent catastrophes as they polymerise against the retrograde flow of actin [188]. The actin retrograde flow and microtubules within growth cones *in vitro* displayed a similar behaviour to what I ob-

served in the initial stages of CIL [189]. These results suggested that as the actin network reorganises (i.e. the retrograde flow rate decreases and changes it's direction) it creates a path of little resistance which then the MTs take to extend towards the site of cell-cell contact. Alternatively, the microtubules and actin stress fibre might be linked together via an actin-microtubule crosslinker, such as Short stop (Shot), a member of the spectraplakin family which links actin and microtubules together in *Drosophila* [190]. Unfortunately, the current resolution of the movies used in this work is insufficient to be able to investigate this in more details and as such the interaction between actin and microtubules remains a mystery. Conducting the same quantification as in this work on time lapse images acquired at a much higher spatial and temporal resolution should establish if microtubule bundles are pushed inside the low retrograde region by the actin flow or they simply choose the path of least resistance to get from the region surrounding the cell body to the site of cell-cell contact.

Microtubules are clearly important for contact inhibition of locomotion in a number of cell-types, but their role is unclear (see section 2.2). During hemocyte CIL, the alignment of the microtubules bundle coincides with the time of a synchronous back acceleration in colliding partners, suggesting that they are playing a role in inhbiting the forward movement. Another possible role for microtubules in my system might be to determine the precise internuclear spacing of hemocytes during CIL which has been proven to be critical for their even dispersal pattern [5]. It could be that this spacing emerges partially from the regular size of hemocyte cell bodies and partially from the physical and dynamic properties of the microtubules and that hemocytes achieve this level of structural stability by balancing out tensional elements (such as the acto-myosin cytoskeleton) and compression bearing elements (i.e. microtubules). Therefore, by precisely controlling the distribution of these elements and their interaction, hemocytes are able to positively transduce mechanical stimuli in such a way that leads to their even distribution throughout the ventral surface of the embryo. Microtubules can also have additional roles in regulating the cell-cell adhesion. It is still unclear what MTs are doing to cell-cell

adhesions. Research on how microtubules regulate focal adhesion between cell and extracellular matrix showed that MTs are either actively increasing the local stress concentration at adhesions until the bonds are physically broken or they help in delivering different proteins that promote adhesion disengagement [191, 192]. Microtubules might have a similar role for cell-cell adhesions, especially during CIL.

An intercellular actin clutch mechanically couples the two cells allowing the actin cytoskeleton to build up lamellar tension. Prior to cell repolarisation and migration away from the collision, hemocytes synchronously retract their lamellae (section 4.4). The evidence suggests that the tension generated during the response is suddenly released as the cell-cell adhesion is broken, causing the collapse of the entire leading edge. As the cells are not connected anymore through the intercellular adhesion, it means that all the tension generated prior to the break of the adhesion has to be dissipated. I propose that the easiest way in which this tension can be dissipated by collapsing the entire leading edge. This collapse causes an assymetry in the actin cytoskeleton that could be the necessary trigger for the subsequent migration away from the collision. Several studies have showed travelling waves of actin disassembly emerge as a consequence of myosin-induced network disassembly which lead to very fast changes in the direction of movement [63, 193]. During CIL a large accumulation of myosin occurs along the transient stress fibre connecting the two colliding cells which could lead to sudden collapse of the network by inducing a wave of disassembly. Alternatively, mechanical failure of both the actin stress-fibre like structure and the microtubule bundle to withstand the tension developed inside the network during CIL might result in a sudden collapse of the leading edge which gives rise to the rapid retraction event. Irrespective of the exact mechanism leading to this rapid retraction of the leading edge, the increased lamellar tension it is likely to be significant. Therefore, this tension release is crucial for orchestrating the hemocyte CIL response. Interestingly, the lamellae retract prior to new protrusions being formed elsewhere. This behaviour is in contrast with what other studies revelead about CIL. For example, neural crest cells have been shown to first repolarise prior to the collapse of their forward protrusions. It was

speculated that for neural crest cells, the repolarisation is contributing to the development of the tension required for the cells to separate [137]. I hypothesise that at least for hemocytes, the release of tension and collapse of the leading edge acts as a trigger for the subsequent repolarisation of cells. In other cell-types it was showed that symmetry breaking and polarisation can be indeed induced by the uneven contraction of the acto-myosin cytoskeleton [194, 176]. These studies have also observed that prior to polarisation, the actin network begins to change from the rear to the cell edge, in a similar fashion to what I observed it happens during CIL. Nevertheless, the mechanisms of this redistribution are still unclear.

The final step of a type 1 CIL response, migration away from the collision, is just now starting to be investigated. Irrespective of the mechanisms that stop cells to migrate over each other, it is important to understand what happens to the cells after they break from a collision. In section 2.1.6 I showed that cell-ECM adhesions are crucial for normal cell migration. Therefore, in order to migrate away from their colliding partner, the cell-substrate traction forces need reorganise. A possible mechanism for this is that the focal adhesions are modified, with more FAs being recruited away from the collision. This behaviour was observed in *in vitro Xenopus* neural crest cells undergoing CIL where the distribution of proteins forming the focal adhesions altered following a collision, with less focal adhesion kinase and paxilin near the collision compared to the distal regions. This redistribution of FAs could cause an inbalance in local traction forces, with more force being generated away from the contact site. It would be interesting to investigate if a similar behaviour is at play during hemocytes contact inhibition and what is the ratio between the intercellular forces developed while cells are in contact and the subsequent traction forces required for the cells to migrate away from the collision.

As mentioned in the beginning of this chapter, hemocyte contact inhibition involves a sequence of stereotypical steps that lead to cells retracting from one another and subsequently repolarising to migrate away from the collision. This behaviour is characteristic of a type 1 contact inhibition response where cells are actively repelling from each other, in contrast to them being randomly deflected or stopped

altogether as it is characteristic for a type 2 response [8]. Perhaps more surprising, hemocyte CIL response appears to be very similar to the original description of the process in chick heart fibroblasts where ”a spasm of contraction” immediately after cell-cell contact ”obliterates the process of ruffling” and ”as a result of the adhesion ... they [cells] push or pull against each other to some extent; some of the energy which would normally go into movement is thereby dissipated or becomes potential energy of elastic tension between the cells. When an adhesion breaks, the release of potential energy stored as elastic tension produces the sudden acceleration” [9].

In this work I showed that as hemocytes collide, their actin networks undergo a very rapid reorganisation which happens synchronously in both cells via an inter-cellular actin clutch that develops between the two cells. Furthermore, lamellar tension increases from the region surrounding the cell body to the site of cell-cell contact. The release of this tension when the cell-cell contact breaks is sufficient to induce the repolarisation of the two colliding partners, causing them to migrate in opposite direction. This is consistent with an inter-cellular actin clutch as the perfect choreographer of CIL hemocyte response.

Taking a step back from contact inhibition, this work also provided additional insights into the mechanisms controlling the retrograde flow *in vivo*. I have showed that myosin II driven contraction is playing an important role in the generation of the actin retrograde flow in hemocytes. Prior studies of the regulation of retrograde flow have showed that a combination of polymerisation at the leading edge and myosin contraction deep inside the lamella are required to generate the centripetal motion of the network [87]. In this system, myosin mutant hemocytes had severe defects in retrograde flow dynamics which perhaps are the main reason behind the defects in cell motility that we observed. Furthermore, myosin II mutant hemocyte motility was also greatly affected. This could be because polymerisation alone is not sufficient to generate enough force to consistently move the whole cell forward. Myosin II contraction has been showed to promote network disassembly allowing for fast recycling of the actin monomers within the lamella [1]. It could be that in the absence of myosin II contraction the network becomes more stable, preventing

it to be remodelled as frequently as it is needed for normal cell migration. Thus, in contrast to cells migrating *in vitro* [195], myosin II generated contraction is absolutely necessary for providing cells with a functional locomotory machinery *in vivo*.

7.1 Further work

CIL offers numerous exploratory avenues as it allows one to study all aspects of cell migration from leading edge dynamics and cell-matrix and cell-cell adhesions to the force generation and transduction pathways that make a cell move. Nevertheless, this complexity is also an obstacle because there are myriad of variables to control for when testing any hypothesis. Although we have a lot of information about the separate processes that are involved in cell migration such as leading edge extension, adhesion to the extracellular matrix, generation of traction forces (see section 2.1), our understanding is lacking an overarching cell motility theory that integrates all these separate findings. Therefore, I believe that to achieve a complete understanding of contact inhibition of locomotion and it's regulation, we need to take a step back and focus on single cell migration. My main reason for going down this reductionist route is that once we will understand how a cell integrates mechanics to choose where to move and what governs the direction in which it moves, we will be more equipped to tackle the problem of direction reversal or cell stopping that are central contact inhibition (section 2.2). Nevertheless, to be able to understand how all the separate processes involved in cell migration are integrated, we need adequate tools that allow us to "look at the thing" (Feynman c. 1960).

The current theoretical framework for understanding cell motility proposes that cells migration is a cyclical step-wise process where a cell first extends its leading edge, adheres to the substratum, and then the whole cell contracts and translocates (see section 2.1). Each these processes has been extensively studied independently (see section 2.1), however, very few studies addressed the entire motility cycle and the integration of these apparently uncoupled steps [31]. The tools that I developed to investigate the role of forces during contact inhibition can be extended to

understand general aspects of cellular motility. A first step towards this goal, is to combine the kinematics analysis and PIV quantification of the actin flow to examine if there is any connection between actin dynamics and the direction in which a cell migrates. Furthermore, the PIV measurements of actin flows can be used to investigate different aspects of the actin network such as network coherence, regions of network assembly and disassembly, or the effects of the actin flows on edge extension/retraction activity.

One big unknown in the field is how a cell migrating at random decides where to go. It is a well established fact that cellular movements in general have some degree of persistence [169]. In other words, in the absence of an external cue, there is something that gives a bias to the random walk allowing cells to consistently move in a direction within a limited time window. The current model for this is that a cell extends its leading edge in multiple direction and then it simply follows the side that extended the most [196]. Clearly this is an incomplete model of cellular motility. As we saw before, moving cells have to integrate a multitude of signals and processes prior to deciding where to migrate next (section 2.1). Most importantly, this edge centric model makes no reference to the retrograde flow or the inter-cellular forces that need to be transduced into positive traction forces.

To better understand how cells migrate, I started designing tools that would allow us to investigate the relationship between retrograde flow dynamics, leading edge activity, and whole cell translocation. To this aim, I make the cells stationary, i.e. eliminate the translation and rotation of the cell as it migrates (Movie 25) [197]. This allows one to uncouple the retrograde flow dynamics from cell translocation. In this way, we will have 'an inside' view of the retrograde flow, similar to what a cell would experience. By making cells stationary, I am able to obtain much more accurate edge dynamics maps because in a non moving cell we have a 1-to-1 correspondence between all edge points over time. Finally, by transforming the retrograde flow velocity vectors from the the frame of a moving cell to the frame of a stationary cell I could infer regions where most of the forces developed within the actin network are transduced into traction stresses.

It remains an open question how actin polymerisation at the leading edge combines with myosin II contraction to generate persistent cellular motion. To address this question, I begun developing new tools for further quantifying actin dynamics during cell migration. Using the actin flow velocity, I quantified the paths of least resistance within the actin flow field (i.e. streamlines) which describes how does a 'massless' particle from the actin network move at a certain instant in time [198].

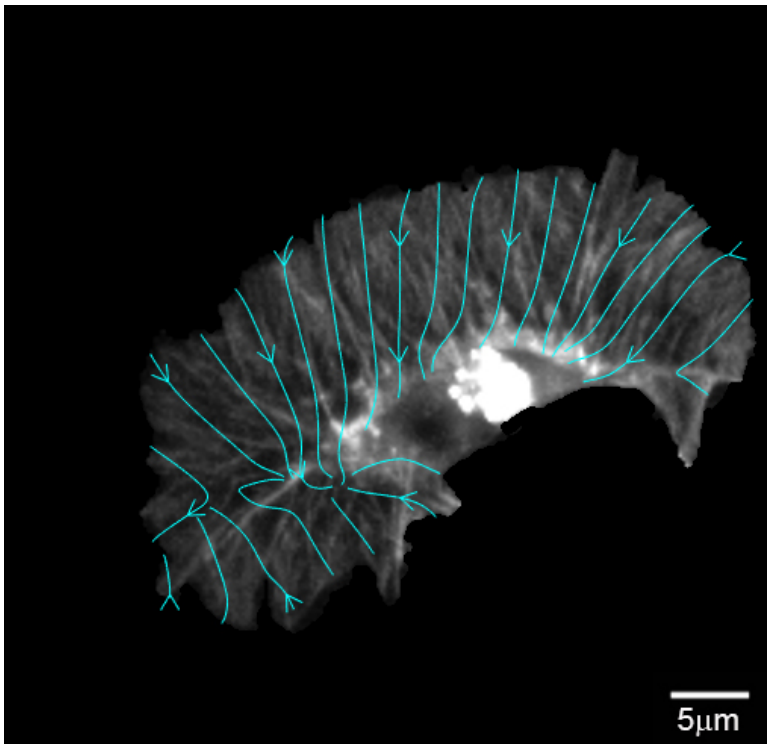

Figure 7.2: Example of actin retrograde flow streamlines in a freely moving hemocyte. Blue lines represent equally spaced streamlines seeded from around the cell outline. End of each streamline highlights the region where actin particles converge. Note that for a freely moving hemocyte, the majority of streamlines converge to the same location within the lamella, suggesting that most of the network is taken apart in this region.

Preliminary analysis of flow streamlines seeded from around the edge of the cell in freely moving hemocytes reveals that the actin cytoskeleton is consistently flowing towards one region within the lamella (as highlighted by the convergence of all streamlines to one point) (Figure 7.2; Movie 26). This suggests that even if the dynamics of the network is varying spatially at the microscale, at the length scale of the cell it behaves as a coherent structure. It would be interesting to further

quantify the convergence of the actin retrograde flow in hemocytes. I speculate that a coherent network is more efficient at sensing and propagating changes in stress and/or strain to allow cells to rapidly adapt to their environment, such as the presence of another cell during collisions.

In parallel to this I am also developing a method for investigating how changes in the geometry of the actin cytoskeleton are affecting cell movement. Using the retrograde flow velocity I am able to quantify the direction in which the network is changing shape the fastest. A previous study on fish keratocytes *in vitro* investigating the relation between lamellar strain and movement has showed that negative strain directly regulates the actin dynamics possibly by enhancing network disassembly which affects cell motility [199]. I am curious to test if the same hypothesis is true for hemocytes too. Furthermore, by combining these different quantifications, my hope is that I will be able to formulate a statistical model for cell motility to test the relative significance of these parameters to whole cell translocation, and in the process provide a unified theory of cell migration.

Appendix A

Movie legends

Movie 1. Timelapse movie of hemocyte developmental dispersal Developmental dispersal of *Drosophila* hemocytes where cell nuclei were labelled using a red marker. Note the change in hemocyte migration pattern from linear migration along the ventral midline to lateral dispersion throughout the embryo until a uniform dispersal pattern is acquired. Movie reporoduced from [6].

Movie 2. Example tracking of hemocyte collisions. Automatic tracking of hemocytes over an 8-minute period surrounding a collision event. Nuclei were labelled using UAS-RedStinger (red) and microtubules were labelled using UAS-Clip-GFP (green). Time is recorded with respect to the initial microtubule contact. Note that the time of microtubule contact was used as a termporal register for analysing hemocyte kinematics. Scale bar = $5\mu m$. Movie reproduced from [6].

Movie 3. Synchronous changes in hemocyte motion during CIL. Timelapse movie of the mean velocities of colliding partners normalised to the direction of the incoming cell. Movie recreated from [6].

Movie 4. F-actin and microtubules dynamics during CIL. Example timelapse movie of colliding hemocytes with fluorescently labelled actin cytoskeleton (magenta) and microtubules (green). Time was recorded with respect to the initial microtubule contact. Scale bar = $5\mu m$. Movie recreated from [6].

Movie 5. Hemocyte fail to contact inhibit when undergo collisions with the rear of another migratory cell. Example timelapse movie of a migrating hemocyte undergoing a collision with the rear of another migratory cell. Note that the absence

of cytoskeletal changes or repulsion. A fluorescent marker was used to label the F-actin network. Scale bar = $5\mu m$. Movie recreated from [6].

Movie 6. Hemocyte fail to contact inhibit during collisions with a static cell Example timelapse movie of a migrating hemocyte undergoing a collision with a static cell. Note that there are no cytoskeletal changes or repulsion. A fluorescent probe was used to label the F-actin network. Scale bar = $5\mu m$. Movie recreated from [6].

Movie 7. Actin retrograde flow within freely moving hemocytes. Example of time-lapse movie of freely moving hemocytes containing a fluorescent F-actin proble (left panel) and the pseudo-speckle quantification of the flow as a vector field (middle panel) and heat map of flow velocity (right panel). Scale bar = $5\mu m$. Movie recreated from [6].

Movie 8. Quantification of actin retrograde flow in freely moving Myosin II mutant hemocytes. Left panel shows a time-lapse movie of a freely moving *myosin II* mutant hemocyte with fluorescently labelled actin cytoskeleton. Right panel shows the heat map of the actin retrograde flow for the same freely moving *myosin II* mutant cell as in the left panel. Note the reduction in actin flow speed compared to control cells in Movie 7. Scale bar = $5\mu m$. Movie recreated from [6].

Movie 9. Pseudo-speckle analysis of the actin retrograde flow during hemocyte collisions. Example time-lapse movie with colliding hemocytes undergoing CIL where the actin cytoskeleton was labeled with a fluorescent probe (left panel). Right panel shows the heat map of flow velocity. Time is recorded with reference to the moment when cells lamellae first overlap. Scale bar = $5\mu m$. Movie recreated from [6].

Movie 10. Quantification of instantaneous changes in actin flow speed during contact inhibition. Time-lapse movie with heat maps of instantaneous changes in actin flow speed superimposed onto a movie of colliding hemocytes where the actin cytoskeleton was labelled using an F-actin probe. As cells separate, note the sudden increase in speed (red) that takes place in both cells. Time is recorded with reference to the moment when cells first separate. Scale bar = $5\mu m$. Movie recre-

ated from [6].

Movie 11. Reorientation of the actin retrograde flow vectors during CIL. Time-lapse movie with heat maps of the quantified actin retrograde flow velocity (left panel). Rose plot highlighting the flow direction with respect to the horizontal axis (right panel). Time is recorded with reference to the moment when lamellae first overlap. Movie recreated from [6].

Movie 12. Analysis of actin retrograde flow and microtubule dynamics during hemocyte collisions. Example time-lapse movie with the pseudo-speckle analysis of actin retrograde flow colocalised with microtubules (pseudo-coloured white). Time is recorded with reference to the moment of microtubules alignment. Scale bar = $5\mu m$. Movie recreated from [6].

Movie 13. Colocalisation of actin and zyxin during hemocyte contact inhibition of locomation. Colocalisation of Zyxin and actin during contact inhibition. Righ panel shows an overlay of Zyxin (pseudocolored white) onto the actin retrograde flow heatmap. Note the that the slowing of the actin flow occurs synchronously with the development of Zyxin puncta. Time was recorded with respect to the initial lamellae overlap. Scale bar = $5\mu m$. Movie recreated from [6].

Movie 14. Colocalisation of Zyxin and microtubules during hemocyte contact inhibition of locomotion. Time-lapse movie dispalying an overlay of fluorescently labeled zyxin and microtubules. Note the microtubules targeting the Zyxin puncta (right panel). Time is recorded with respect to the initial microtubule contact. Scale bar = $5\mu m$. Movie recreated from [6].

Movie 15. Quantification of actin retrograde flow in colliding Myosin II mutant hemocytes. Left panel shows a time-lapse movie of an example collision between *myosin II* mutant hemocytes containing fluorescently labelled F-actin. Right panel shows the heat map of the actin retrograde flow. Time is recorded with respect to the initial lamellae contact. Scale bar = $5\mu m$. Movie recreated from [6].

Movie 16. Quantification of Myosin II during CIL. Colocalisation of Myosin II and F-actin during hemocyte contact inihibtion of locomotion. Myosin II particles move in a retrograde fashion before and after collision. However, during lamellae

contact Myosin II particles decorate the actin fibre. Time is recorded with respect to the initial lamellar contact. Scale bar = $5\mu m$. Movie recreated from [6].

Movie 17. Expression of constitutively active *Diaphanous* in a freely moving hemocyte. Time-lapse movie of a freely moving hemocyte expressing constitutively active *Diaphanous* where the actin cytoskeleton (pseudo-coloured mangenta) and Myosin II (green) were fluorescently labelled. Myosin II accumulation is enhanced in the lamella leading to a sudden contraction of the network. Scale bar = $5\mu m$. Movie recreated from [6].

Movie 18. Quantification of actin retrograde flow in freely moving *diaphanous* mutant hemocytes. Left panel shows a time-lapse movie of a freely moving *diaphanous* mutant hemocyte containing fluorescently labelled F-actin. Righ panel shows the heat map of the actin retrograde flow. Note that there are no significant differences in flow speed and direction compared to the control cell in Movie 7. Scale bar = $5\mu m$. Movie recreated from [6].

Movie 19. Quantification of actin retrograde flow in *diaphanous* mutant hemocytes during a collision. Two example collisions between *diaphanous* mutant hemocytes highlighting the variability in the response. Left panel shows *diaphanous* mutant hemocytes with labelled F-actin undergoing a collision. Right panel shows the heat map of the actin retrograde flow in the cells from left panel. Note that in collision one a clear corridor of low retrograde flow fails to appear even if there is some resemblance of a stress fibre forming towards the end of the response. In the second collision, both the low actin flow corridor and the actin fibre fail to develop upon lamellar overlap. Time is recorded with respect to the initial lamellar overlap. Scale bar = $5\mu m$. Movie recreated from [6].

Movie 20. Lamellar recoil upon laser abscission during CIL. Time-lapse movie of the lamellar recoil upon laser abscision of both freely moving and colliding cells (arrowheads highlight the ablation region). Left panels show an example ablation of the leading edge or the intracellular actin cytoskeleton (labelled using LifeAct-GFP). Note the small recoil of the network. Right panels show an example ablation of the actin fibre developing the in overlap region between colliding cells.

Note the rapid and synchronous lamellar recoil. Scale bar = $5\mu m$. Movie recreated from [6].

Movie 21. Quantification of cell migration upon laser abscission. The movement of freely moving and colliding hemocytes labelled with LifeAct-GFP and a red nuclear marker was analysed after laser ablation and mock ablation. Note that hemocyte igration was quantified by measuring the nuclear displacement. Freely moving cells showed no significant changes in their movement. Mock ablation of collisions also resulted in no changes in cell movement, with hemocytes continuing to migrate towards the colliding partner. In contrast, ablation of the actin fibre in the lamellar overlap region during CIL induced a very sudden rearward movement of both colliding partners. Scale bar = $5\mu m$. Movie recreated from [6].

Movie 22. Viscoelastic model of the actin network stress during hemocyte contact inhibition of locomotion. Left panel shows an example of a hemocyte undergoing a collision where the actin cytoskeleton was fluorescently labelled. Right panel shows a heat map of the modelled viscoelastic forces developed within the actin cytoskeleton during CIL. Note the redistribution of forces during collisions from the region surrounding the cell body to the region where the actin fibre is developing. Red = high force, Blue = low force. Time is recorded with respect to cell separation. Scale bar = $5\mu m$. Movie recreated from [6].

Movie 23. Hemocyte dispersal in wild-type and *diaphanous* mutant embroys. Time-lapse movies showing hemocytes migrating on the ventral surface of the embryo where the actin cytoskeleton (green) and nuclei (magenta) were fluorescently labelled. Note that even if *dia* ^{5} mutant hemocytes are capable of dispersing, they show regions of clumping (magenta arrows). Scale bar = $20\mu m$. Movie recreated from [6].

Movie 24. Simulation of hemocyte dispersal with different repulsion parameters. Simulations of hemocyte dispersal comparing wild-type CIL parameters to randomised repulsion. Left panel shows a simulation where cells take into account the direction of their colliding partner during the repulsion phase. Right panel shows a simulation in which cells are allowed to respond randomly to the presence

of their colliding partners. Movie recreated from [6].

Movie 25. Time-lapse movie where a freely moving cell has been made stationary. (Left panel) Time-lapse movie of a freely moving hemocyte containing fluorescently labelled F-actin. (Right panel) Time-lapse movie of the freely moving hemocyte from left panel where the cell translation and rotation has been removed.

Movie 26. Actin retrograde flow within freely moving hemocytes converges to a single location inside the lamella. Time-lapse movie of a freely moving hemocyte containing fluorescently labelled F-actin. Magenta lines highlight retrograde flow streamlines computed using equidistant seeding points along the cell edge. Note the development of a single zone of convergence within the network where the majority of the streamlines end.

Bibliography

[1] L. Blanchoin, R. Boujemaa-Paterski, C. Sykes, and J. Plastino. Actin dynamics, architecture, and mechanics in cell motility. *Physiological reviews*, 94(1):235–63, 2014.

[2] M. D. Welch, A. Mallavarapu, J. Rosenblatt, and T. J. Mitchison. Actin dynamics in vivo. *Current Opinion in Cell Biology*, 9(1):54–61, 1997.

[3] M. Abercrombie. The croonian lecture, 1978: The crawling movement of metazoan cells. *Proc. R. Soc. Lond. B Bioo. Sci.*, 207:129–147, 1980.

[4] C. Carmona-Fontaine, H. K. Matthews, S. Kuriyama, M. Moreno, G. A. Dunn, M. Parsons, C. D. Stern, and R. Mayor. Contact inhibition of locomotion in vivo controls neural crest directional migration. *Nature*, 456(7224):957–961, 2008.

[5] J. R. Davis, C.-Y. Huang, J. Zanet, S. Harrison, E. Rosten, S. Cox, D. Y. Soong, G. A. Dunn, and B. M. Stramer. Emergence of embryonic pattern through contact inhibition of locomotion. *Development*, 139(24):4555–60, 2012.

[6] J. R. Davis, A. Luchici, F. Mosis, J. Thackery, J. A. Salazar, Y. Mao, G. A. Dunn, T. Betz, M. Miodownik, and B. M. Stramer. Inter-Cellular Forces Orchestrate Contact Inhibition of Locomotion. *Cell*, 161(2):361–373, 2015.

[7] T. Betz, D. Koch, Y.-B. Lu, K. Franze, and J. A. Käs. Growth cones as soft and weak force generators. *Proceedings of the National Academy of Sciences of the United States of America*, 108(33):13420–13425, 2011.

[8] M. Abercrombie, J. E. Heaysman, and S. M. Pegrum. The locomotion of fibroblasts in culture. I. Movements of the leading edge. *Experimental cell research*, 59(3):393–398, 1970.

[9] M. Abercrombie and Joan E.M. Heaysman. Observations on the social behaviour of cells in tissue culture. *Experimental Cell Research*, 5(1):111–131, 1953.

[10] S. W. Paddock and G. A. Dunn. Analysing collisions between fibroblasts and fibrosarcoma cells: fibrosarcoma cells show an active invasionary response. *Journal of cell science*, 81:163–187, 1986.

[11] S. Kadir, J. W. Astin, L. Tahtamouni, P. Martin, and C. D. Nobes. Microtubule remodelling is required for the front-rear polarity switch during contact inhibition of locomotion. *Journal of cell science*, 124:2642–2653, 2011.

[12] B. Stramer, S. Moreira, T. Millard, I. Evans, C.-Yin Huang, O. Sabet, M. Milner, G. Dunn, P. Martin, and W. Wood. Clasp-mediated microtubule bundling regulates persistent motility and contact repulsion in. 189(4), 2010.

[13] V. Villar-Cerviño, M. Molano-Mazón, T. Catchpole, M. Valdeolmillos, M. Henkemeyer, L. M. Martinez, V. Borrell, and O. Marin. Contact repulsion controls the dispersion and final distribution of cajal-retzius cells. *Neuron*, 77:457 – 471, 2013.

[14] M. Abercrombie. Contact inhibition: the phenomenon and its biological implications. *Natl Cancer Inst Monogr*, 26:249 – 277, 1967.

[15] S. Vedel, S. Tay, D.M. Johnston, H. Bruus, and S.R. Quake. Migration of cells in a social context. *Proc Natl Acad Sci U S A*, 110:129 – 134, 2013.

[16] S. F. Becker, R. Mayor, and J. Kashef. Cadhering-11 mediates contact inhibition of locomotion during xenopus neural crest cell migration. *PLOS One*, 8, 2013.

[17] Y. Takai, J. Miyoshi, W. Ikeda, and H. Ogita. Nectins and nectin-like molecules: roles in contact inhibition of cell movement and proliferation. *Nat Rev Mol Cell Biol*, 9:603 – 615, 2008.

[18] A. Huttenlocher, M. Lakonishok, M. Kinder, S. Wu, T. Truong, K. A. Knudsen, and Horwitz A. F. Integrin and cadherin synergy regulates contact inhibition of migration and motile activity. *J Cell Biol*, 141:515–526, 1998.

[19] W. C. Chen and B. Obrink. Cell-cell contacts mediated by e-cadherin (uvomorulin) restrict invasive behavior of l-cells. *Journal of Cell Biology*, 114:319–327, 1991.

[20] E. Theveneau, L. Marchant, S. Kuriyama, M. Gull, B. Moepps, M. Parsons, and R. Mayor. Collective Chemotaxis Requires Contact-Dependent Cell Polarity. *Developmental Cell*, 19(1):39–53, 2010.

[21] M. Tanaka, S. Kuriyama, and N. Aiba. Nm23-H1 regulates contact inhibition of locomotion which is affected by ephrin-B1. *Journal of Cell Science*, 2012.

[22] J. W. Astin, J. Batson, S. Kadir, J. Charlet, R. Persad, D. Gillatt, J. D. Oxley, and C. D. Nobes. Competition amongst Eph receptors regulates contact inhibition of locomotion and invasiveness in prostate cancer cells. *Nature cell biology*, 12(12):1194–1204, 2010.

[23] J. Batson, J. W. Astin, and C. D. Nobes. Regulation of contact inhibition of locomotion by Eph-ephrin signalling. *Journal of Microscopy*, 251(3):232–241, 2013.

[24] Robert H. Insall and Laura M. Machesky. Actin Dynamics at the Leading Edge: From Simple Machinery to Complex Networks. *Developmental Cell*, 17(3):310–322, 2009.

[25] W. Wood, C. Faria, and A. Jacinto. Distinct mechanisms regulate hemocyte chemotaxis during development and wound healing in Drosophila melanogaster. *Journal of Cell Biology*, 173(3):405–416, 2006.

[26] T. J. Parsons, A. R. Horwitz, and M. A. Schwartz. Cell adhesion: integrating cytoskeletal dynamics and cellular tension. *Nature Reviews Molecular Cell Biology*, 11:633 – 643, 2010.

[27] Y. Aratyn-Schaus and M. L. Gardel. Clutch dynamics. *Science*, 322:1646 – 1647, 2008.

[28] A. J. Ridley, M. A. Schwartz, K. Burridge, R. A. Firtel, M. H. Ginsberg, G. Borisy, J. T. Parsons, and A. R. Horwitz. Cell migration: integrating signals from front to back. *Science*, 302(5651):1704–1709, 2003.

[29] D. A. Lauffenburger and A. F. Horwitz. Cell migration: A physically integrated molecular process. *Cell*, 84(3):359–369, 1996.

[30] T. J. Mitchison and L. P. Cramer. Actin-based cell motility and cell locomotion. *Cell*, 84(3):371–379, 1996.

[31] S. M Rafelski and J. A. Theriot. Crawling toward a unified model of cell mobility: spatial and temporal regulation of actin dynamics. *Annual Review of Biochemistry*, 73:209–239, 2004.

[32] A. J. Ridley. Life at the leading edge. *Cell*, 145(7):1012–1022, 2011.

[33] T. Pollard and G. Borisy. Cellular motility driven by assembly and disassembly of actin filaments. *Cell*, 112:453 – 465, 2003.

[34] L. Blanchoin and T. D. Pollard. Hydrolysis of ATP by Polymerized Actin Depends on the Bound Divalent Cation but Not Profilin . 2002.

[35] M. F. Carlier and D. Pantaloni. Direct evidence for adp-pi-f-actin as the major intermediate in atp-actin polymerisation. rate of dissociation of pi from actin filaments. *Biochemistry*, 25:7789 – 7792, 1986.

[36] N. Selve and D. Wegner. Rate of treadmilling of actin filaments in vitro. *Journal of Molecular Biology*, 187:627–631, 1986.

[37] A. J. Ridley. Rho gtpases and cell migration. *J Cell Sci*, 114:2713 – 2722, 2001.

[38] M. Harasim, B. Wunderlich, O. Peleg, M. Kroger, and A. R. Bausch. Direct observation of the dynamics of semiflexible polymers in shear flow. *Phys Rev Lett*, 110, 2013.

[39] J. Howard. *Mechanics of motor proteins and the cytoskeleton*. 2001.

[40] D. R. Kovar and T. D. Pollard. Insertional assembly of actin filaments barbed ends in association with formins produces piconewton forces. *Proc Natl Acad Sci USA*, 101:14725 – 14730, 2004.

[41] J. Berro, A. Michelot, L. Blanchoin, D. R. Kovar, and J. L. Martiel. Attachment conditions control actin filament buckling and the production of forces. *Biophysical Journal*, 92:2546 – 2558, 2007.

[42] H. Isambert, P. Venier, A. C. Maggs, A. Fattoum, R. Kassab, D. Pantaloni, and M. F. Carlier. Flexibility of actin filaments derived from thermal fluctuations. *J Biol Chem*, 270:11437 – 11444, 1995.

[43] H. Kang, M. J. Bradley, B. R. McCullough, A. Pierre, E. E. Grintsevich, E. Reisler, and E. M. De La Cruz. Identification of cation-binding sites on actin that drive polymerization and modulate bending stiffness. *Proc Natl Acad Sci USA*, 109:16923 – 16927, 2012.

[44] A. Mogilner and G. Oster. Cell motility driven by actin polymerization. *Biophysical Journal*, 71(6):3030–3045, 1996.

[45] L. Blanchoin, K. J. Amann, H. N. Higgs, J.-B. Marchand, D. A. Kaiser, and T. D. Pollard. Direct observation of dendritic actin complex and WASP / Scar proteins. 171(1994):1007–1011, 2000.

[46] F. Gittes, B. Mickey, J. Nettleton, and J. Howard. Flexural rigidity of microtubules and actin filaments measured from thermal fluctuations in shape. *J Cell Biol*, 120:923 – 934, 1993.

[47] J. V. Small, T. Stradal, E. Vignal, and K. Rottner. The lamellipodium: Where motility begins. *Trends in Cell Biology*, 12(3):112–120, 2002.

[48] T. D. Pollard, L. Blanchoin, and Mullinds R. D. Molecular mechanisms controlling filament dynamics in nonmuscle cells. *Annual Review of Biophysics and Biomolecular Structure*, 29:545–576, 2000.

[49] M. Pring, A. Weber, and M. R. Bubb. Profilin-Actin Complexes Directly Elongate Actin Filaments at the Barbed End ? pages 1827–1836, 1992.

[50] L. M. Machesky and A. Li. Invasive filopodia promoting metastasis. pages 263–270, 2010.

[51] A.-C. Reymann, C. Suarez, C. Guérin, J.-L. Martiel, and F. Chang. Turnover of branched actin filament networks by stochastic fragmentation with ADF / cofilin. 22, 2011.

[52] E. Ingerman, J. Y. Hsiao, and R. D. Mullins. dispensable for assembly. 200(5):619–633, 2013.

[53] B. R. McCullough, L. Blanchoin, J. L. Martiel, and E. M. De la Cruz. Cofilin increases the bending flexibility of actin filaments: implications for severing and cell mechanics. *J Mol Biol*, 381:550 – 558, 2008.

[54] L. Blanchoin and T. D. Pollard. Mechanism of Interaction of Acanthamoeba Actophorin (ADF / Cofilin) with Actin Filaments *. 274(22):15538–15546, 1999.

[55] I. Mabuchi. An Actin-depolymerizing Protein (Depactin) from Starfish Oocytes " Properties and Interaction with Actin. 97(November), 1983.

[56] E. M. De La Cruz. How cofilin severs an actin filament. *Biophys Rev*, 1:51–59, 2009.

[57] B. R. Mccullough, E. E. Grintsevich, C. K. Chen, H. Kang, A. L. Hutchison, A. Henn, W. Cao, C. Suarez, J.-L. Martiel, L. Blanchoin, E. Reisler, and

E. M. De La Cruz. Cofilin-Linked Changes in Actin Filament Flexibility Promote Severing. *Biophysical Journal*, 101(1):151–159, 2011.

[58] D. Breitsprecher, S. A. Koestler, I. Chizhov, M. Nemethova, J. Mueller, B. L. Goode, J. V. Small, K. Rottner, and J. Faix. Cofilin cooperates with fascin to disassemble filopodial actin filaments. 2011.

[59] C. Suarez, R. Boujemaa-Paterski, H. Kang, B. R Mccullough, E. M. De La Cruz, and L. Blanchoin. Report Cofilin Tunes the Nucleotide State of Actin Filaments and Severs at Bare and Decorated Segment Boundaries. pages 862–868, 2011.

[60] B. Alberts, A. Johnson, J. Lewis, M. Raff, K. Roberts, and P. Walter. *Molecular Biology of the Cell*. Garland Science, Taylor and Francis Group, 5 edition, 2012.

[61] C. Bustamante, D. Keller, and G. Oster. The physics of molecular motors. *Acc Chem Res*, 34:412–420, 2001.

[62] L. Haviv, D. Gillo, F. Backouche, and A. Bernheim-Groswasser. A cytoskeletal demolition worker: myosin ii acts as an actin depolymerization agent. *J Mol Biol*, 375:325 – 330, 2008.

[63] Actin network architecture can determine myosin motor activity. *Science*, 336:1310 – 1314, 2012.

[64] J. Stricker, T. Falzone, and M.L. Gardel. Mechanics of the f-actin cytoskeleton. *Journal of Biomechanics*, 43:9–14, 2010.

[65] M. L. Gardel, J. H. Shin, F. C. MacKintosh, L. Mahadevan, P. Matsudaira, and D. A. Weitz. Elastic behavior of cross-linked and bundled actin networks. *Science*, 304(5):1301–1305, 2004.

[66] Gardel M.L., Kasza K.E., Brangwynne C.P., Liu J., and Weitz D.A. Chapter 19: Mechanical respose of cytoskeletal networks. *Methods Cell Biology*, 89:487–519, 2008.

[67] L. Ji, J. Lim, and G. Danuser. Fluctuations of intracellular forces during cell protrusion. *Nature cell biology*, 10(12):1393–1400, 2008.

[68] O. Chaudhuri, S. H. Parekh, and D. A. Fletcher. Reversible stress softening of actin networks. *Nature*, 445:295–298, 2007.

[69] B. Fabry, G. N. Butler, M. Glogauer, J. Navajas, and J. J. Fredberg. Scaling the microrheology of living cells. *Physical Review Letters*, 87:148102, 2001.

[70] D. A. Fletcher and R. D. Mullins. Cell mechanics and the cytoskeleton. *Nature*, 463:485–492, 2010.

[71] D.A Head, A. J. Levine, and F. C. MacKintosh. Distinct regimes of elastic response and deformation models of cross-linked cytoskeletal and semiflexible polymer networks. *Physical Review E Statistical, Nonlinear, Soft Matter Physics*, 68:06190ss, 2003.

[72] D.A Head, A. J. Levine, and F. C. MacKintosh. Deformation of cross-linkced semiflexible polymer networks. *Physical Review Letters*, 91:109102ss, 2003.

[73] J. Liu, G. H. Koenderink, Kasza, and and MacKintosh, F. C. Visualizing the strain field in semiflexible polymer networks: Strain fluctuations and nonlinear rheology of f-actin visualizing the strain field in semiflexible polymer metworks: Strain fluctuations and nonlinear rheology of f-actin gets. *Physical Review Letters*, 98:198304, 2007.

[74] D. Mizuno, C. Tardin, C. F. Schmidt, and F. C. MacKintosh. Nonequilibrium mechanics of active cytoskeletal networks. *Science*, 315:370–373, 2007.

[75] C. Storm, J. Pastore, F. C. MacKintosh, T. C. Lubensky, and P. A. Janmey. Nonlinear elasticity in biological cells. *Nature*, 435:191–194, 2005.

[76] K. Burridge and E. S. Wittchen. The tension mounts: Stress fibers as force-generating mechanotransducers. *Journal of Cell Biology*, 200(1):9–19, 2013.

[77] L. J. Peterson, Z. Rajfur, A. S. Maddox, C. D. Freel, Y. Chen, M. Edlund, C. Otey, and K. Burridge. Simultaneous stretching and contraction of stress fibers in vivo. *Mollecular Biology of the Cell*, 15:3497–3508, 2004.

[78] N. Q. Balaban, U. S. Schwarz, D. Riveline, P. Goichberg, G. Tzur, I. Sabanay, D. Mahalu, S. Safran, A. D. Bershadsky, L. Addadi, and B. Geiger. Force and focal adhesion assembly: a close relationship studied using micropatterned substrates. *Nature Cell Biology*, 3:466–472, 2001.

[79] K. A. Beningo, M. Dembo, I. Kaverina, J. V. Small, and Y. L. Wang. Nascent focal adhesions are responsible for the generation of strong propulsive forces in migrating fibroblasts. *The Journal of Cell Biology*, 153:881–888, 2001.

[80] B. Geiger, J. P. Spatz, and A. D. Bershadsky. Environmental sensing through focal adhesions. *Nat Rev Mol Cell Biol*, 10:21 – 33, 2009.

[81] P. Houlainen and P. Lappalainen. Stress fibers are generated by two distinct actin assembly mechanisms in motile cells. *The Journal of Cell Biology*, 173:383–394, 2006.

[82] P. W. Oakes, Y. Beckham, J. Stricker, and M.L. Gardel. Tension is required but not sufficient for focal adhesion maturation without a stress fiber template. *The Journal of Cell Biology*, 196:363–374, 2012.

[83] J. Colombelli, A. Besser, H. Kress, E. G. Reynaud, P. Girard, E. Caussinus, U. Haselmann, J Small, U. S. Schwarz, and E. H. Stelzer. Mechanosensing in actin stress fibers revealed by a close correlation between force and protein localization. *Journal of cell science*, 122:1665–1679, 2009.

[84] A. Ponti, M. Machacek, S. L. Gupton, C. M. Waterman-Storer, and G. Danuser. Two distinct actin networks drive the protrusion of migrating cells. *Science*, 305(5691):1782–1786, 2004.

[85] P. Vallotton, G. Danuser, S. Bohnet, J.-J. Meister, and A. B. Verkhovsky.

Tracking retrograde flow in keratocytes: news from the front. *Mol. Biol. Cell*, 16:1223 – 1231, 2005.

[86] P. Vallotton and J. V. Small. Shifting views on the leading role of the lamellipodium in cell migration: speckle tracking revisited. *Journal of cell science*, 122:1955–1958, 2009.

[87] C. H. Lin, E. M. Espreafico, and M. S. Mooseker. Myosin Drives Retrograde F-Actin Flow in Neuronal Growth Cones. 16:769–782, 1996.

[88] J. H. Henson, T. M. Svitkina, A. R. Burns, H. E. Hughes, K. J. Macpartland, R. Nazarian, and G. G. Borisy. Two Components of Actin-based Retrograde Flow in Sea Urchin Coelomocytes. 10:4075–4090, 1999.

[89] C.-H. Lin and P. Forscher. Growth cone advance is inversly proportional to retrograde f-actin flow. *Neuron*, 14:763 – 777, 1995.

[90] G. Danuser and C. M. Waterman-Storer. Quantitative fluorescent speckle microscopy of cytoskeleton dynamics. *Annual review of biophysics and biomolecular structure*, 35:361–387, 2006.

[91] G. Danuser and C. M. Waterman-Storer. Quantitative fluorescent speckle microscopy of cytoskeleton dynamics. *Annual Review of Biophysics and Biomolecular Structure*, 35:361–389, 2006.

[92] A. Ponti, A. Matov, M. Adams, S. Gupton, C. M. Waterman-Storer, and G. Danuser. Periodic patterns of actin turnover in lamellipodia and lamellae of migrating epithelial cells analyzed by quantitative Fluorescent Speckle Microscopy. *Biophysical Journal*, 89(5):3456–3469, 2005.

[93] P. Vallotton, S. L. Gupton, C. M. Waterman-Storer, and G. Danuser. Simultaneous mapping of filamentous actin flow and turnover in migrating cells by quantitative fluorescent speckle microscopy. *Proceedings of the National Academy of Sciences of the United States of America*, 101(26):9660–9665, 2004.

[94] S. Schaub, S. Bohnet, V. M. Laurent, JJ Meister, and A. B. Verkhovsky. Comparative maps of motion and assembly of filamentous actin and myosin ii in migrating cells. *Mollecular Biology of the Cell*, 18:3723–3732, 2007.

[95] A. Y. Alexandrova, K. Arnold, S. Schaub, J. M. Vasiliev, J. J. Meister, A. D. Bershadsky, and A. B. Verkhovsky. Comparative dynamics of retrograde actin flow and focal adhesions: Formation of nascent adhesions triggers transition from fast to slow flow. *PLoS ONE*, 3(9):1–9, 2008.

[96] C. Jurado, J. R. Haserick, and J. Lee. Slipping or gripping? fluorescent speckle microscopy in fish keratocytes reveals two different mechanisms for generating a retrograde flow of actin. *Molecular Biology of the Cell*, 16:507 – 518, 2005.

[97] A. D. Bershadsky, N. Q. Balaban, and B. Geiger. Adhesion-dependent cell mechanosensitivity. *Annual Review of Cell and Developmental Biology*, 19:677–695, 2003.

[98] E. Zamir and B. Geiger. Molecular complexity and the dynamics of cell-matrix adhesions. *Journal of cell science*, 2:191–196, 2001.

[99] G. Giannone, R. M. Mège, and O. Thoumine. Multi-level molecular clutches in motile cell processes. *Trends in Cell Biology*, 19(9):475–486, 2009.

[100] U. S. Schwarz and M. L. Gardel. United we stand - integrating the actin cytoskeleton and cell-matrix adhesions in cellular mechanotransduction. *Journal of Cell Science*, 125(13):3051–3060, 2012.

[101] J. Stricker, Y. Beckham, W. Davidson, and M.L. Gardel. Myosin ii-mediated focal adhesion maturation is tension insensitive. *PLoS One*, 8:e70652, 2013.

[102] J. Stricker, Y. Aratyn-Schaus, P. W. Oakes, and M.L. Gardel. Spatiotemporal contrains on the force-dependent growth of focal adhesions. *Biophysical Journal*, 100:2883–2893, 2011.

[103] C. E. Chan and D. J. O. Traction dynamics of filopodia on compliant substrates. *Science*, 322(5908):1687–1691, 2008.

[104] M. L. Gardel, B. Sabass, L. Ji, G. Danuser, U. Schwarz, and Waterman C. M. Traction stress in focal adhesions correlates biphasically with actin retrograde flow speed. *The Journal of Cell Biology*, 183(6):999–1005, 2008.

[105] C. S. Chen, J. Tan, and J. Tien. Mechanotransduction at cell-matrix and cell-cell contacts. *Annual Review of Biomedical Engineering*, 6:275–302, 2004.

[106] V. Vogel and M. Sheetz. Local force and geometry sensing regulate cell functions. *Nature Reviews Molecular Cell Biology*, 7:265–275, 2006.

[107] K Hayakawa, N Sato, and T Obinata. Dynamic reorientation of cultured cells and stress fibers under mechanical stress from periodic stretching. *Exp Cell Res*, 268:104–114, 2001.

[108] S. Jungbauer, H. Gao, J. P. Spatz, and R. Kemkemer. Two characteristic regimes in frequency-dependent dynamic reorientation of fibroblasts on cyclically stretched substrates. *Biophysical Journal*, 196:641–652, 2008.

[109] U. Faust, N. Hampe, W. Rubner, N. Kirchgessner, S. Safran, B. Hoffmann, and R. Merkel. Cyclic stress at mhz frequencies aligns fibroblasts in direction of zero strain. *PLoS One*, 6:e28963, 2011.

[110] M. A. Smith, M. L. Blankman, M. L. Gardel, L. Luettjohann, Waterman C. M., and M. C. Beckerle. A zyxin-mediated mechanism for actin stress fiber maintenance and repair. *Developmental Cell*, 19:365–376, 2010.

[111] L. M. Hoffman, C. C. Jensen, A. Chaturvedi, M. Yoshigi, and M. C. Beckerle. Stretch-induced actin remodeling requires targeting of zyxin to stress fibers and recruitment of actin regulators. *Mollecular Biology of the Cell*, 23:1846–1859, 2012.

[112] Y. Fukui, T. Kitanishi-Yumura, and S. Yumaura. Myosin-ii indepen- dent f-actin flow contributes to cell locomotion in dictyostelium. *J. Cell Sci.*, 112:877–886, 1999.

[113] N. Watanabe and T. J. Mitchison. Single-Molecule Speckle Analysis of Actin Filament Turnover in Lamellipodia. 295:1083–1087, 2002.

[114] D. G. Jay. The clutch hypothesis revisited: ascribing the roles of actin-associated proteins in filopodial protrusion in the nerve growth cone. *Review. J. Neurobiol*, 44:114–125, 2000.

[115] P. A. DiMilla, K. Barbee, and D. A. Lauffenburger. Mathematical model for the effects of adhesion and mechanics on cell migration speed. *Biophysical Journal*, 30:15 – 37, 1991.

[116] P. A. DiMilla, J. A. Stone, J. A. Quinn, S. M. Albelda, and D. A. Lauffenburger. Maximal migration of human smooth muscle cells on fibornectin and type iv collagen occurs at an intermediate attachement strength. *J Cell Biol*, 122:729 – 737, 1993.

[117] S. P. Palecek, J. C. Loftus, M. H. Ginsberg, D. A. Lauffenberger, and A. F. Horwitz. Integrin-ligand binding properties govern cell migration speed through cell-substratum adhesiveness. *Nature*, 385:537–540, 1997.

[118] G. Danuser, J. Allard, and A. Mogilner. Mathematical modeling of eukaryotic cell migration: insights beyond experiments. *Annual review of cell and developmental biology*, 29:501–28, 2013.

[119] B. Rubinstein, M. Fournier, K. Jacobson, A. B. Verkhovsky, and A. Mogilner. Actin-myosin viscoelastic flow in the keratocyte lamellipod. *Biophysical Journal*, 97:1853–1863, 2009.

[120] E. M. Craig, D. Van Goor, P. Forscher, and A. Mogilner. Membrane tension, myosin force, and actin turnover maintain actin treadmill in the nerve growth cone. *Biophysical Journal*, 102:1503–1513, 2012.

[121] J. F. Joanny and J. Prost. Active gels as a description of the actin-myosin cytoskeleton. *HFSP Journal*, 3:94–104, 2009.

[122] M. Abercrombie and J. E. Heaysman. Observations on the social behaviour of cells in tissue culture. II. Monolayering of fibroblasts. *Experimental cell research*, 6(2):293–306, 1954.

[123] M. Abercrombie. Contact inhibition of malignancy. *Nature*, 281(259–262), 1979.

[124] M. Abercrombie, Joan E. M. Heaysman, and H. M. Karthauser. Social behaviour of cells in tissue culture. III. Mutual influance of sarcoma cells and fibroblasts. *Experimental Cell Research*, 13(2):276–291, 1957.

[125] M. Abercrombie and J. E. M. Heaysman. Invasive behaviour between sarcoma and fibroblast populations in cell culture. *J. Natn. Cancer Inst.*, 56:561 – 570, 1976.

[126] G. A. Dunn and S. W. Paddock. Analysing the motile behaviour of cells: a general approach with special reference to pairs of cells in collision. *Philosophical transactions of the Royal Society of London*, 299:147–157, 1982.

[127] P. Vesely and R.A. Weiss. Cell locomotion and contact inhibition of normal and neoplastic rat cells. *International journal of cancer Journal international du cancer*, 11:64–76, 1973.

[128] E. K. Parkinson and J. G. Edwards. Non-reciprocal contact inhibition of locomotion of chick embryonic choroid fibroblasts by pigmented retina epithelial cells. *Journal of cell science*, 33:103–120, 1978.

[129] E. Martz and M. S. Steinberg. Contact inhibition of what? analytical review. *J Cell Physiol*, 81:25 – 37, 1973.

[130] M. Abercrombie and E. J. Ambrose. Interference microscope studies of cell contacts in tissue culture. *Expl. Cell Res.*, 15:332 – 345, 1958.

[131] M. Abercrombie. The bases of the locomotory behaviour of fibroblasts. *Experimental cell research*, Suppl 8:188–198, 1961.

[132] M. Abercrombie. Contact inhibition in tissue culture. *In vitro*, 6:128 – 142, 1970.

[133] M. Abercrombie. Control mechanisms in cancer. *Eur J Cancer*, 6:7 – 13, 1970.

[134] M. Abercrombie, J. E. M. Heaysman, and S. M. Pegrum. The locomotion of fibroblasts in culture iv. electron microscopy of the leading lamella. *Expl. Cell Res.*, 67:359 – 367, 1971.

[135] J.P. Trinkaus, T. Betchaku, and L.S. Krulikowski. Local inhibition of ruffling during contact inhibition of cell movement. *Exp. Cell Res.*, 64:291 – 300, 1971.

[136] G. A Dunn. Mutual contact inhibition of extension of chick sensory nerve fibres in vitro. *The Journal of comparative neurology*, 143:491 – 507, 1971.

[137] E. Scarpa, A. Szabó, A. Bibonne, E. Theveneau, M. Parsons, and R. Mayor. Cadherin Switch during EMT in Neural Crest Cells Leads to Contact Inhibition of Locomotion via Repolarization of Forces. *Developmental Cell*, pages 1–14, 2015.

[138] J. E. M. Heaysman and S. M. Pegrum. Early contacts between normal fibroblasts and mouse sarcoma cells: An ultrastructural study. *Expl. Cell Res.*, 78:479 – 481, 1973.

[139] E. J. Sanders and S. Prasad. Contact inhibition of locomotion and the structure of homotypic and heterotypic intercellular contacts in embryonic epithelial cultures. *Experimental cell research*, 135(1):93–102, 1981.

[140] E. Anear and Roger W. Parish. The effects of modifying RhoA and Rac1 activities on heterotypic contact inhibition of locomotion. *FEBS Letters*, 586(9):1330–1335, 2012.

[141] S. Nakao, A. Platek, S. Hirano, and M. Takeichi. Contact-dependent promotion of cell migration by the ol-protocadherin-nap1 interaction. *J. Cell Biol.*, 182:395–410, 2008.

[142] R. Mayor and C. Carmona-Fontaine. Keeping in touch with contact inhibition of locomotion. *Trends in Cell Biology*, 20(6):319–328, 2010.

[143] B. M. Gumbiner. Regulation of cadherin-mediated adhesion in morphogenesis. *Nature Reviews of Mollecular Cell Biology*, 6:622–634, 2005.

[144] E. Theveneau, B. Steventon, E. Scarpa, S. Garcia, X. Trepat, A. Streit, and R. Mayor. Chase-and-run between adjacent cell populations promotes directional collective migration. *Nature Cell Biology*, 15(7):763–772, 2013.

[145] D. Devenport. The cell biology of planar cell polarity. *JCB*, 207:171 – 179, 2014.

[146] E. Scarpa, A. Roycroft, E. Theveneau, E. Terriac, M. Piel, and R. Mayor. A novel method to study contact inhibition of locomotion using micropatterned substrates. *Biology Open*, 2(9):901–6, 2013.

[147] T. Nagasaki, C. J. Chapin, and G. G. Gundersen. Distribution of detyrosinated microtubules in motile nrk fibroblasts is rapidly altered upon cell-cell contact: implications for contact inhibition of locomotion. *Cell Moltil. Cytoskeleton*, 23:45 – 60, 1992.

[148] X. Huang and J.P. Saint-Jeannet. Induction of the neural crest and the opportunities of life on the edge. *Developmental Biology*, 275:1–11, 2004.

[149] J. F. Crane and P. A. Trainor. Neural crest stem and progenitor cells. *Annual Review of Cell and Developmental Biology*, 22:267 – 286, 2006.

[150] M.J. Hendrix, E.A. Seftor, R.E. Seftor, J. Kasemeier-Kulesa, P.M. Kulesa, and L.M. Postovit. Reprogramming metastatic tumour cells with embryonic microenvironments. *Nature Rev. Cancer*, 7:246–255, 2007.

[151] P.M. Kulesa, J.C. Kasemeier-Kulesa, J.M. Teddy, N.V. Margaryan, E.A. Seftor, R.E. Seftor, and M.J. Hendrix. Reprogramming metastatic melanoma cells to assume a neural crest cell-like phenotype in an embryonic microenvironment. *Proc. Natl. Acad. Sci. USA*, 103:3752 – 3757, 2006.

[152] M. L. Woods, C. Carmona-Fontaine, C. P. Barnes, I. D. Couzin, R. Mayor, and K. M. Page. Directional Collective Cell Migration Emerges as a Property of Cell Interactions. *PLoS ONE*, 9(9):e104969, 2014.

[153] Y. T. Ip and M. Levine. Molecular genetics of drosophila immunity. *Curr. Opin. Genet. Dev.*, 4:672 – 674, 1994.

[154] W. Wood and A. Jacinto. Drosophila melanogaster embryonic haemocytes : masters of multitasking. 8:542–551, 2007.

[155] B. Stramer, W. Wood, M. J. Galko, M. J. Reed, A. Jacinto, S. M. Parkhurst, and P. Martin. Live imaging of wound inflamation in drosophila embryos reveals key roles for small gtpases during *in vivo* cell migration. *J. Cell Biol.*, 168:567 – 573, 2005.

[156] C. F. Homem, M. Peifer, C. Hill, and C. Hill. Exploring the Roles of Diaphanous and Enabled Activity in Shaping the Balance between Filopodia and Lamellipodia. 20:5138–5155, 2009.

[157] J.D. Franke, R.A. Montague, and D.P. Kiehart. Nonmuscle myosin II generates forces that transmit tension and drive contraction in multiple tissues during dorsal closure. *Current Biology*, 15:2208–2221, 2005.

[158] H. Goldstein, C. Poole, and J. Safko. *Classical Mechanics*. Addison-Wesley, third edition edition, 2002.

[159] H. C. Corben and P. Stehle. *Classical mechanics*. John Wiley and Sons, Inc., second edition edition, 1960.

[160] J. D. Foley, A. van Dam, S. K. Feiner, and J. F. Hughes. *Computer graphics: principles and practice*. Addison-Wesley, second edition edition, 1996.

[161] S. R. Jammalamadaka and A. SenGupta. *Topics in circular statistics*. World Scientific, first edition edition, 2001.

[162] K. V. Mardia and P. E. Jupp. *Directional statistics*. John Wiley and Sons, Ltd, second edition, 2000.

[163] MATLAB. *version 7.11.0.584 (R2010b)*. The MathWorks Inc., 2010.

[164] P Berens. CircStat: A Matlab Toolbox for Circular Statistics. *Journal of Statistical Software*, 31, 2009.

[165] S. Siegel and N. J. Castellan Jr. *Nonparametric statistics for the behavioral sciences*. 1988.

[166] T. Betz. *Actin Dynamics and Forces of Neuronal Growth*. PhD thesis, University of Leipzig, 2007.

[167] D. Boal. *Mechanics of the Cell*. Cambridge University Press, 1 edition, 2002.

[168] L. D. Landau and E. M. Lifshitz. *Theory of elasticity*. Elsevier Ltd, 1986.

[169] R. Gorelik and A. Gautreau. Quantitative and unbiased analysis of directional persistence in cell migration. *Nat. Protoc.*, 9:1931 – 1943, 2014.

[170] T. Betz, D. Koch, D. Lim, and J. A. Käs. Stochastic actin polymerization and steady retrograde flow determine growth cone advancement. *Biophysical Journal*, 96(12):5130–5138, 2009.

[171] H. Hirata, H. Tatsume, and M. Sokabe. Zyxin emerges as a key player in the mechanotransduction at cell adhesive structures. *Commun Integr Biol*, 1:192 – 195, 2008.

[172] K. Afshar, B. Stuart, and S. A. Wasserman. Functional analysis of the Drosophila Diaphanous FH protein in early embryonic development. 1897:1887–1897, 2000.

[173] M. Roh-Johnson, G. Shemer, C.D. Higgins, J. H. McClellan, A. D. Werts, U. S. Tulu, L. Gao, E. Betzig, D. P. Kiehart, and B. Goldstein. Triggering a cell shape change by exploiting preexisting actomyosin contractions. *Science*, 335:1232–1235, 2012.

[174] Adam C. Martin. Pulsation and stabilization: Contractile forces that underlie morphogenesis. *Developmental Biology*, 341:114 – 125, 2010.

[175] T.M. Svitkina, A.B. Verkhovsky, K.M. McQuade, and G.G. Borisy. Analysis of the actin-myosin ii system in fish epidermal keratocytes: mechanism of cell body translocation. *J. Cell Biol.*, 139:397–415, 1997.

[176] P. T. Yam, C. A. Wilson, L. Ji, B. Hebert, E. L. Barnhart, N. A. Dye, P. W. Wiseman, G. Danuser, and J. A. Theriot. Actin-myosin network reorganization breaks symmetry at the cell rear to spontaneously initiate polarized cell motility. *J Cell Biol*, 178:1207 – 1221, 2007.

[177] M. L. Gardel, B. Sabass, L. Ji, G. Danuser, U. S. Schwarz, and C. M. Waterman. Traction stress in focal adhesions correlates biphasically with actin retrograde fl ow speed. *Journal of Cell Biology*, 183(6):999–1005, 2008.

[178] N.A. Gloushankova, M.F. Krendel, N.O. Alieva, E.M. Bonder, H.H. Feder, J.M. Vasiliev, and I.M. Gelfand. Dynamics of contacts between lamellae of fibroblasts: essential role of the actin cytoskeleton. *Proceedings of the National Academy of Sciences of the United States of America*, 95:4362–4367, 1998.

[179] J. Batson, L. Maccarthy-Morrogh, a. Archer, H. Tanton, and C. D. Nobes. Epha receptors regulate prostate cancer cell dissemination through vav2-rhoa mediated cell-cell repulsion. *Biology Open*, 3(6):453–462, 2014.

[180] S. Huveneers and J. de Rooij. Mechanosensitive systems at the cadherin-f-actin interface. *J. Cell Sci.*, 126:403–413, 2013.

[181] S. Huveneers, J. Oldenburg, E. Spanjaard, G. van der Krogt, I. Grigoriev, A. Akhmanova, H. Rehmann, and J. de Rooij. Vinculin associates with endothelial ve-cadherin junctions to control force-dependent remodeling. *J. Cell Biol.*, 196:641–652, 2012.

[182] C.L. Adams, Y.T. Chen, S.J. Smith, and W.J. Nelson. Mechanisms of epithelial cell-cell adhesion and cell compaction revealed by high-resolution tracking of e-cadherin-green fluorescent protein. *J. Cell Biol.*, 142:1105–1119, 1998.

[183] F. Peglion, F. Llense, and S. Etienne-Manneville. Adherens junction treadmilling during collective migration. *Nat. Cell Biol.*, 16:639–651, 2014.

[184] R. Ananthakrishnan and A. Ehrlicher. The forces behind cell movement. *International Journal of Biological Sciences*, 3:303 – 317, 2007.

[185] L. Trichet, J. Le Digabel, R.J. Hawkins, S.R. Vedula, M. Gupta, C. Ribrault, P. Hersen, R. Voituriez, and B. Ladoux. Evidence of a large-scale mechanosensing mechanism for cellular adaptation to substrate stiffness. *Proc. Natl. Acad. Sci. USA*, 109:6933–6938, 2012.

[186] O.M. Rossier, N. Gauthier, N. Biais, W. Vonnegut, M.A. Fardin, P. Avigan, E.R. Heller, A. Mathur, S. Ghassemi, and M.S. Koeckert. Force generated by actomyosin contraction builds bridges between adhesive contacts. *EMBO J.*, 29:1055–1068, 2010.

[187] R. Mayor and E. Theveneau. The role of the non-canonical Wnt-planar cell polarity pathway in neural crest migration. *The Biochemical journal*, 457(1):19–26, 2014.

[188] C.M. Waterman-Storer and E.D. Salmon. Actomyosin-based retrograde flow of microtubules in the lamella of migrating epithelial cells influences microtubule dynamic instability and turnover and is associated with microtubule breakage and treadmilling. *J. Cell Biol.*, 139:417–434, 1997.

[189] A. W. Schaefer, V. T. G. Schoonderwoert, L. Ji, N. Mederios, G. Danuser, and P. Forscher. Cytoskeletal Dynamics Underlying Neurite Outgrowth. *Developmental Cell*, 15(1):146, 2008.

[190] D. A. Applewhite, K. D. Grode, M. C. Duncan, S. L. Rogers, and P. Forscher. The actin-microtubule cross-linking activity of Drosophila Short stop is regulated by intramolecular inhibition. 24, 2013.

[191] A. Bershadsky, A. Chausovsky, E. Becker, A. Lyubimova, and B. Geiger. Involvement of microtubules in the control of adhesion- dependent signal transduction. pages 1279–1289.

[192] I. Kaverina, O. Krylyshkina, and J. V. Small. Regulation of substrate adhesion dynamics during cell motility. 34:746–761, 2002.

[193] J. Allard and A. Mogilner. Traveling waves in actin dynamics and cell motility. *Curr Opin Cell Biol*, 25:107 – 1152, 2013.

[194] L.P. Cramer. Forming the cell rear first: breaking cell symmetry to trigger directed cell migration. *Nat. Cell Biol.*, 12:628–632, 2010.

[195] A. D. Doyle, M. L. Kutys, M. A. Conti, K. Matsumoto, R. S. Adelstein, and K. M. Yamada. Micro-environmental control of cell migration-myosin iia is required for efficient migration in fibrillar environments through control of cell adhesion dynamics. J Cell Sci:2244 – 2256, 2012.

[196] R. J. Petrie, A. D. Doyle, and K. M. Yamada. Random versus directionally persistent cell migration. *Nature reviews. Molecular cell biology*, 10(8):538–549, 2009.

[197] C. A. Wilson and J. A. Theriot. A correlation-based approach to calculate rotation and translation of moving cells. *IEEE Transations on Image Processing*, 15:1939 – 1951, 2006.

[198] B. R. Munson, D. F. Young, and T. H. Okiishi. *Fundamentals of Fluid Mechanics*. John Wiley & Sons, 2002.

[199] T. Adachi, K. O. Okeyo, Y. Shitagawa, and M. Hojo. Strain field in actin filament network in lamellipodia of migrating cells: Implication for network reorganization. *Journal of Biomechanics*, 42(3):297–302, 2009.